PEOPLE'S DEMOCRATIC REPUBLIC OF ALGERIA
MINISTRY OF HIGHER EDUCATION AND SCIENTIFIC RESEARCH

LARBI BEN M'HIDI UNIVERSITY, OUM EL BOUAGHI

FACULTY OF EXACT SCIENCES, NATURAL SCIENCES AND LIFE
DEPARTMENT OF SCIENCE OF MATTER

Order N°:
Series:

THESIS SUBMITTED IN FULFILMENT OF THE REQUIREMENTS FOR THE "DOCTORATE LMD" DEGREE IN

SEMICONDUCTOR PHYSICS AND MATERIALS

By

NOUA ABDELOUAHAB

Preparation and characterization of thin films nanostructures based on ZnO and other oxides

Board of Examiners

Chairman	***Pr.***	A. NOUIRI	Oum El Bouaghi University
Supervisor	***Pr.***	R.GUEMINI	Oum El Bouaghi University
Examiners	***Pr.***	A. BOUBERTAKH	Constantine I University
	M.C.A.	A. HAFDALLAH	Tebessa University
Co-supervisor	***M.C.A.***	H. FARH	Tebessa University

DEDICATED

To my family and friends

To my teachers and colleagues

Noua Abdelouahab

Acknowledgments

The work presented in this thesis is a result of cooperation, guidance, inspiration and encouragement of several people. I wish to express my sincere thanks and gratitude to all of them.

First and foremost, I would like to thank my research supervisor **Pr. Guemini Rebai** for giving his time and offered me the position to work on this topic. His experience prepared me to be an independent researcher by allowing me to develop my research ideas, thanks to his support and advice. I would also like to thank my co-supervisor, **Dr. Farh Hichem** for his continuous support and encouragement during my Ph.D. journey. It has been an excellent learning experience working together with them.

I would like also to thank the members of the committee, **Pr. A. Nouiri, Pr. A. Boubertakh and M.C.A. A. Hafdallah** for accepting to read and to evaluate this work.

I would like to thank the **Pr. M. Zaabat** and all the members and staff of the Laboratory of Active Components and Materials, Larbi Ben M'Hidi University, Oum El Bouaghi for their support and assistance during this study.

Last but not the least; I am deeply thankful to my family for their love and support. My parents have made countless sacrifices for me, and have provided me with steady guidance and encouragement. This thesis is dedicated to them.

TABLE OF CONTENTS

Chapter II Bibliographic on ZnO and NiO and their applications

Chapter III Experimental details and characterization methods

Chapter IV Results and discussion

LIST OF FIGURES

LIST OF TABLES

GENERAL INTEROCUCTION

Introduction

With the new technological advanced research, nanomaterials have been the core of numerous studies based on their interesting optical, electrical and mechanical properties which cannot be found in normal bulk materials. Nanomaterials are widely used in different applications such as solar cells, photodetectors, gas sensors, photocatalysis, etc.

Among nanomaterials, Transparent conducting oxides (TCOs) are the most investigated materials due to the co-existence of both electrical and optical properties. Typically, TCOs based on their wide bandgap (≥3eV), high efficient electrical conductivity. TCOs can be classified into two types, n-type and p-type, the famous and the promising n-type the well-known zinc oxide. Zinc oxide (ZnO) attracts much interest due to its typical properties such as high chemical and mechanical stability in hydrogen plasma, so as a large excitation binding energy (60 meV), a low cost, non-toxicity and ease of doping, with a high optical transparency in the visible and near-infrared region [1-3]. Due to those properties, ZnO is a promising material for electronic or optoelectronic applications such as solar cells (anti-reflecting coating and transparent conducting materials), gas sensors, liquid crystal displays, heat mirrors, surface acoustic wave devices.

The p-type TCOs are rarely reported in researches compared to n-type. It worth to mention that the first report p-type TCO was published in 1993. In this study, we are interested in NiO due to its wide bandgap energy 3.5-4eV and good thermal and chemical stability. Otherwise, both of NiO and ZnO properties can be improved by doping and co-doping processes.

Overall, the transparent conducting oxides can be synthesized by different techniques such as DC magnetrone technique, electron beam deposition, spin coating, hydrothermal, sol-gel dip- coating, spray pyrolysis, chemical bath deposition. In this study, we used sol-gel dip-coating method for its simplicity, low-temperature deposition and the promising control upon the deposition processes.

In order to achieve the main characteristic properties of prepared thin films, samples were examined using X-ray diffraction (XRD) to investigate structural properties such as the crystalline quality and nature of the layers, the grain size, dislocation density, and the strain. Atomic force microscopy (AFM) was used to characterize the surface morphology

of samples; UV-visible spectrophotometer was also used to analyze the optical characteristics such as the spectrum of the transmittance and the optical gap energy.

Recently, many studies revealed the possibility of adoption of many approaches to enhance the TCOs properties except doping and co-doping, among those approaches the p-n heterostructure allows better separation of electrons/holes due to the existence of the inner electric field between the n-type and the p-type materials.

This thesis is divided into four chapters:

In the first chapter, we will give concepts of nanomaterials, background on Transparent conducting oxides and the thin films deposition techniques.

The second chapter was devoted to the bibliographic study of the essential properties (structural, optical and electrical) of zinc oxide and nickel oxide and their potential applications.

The third chapter is dedicated to summarizing the different parameters affecting the sol-gel deposition. The experimental details of the elaboration of films and a brief review of the different characterization techniques used in this work are also given.

The last chapter relates the obtained results with discussion of different properties (structural, morphological and optical properties) of NiO, Ag-doped ZnO, and ZnO/NiO heterostructure thin films prepared by sol-gel dip-coating method. The photocatalytic properties of ZnO/NiO heterostructure are also presented.

In the end, a general conclusion summarizes the main results obtained in this thesis.

CHAPTER I

Background on TCOs and deposition methods

I.1 Introduction

In This chapter, we give a brief outlines on nanomaterials and their classification especially the Transparent Conductive Oxides (TCOs) because of their optical and electrical duality, also presents approaches including doping and heterostructures to enhance their properties. Besides this, we have presented the different processes to fabricate nanomaterials (physical and chemical depositions) with focusing on the sol-gel method.

I.2 Nanomaterials

I.2.1 Definition

Nanomaterials are defined as a group of materials whose structure has at least one dimension less than about 100 nanometers. In these dimensions, considerable changes occur in materials with all the basic characteristics, which led all researchers to study the different changes and report the results.

The quest for improvement and control of the different properties of materials at the nanoscale is what has led to the emergence of many applications of these materials, including Solar cells; Photodetectors; Electroluminescent diodes; Gas sensors; Biosensors...

I.2.2 Classification of nanomaterials

A lot of research in the field of nanotechnology has been done and many forms have been found. It is, therefore, necessary to develop nomenclatures to classify these materials; nanomaterials can be classified in 0-D, 1-D, 2-D and 3-D (bulk cases) according to their dimensions figure I.1. The density of states (DOS) (number of electronic states per unit of volume and energy) is strongly modified for different types of nanostructures depending on the degree of confinement, as shown in the figure I.2 and as explained below [1]:

- ***0-dimension***

In the 0-D system, for example the quantum dot, the electrons are confined in their movement in the three directions.

- ***1-dimension***

In the 1-D system, such as nanofibres and nanorods, the electrons are free to travel in one direction and confined in the other two directions.

- ***2-dimension***

In the 2D system, for example the nanowires, nanoplates, electrons can easily move in two directions and are confined in one direction.

- ***3-dimension***

In the 3D system, the bulk case, the electrons are free to move in all three directions and there is no confinements and limitations.

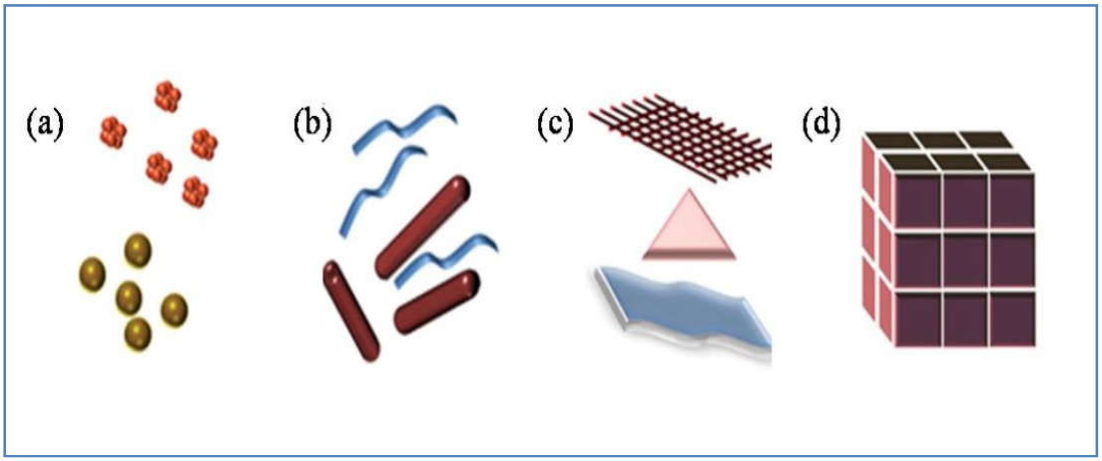

Figure I. 1 Classification of Nanomaterials (a) 0D spheres and clusters,(b) 1D nano-fibers, wires and rods, (c) 2D films, plates and networks, (d) 3D nanomaterials [2].

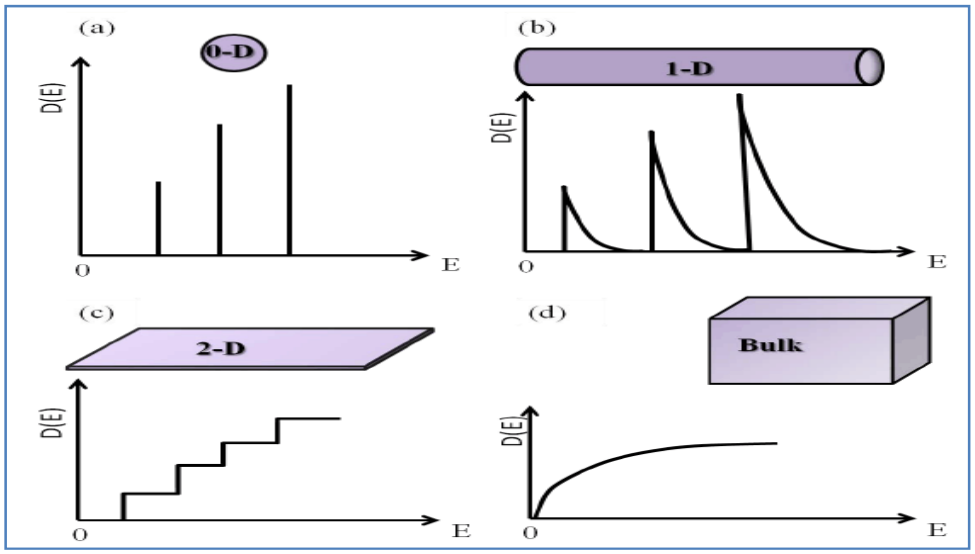

Figure I. 2 Schema illustrating: (a) 0-dimensional (0-D), (b) one-dimensional (1-D), (c) two-dimensional 2-D) and (d) three-dimensional (3 -D). The corresponding state densities (DOS) for each type are also presented.

There are different types of materials that can be prepared at the nanoscale, but we are interested in TCO materials because of the duality of their optical and electrical properties. So, we will give an overview of TCOs in the section below.

I.3 Transparent conductive oxides (TCOs)

Transparent Conductive Oxides (TCOs) are materials with high electrical conductivity combined with low visible absorption. TCOs generally have an electrical resistivity (ρ) $\leq 10^{-4}\Omega.\,cm$, an absorption coefficient (α) of less than 10^4 cm^{-1} in the UV-Visible range and specifically a gap energy high than 3.1eV which allow the transmittance of photons of the visible spectrum because of their energy below 3.1eV [3].

The TCOs are discovered at the beginning of the twentieth century by Baedeker [4] who deposits the first layer of CdO. Then, the research presents several materials that can be considered as TCOs, the best known are ZnO, In_2O_3, SnO_2, CdO, Sn-doped In_2O_3 (ITO) and F doped SnO_2 (FTO). Tin-doped indium oxide (ITO) is the most used for the majority of applications (solar cells, flat screens ...) for a long time [5], but the cost and the abundance of indium pushed the researchers to seek for a material that may be a substitute for ITO. Doped and undoped zinc oxide (ZnO) has emerged as a better candidate for its greater transparency in the visible and low resistivity comparable to those of thin layers of ITO, also for its low cost, abundance, and non-toxicity [5].

I.3.1 Electrical and optical properties of TCOs

TCOs are characterized by their optical and electrical properties, the electrical properties of TCOs can be improved either by defects in the structure (imbalance in stoichiometry) of the oxide or by appropriate doping [6, 7]. The conditions of preparation and the technique of the deposition used are also affecting the electrical properties of a TCO.

The crystalline quality of the layers and the grain size play a very important role in understanding the behavior of the μ mobility of the charge carriers, which are electrons in the case of ZnO. μ is influenced by the diffusion phenomenon of the carriers of free charge in the material and the more this phenomenon is important, more μ will be low. The distribution of charge carriers is mainly due to three factors [8, 9]:

- The presence of ionized or neutral impurities: the more impurities in the ZnO layer, the more they cause the charge carriers to diffuse.

- The presence of grain boundaries in the material: this type of diffusion occurs only in polycrystalline materials. Grain boundaries represent potential barriers that electrons must pass. The more grain boundaries there are, the more the electrons are slowed down, and therefore their mobility is reduced.
- The presence of optical or acoustic phonons: the various vibrations ZnO atomic network can cause electron scattering and thus reduce their mobility.

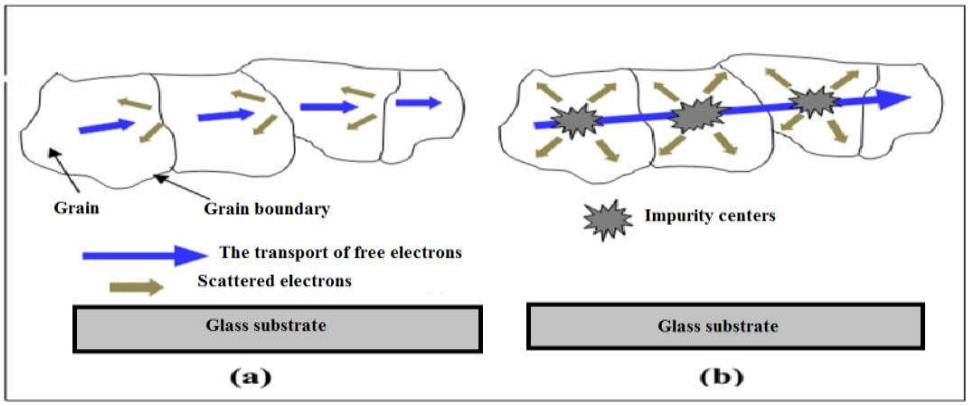

Figure I. 3 Diffusion mechanisms of free electrons: (a) diffusion by grain boundaries and (b) diffusion by impurities [10].

Figure I.3 shows the diffusion phenomenon of the charge carriers in the presence of impurities and the grain boundaries in the material, the choice of dopant and the doping concentration are very important parameters. The dopant is introduced for increased density of the charge carriers but in the case of the TCOs is highly doped, carrier mobility reduced by the diffusion of ionized impurities to a certain point that the conductivity no longer increases.

For the optical properties of TCOs, all searches are done to improve the electrical properties at the same time avoiding the decrease of the optical properties.

I.3.2 Criteria for choosing TCOs

The quantitative assessment of the performance of a TCO is given by the quality factor Q (merit factor or figure of merit) which is defined as the ratio Electrical conductivity σ / optical absorbance in the visible α;

$$Q = \sigma / \alpha = -\left(\frac{1}{R_{sq}\ln(T+R)}\right) \qquad (I.1)$$

Where:

σ [$\Omega^{-1}cm^{-1}$] : Conductivity.

α [cm^{-1}] : Absorption coefficient.

R_{sq}[Ω_{sq}]: Sheet resistance.

T [%]: Total transmission.
R [%]: Total reflection.

It should be noted that the figure of merit gives a good estimate of the performance of the TCOs of the same microstructure [11], but there are other parameters that determine the choice of a TCO such as the stability of TCO (thermal, chemical and mechanical), toxicity and the deposition temperature...

Table I. 1 Factors of different transparent conductive oxides [12].

	Ohm/ sq	A	FoM
ZnO:F	5	0.03	7
Cd_2SnO_4	7.2	0.02	7
ZnO:Al	3.8	0.05	5
In_2O_3:Sn	6	0.04	4
SnO_2:F	8	0.04	3
ZnO:Ga	3	0.12	3
ZnO:B	8	0.06	2
SnO_2:Sb	20	0.12	0.4
ZnO:In	20	0.20	0.2

Table I.1 shows the figure of merits (FoMs) of different transparent conductive oxides. Among them, we notice that ZnO with the appropriate doping (F, Al, GA ...) show good values of FoM and better than tin-doped indium dioxide in the case of ZnO: F and ZnO: Al.

With other dopants, ZnO gives minor FoM values but, in general, we can say that ZnO is a promising TCO and a better replacement of ITO.

I.3.3 Applications of TCOs

TCOs are materials with high transparency in the visible region and good conductivity and for this coexistence of electrical and optical properties, TCOs have been attracted more intentionally in research and industry, they are the basis of many applications and various components [13, 14]:

Solar cell
Optoelectronic systems
Gas sensors
Touchscreens
Flat screens
Electrochromic mirrors and windows
Windows reflecting heat (buildings, ovens ...)

Although they are used in many applications as noted above, TCOs are missing in the application of active devices because of the need of a pn junction [15] and most TCOs are n-type, there is considerable research on the type p are recently reported. The first p-type (NiO) is reported by Sato *et al.* in 1993 [16].

I.4 Principal approaches to change the TCOs properties

I.4.1 Doping

The electrical properties of transparent metal oxides can be changed by introducing dopants. By doping, we introduce energy levels close to the minimum of the conduction band in order to obtain an excess of free electrons (n-type doping) or by introducing energy levels close to the maximum of the valence band and that it is a p-type doping. Much research has been conducted to determine the perfect amount of doping element needed to obtain the optimal properties.

ZnO and NiO are TCO materials with wide band gap energies and good transparency, as well as n-type and p-type conductivities, respectively. The conductivity can vary in case of doping with different elements. The well-known dopants of ZnO are the trivalent metal

cations such as aluminum, gallium, and indium [17-21] and for the NiO different doping element were used [22-24] and well known are the monovalent, especially lithium (Li) [25]. Doping has a limitation at high concentrations; the mobility decreases due to the dispersion of the free carriers and causes the decrease of the conductivity.

The effect of doping on the energy bands in the ZnO, for example, when the ZnO is heavily doped n-type; the energy band edge affected and shifting by increasing in carrier concentration, this case is known by the effect of Burstein - Moss [26].

The conductivity mechanisms are based on the generation and transport of free carriers. In case of the generation of free carriers, we must consider that the concentrations of dopants must be exerted so as not to exceed the solubility limit of the dopants, resulting in phase separation or transformation of the crystalline structure [27]. In the transport case, free carrier mobility must be taken into account.

Many researchers have reported the ideal amount of doping elements to achieve the optimal properties of some materials, using different preparation conditions and of course different preparation methods. From doping to co-doping and mixtures, binary or ternary of different materials, the researchers have tried several ways to report good characteristics for different materials in order to get the ideal TCO candidate. Among these approaches, nano-heterostructure material fabrication was found to be the most promising approach.

I.4.2 Heterostructures

In heterostructures, at least two different materials are combined. In this study, we are interested in oxides-based heterostructured binary semiconductors because of the new features offered by oxide-based materials, which can be a key factor in the development of a new branch of electronics, called "Oxide Electronics" [28].

I.4.2.1 Band alignment in heterostructures

As we said, in heterostructures, at least two semiconductors with different properties and different band gaps are combined, If their carrier type is the same, the heterojunction is called isotype if not it is called anisotype heterojunction. Various models have been developed to predict the band alignment, we simply used Anderson’s rule where band alignment is determined by the electron affinities χ as shown in fig I.4. For a semiconductor, the electron

affinity is the (positive) energy difference between the vacuum level and the conduction band and according to this rule; the conduction and valence bands discontinuities are given by:

$\Delta Ec = \chi 1 - \chi 2$

$\Delta Ev = (\chi 1 + Eg_1) - (\chi 2 + Eg_2)$

With: $\chi 1$, $\chi 2$, and Eg_1, Eg_2 are the electronic affinities and bandgap energies of materials 1 and 2, respectively.

Generally, heterostructures are classified into three types depending on the alignment of the bands of the two semiconductors, as shown in figure I.4.

I. Straddling gap (type I),

II. Staggered gap (type-II),

III. Broken gap (type-III).

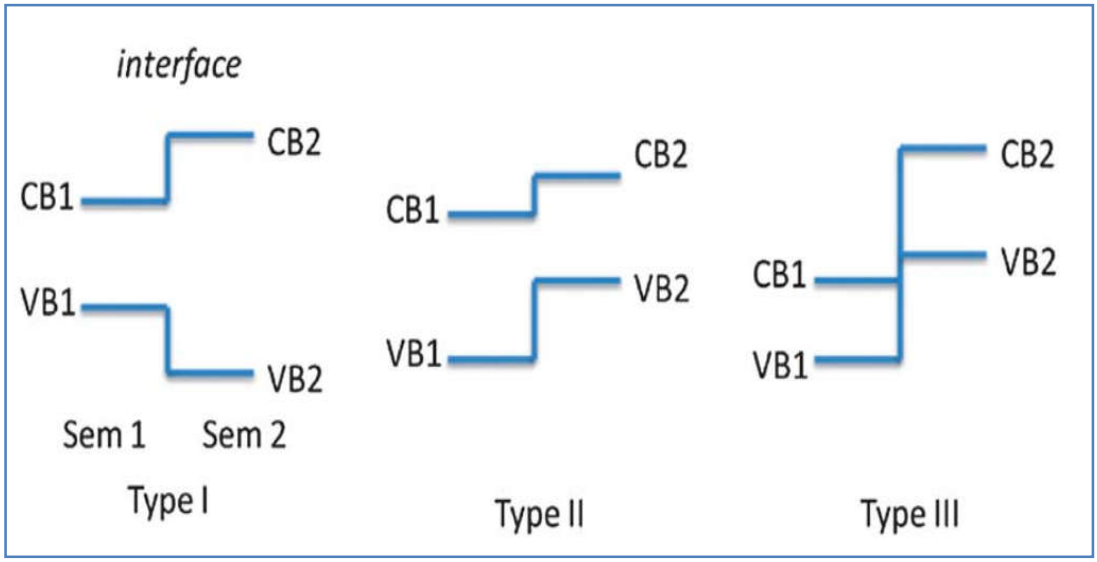

Figure I. 4 Energy band diagram of three types of heterojunctions [29].

Type-I structure (straddled band lineup) is the most studied type. In this type, the band gap of one material overlaps entirely that of the other. In the type-II structure, a staggered lineup is present and electrons will localize in one material and holes will localize in the other materials. In a type-II heterostructure, E_c in one material is lower than E_v of the other material. The researches in the heterostructures try to find a certain physical properties or to fulfill certain application, this is called 'band gap engineering'.

I.4.2.2 The interest of Heterostructures and its applications

The development and manufacture of new functional materials based on hetero-nanostructures have shown interesting opportunities due to the properties emerging from the interface coupling effects and the characteristics of the heterojunction barrier, which is particularly the key to the improvement of gas detection properties as mentioned in [30]. It has been found that various heterostructures materials (in the form of architectures 0D, 1D and 2D, and nano-composites), in various forms such as Field Effect Transistor (FET) detectors or metal/oxide heterocontacts have the ability to adjust the sensitivity and selectivity in the field of gas sensor applications. In addition, the effect of the heterojunction structure on the photocatalyst performance, in particular of type II, the formation of the p-n heterojunction of an n-type semiconductor and a p-type semiconductor develop an n-type directed electric field towards the p-type semiconductor. This can allow getting an efficient separation of photogenerated charges which can improve the photocatalytic performance [31]. Heterostructures have also been used in photodetectors, solar cells, and many other applications. Table I.2 shows the use of different semiconductor heterostructures in different applications.

Table I. 2 The use of different semiconductor heterostructures in different applications.

Heterostructure	Application	Deposition method	Ref.
NiO/SnO2	Gas detection	electron beam evaporation and (RF) magnetron sputtering	[32]
n-ZnO/p-NiO/p-Si	electroluminescence diodes	metal-organic chemical vapor deposition (MOCVD) combined	[33]
NiO/ ZnO	photocatalytic activity	chemical bath deposition	[34]
p-NiO thin film/n-ZnO nanorods	ultraviolet photodetectors	aqueous chemical hydrothermal and thermal evaporation meth-	[35]
SnO_2–TiO_2 nanobelt	Gas detection	hydrothermal process	[36]

NiO nanosheet/TiO_2 nanorod	photocatalytic activity	hydrothermal	[37]
SnO_2–ZnO nanofibers	Gas detection	electrospinning method	[38]
n-ZnO/NiO/p-GaN	Light-emitting diode	MOCVD	[39]
ZnO–SnO_2 nanocomposites	photocatalytic activity	Sol-gel	[40]
p-NiO/n-ZnO	ultraviolet photodetectors	thermal oxidation and hydrothermal	[41]
NiO/WO_3	photoelectrochemical water splitting reaction.	Hydrothermal and dip-coating method	[42]
p-NiO/n-ZnO	ultraviolet photodetectors	Rf-sputtering technique	[43]

As mentioned in the table above, different heterostructure semiconductors have been used for many applications, as we can see; many techniques were used for the manufacture of these heterostructures which also can affect their properties. In the next section, we will discuss various deposition techniques that are used in the preparation of nanomaterials.

I.5 Thin film deposition methods

The processes for producing thin films are divided into two types, the physical and the chemical methods.

I.5.1 Physical vapor deposition (PVD)

Physical Vapor Deposition (PVD) mainly includes evaporation, spraying in all its forms and laser ablation. The most widely used PVD methods are molecular beam epitaxy, cathodic sputtering.

I.5.1.1 Sputtering

Sputtering is a technique used to deposit different materials such as metals, refractory materials, dielectrics, and ceramics. The principle of this technique is the bombardment of the material to be deposited (target) by neutral gas ions generally argon, under the effect of bombardment atoms torn from the target and deposits on the substrate located in front of the target. If the atmosphere (gas) of the discharge is chemically neutral, the sputtering is called simple. However, if it consists of active gases such as oxygen O_2 or nitrogen N_2, sputtering is said to be reactive. The basic scheme of operation of the sputtering is shown in figure I.5.

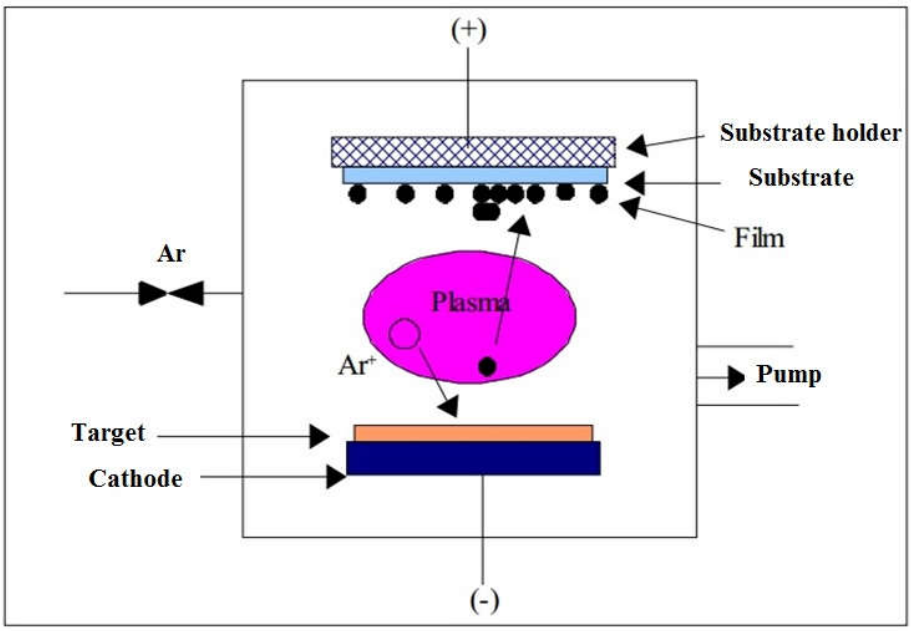

Figure I. 5 The operating principle of sputtering [44].

There are two types of cathodic sputtering depending on the mode of creation of the plasma or the nature of the target (conductive or insulating): direct cathodic sputtering (DC) only in the case of the sputtering of conductive materials and sputtering radiofrequency (RF) which allows the spraying of conductive materials or insulating materials. There are many parameters that affect the deposition process such as base vacuum, sputter gas pressure during deposition, sputter power, target and substrate temperature, etc…The magnetron device has been used to limit the disadvantages and increase the efficiency of the sputtering.

I.5.1.2 Molecular Beam Epitaxy (MBE)

Epitaxy is a compound of two Greek words Epi = on, Taxi = arrangement. It is defined as the formation of a monocrystalline layer called (the epitaxial layer) on a monocrystalline substrate [45].

Molecular beam epitaxy is a method for developing thin films at low temperature with excellent crystalline quality and very low roughness in a very high vacuum (<10-10 Torr). The principle of this technique, figure I.6, is based on the reaction of atomic or molecular fluxes on a monocrystalline substrate which brought to an adequate temperature [46].

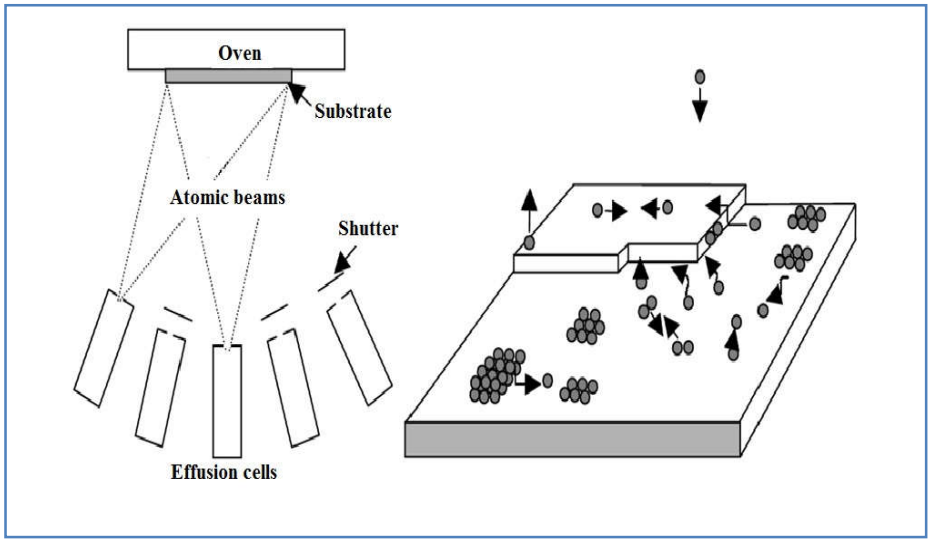

Figure I. 6 the operating principle of MBE [47].

As shown in Figure I.6, the growth process of the molecular beam epitaxy can be summarized in the following steps [47]:

1) Deposition of atoms onto the surface of the substrate

2) Nucleation process (creation of di-atomic islands)

3) Growth of islands by coalescence

4) Formation of a layer by coalescence of islands

Molecular beam epitaxy has the following advantages [45]:

- The low growth rate that allows doping at the atomic level
- Possible controls and in situ analysis (RHEED; Auger XPS)

- Very precise control of the thicknesses of the thin layers
- The ability to control all the steps automatically
- No boundary layer.

I.5.1.3 Pulsed Laser Deposition

Pulsed Laser Deposition (PLD) is a deposition technique that has the advantage of transferring the stoichiometry of the target to the prepared layer, in this method a laser beam focused on a depositing material (target) placed in an ultrahigh vacuum chamber. Under the effect of this laser beam, an amount of the material is pulled away from the target in the form of a dense and light vapor (plasma) and deposited on the substrate placed opposite as presented in figure I.7.

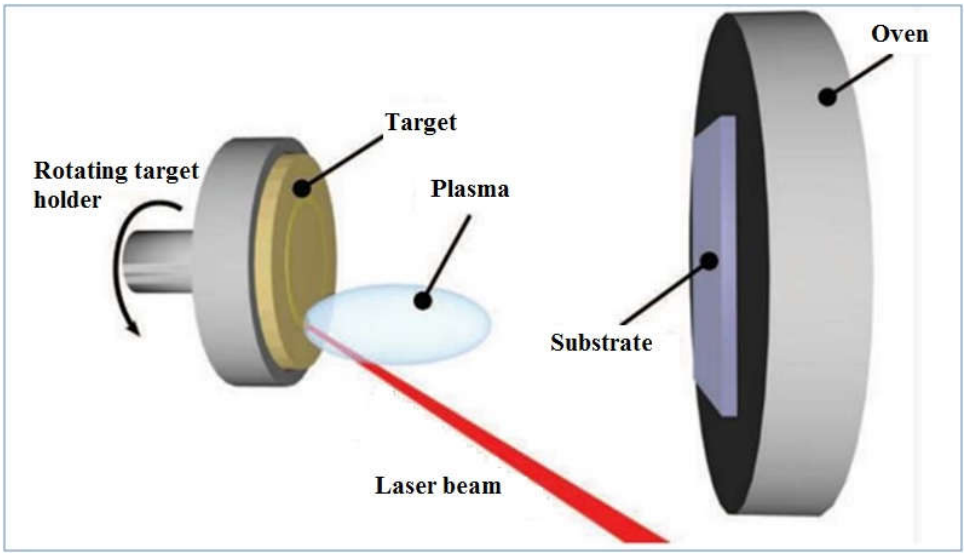

Figure I. 7 Schematic diagram of the Pulsed Laser Deposition (PLD) technique [48].

Laser ablation has a number of advantages, it enables the deposition at room temperature and the coating of all types of the substrate [49], it also allows the manufacture of the complex composition of materials in thin layers.

I.5.2 Chemical deposition

I.5.2.1 Chemical Vapor Deposition (CVD)

The CVD technique consists of developing materials in the form of thin layers from gaseous precursors that chemically react to form these layers on a heated substrate [50], as shown in figure I.8. The CVD process can be summarized in five steps [49]:

- Transporting reactive gas species (or species) to the substrate.
- Adsorption of the reactants on the surface.
- Surface reaction and film growth.
- Desorption of volatile secondary products.
- Transport and evacuation of gaseous products to the reactor outlet.

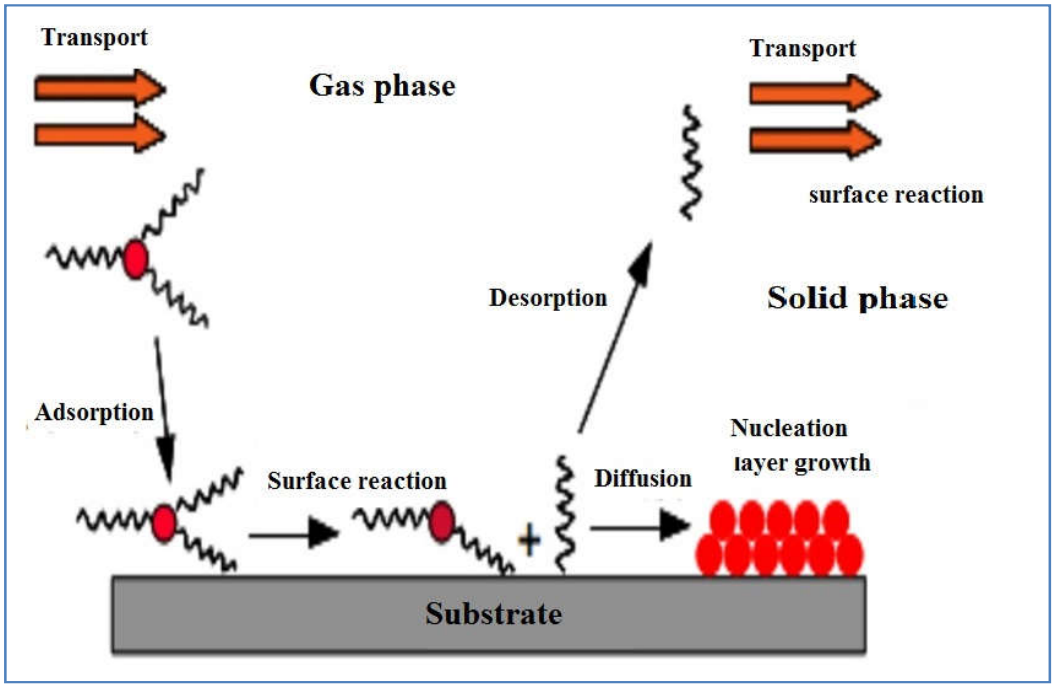

Figure I. 8 The main steps of deposition by the CVD method [45].

The improvement of this technique is to reduce the deposition temperature and the reactor pressure and remedy the low volatility of the precursors. Several CVD type techniques can be given [51]:

- APCVD: (Atmospheric Pressure Chemical Vapor Deposition) deposition under atmospheric pressure;
- LPCVD: (Low-Pressure Chemical Vapor Deposition) low-pressure deposition;
- MOCVD: (Metal Organic CVD) the use of organometallic precursors;
- PACVD: (Plasma Assisted Chemical Vapor Deposition) with the assistance of a plasma.

I.5.2.2 Spray Pyrolysis

The spray pyrolysis is a deposition technique used to prepare thin and thick layers, ceramic coatings and powders [52]. As shown in fig I.9, fine droplets of the precursor solution (containing the material that is to be deposited) are sprayed with a sprayer (nozzle) on a heated substrate. The temperature of the substrate allows the evaporation of the solvents and activates the chemical reactions between the compounds to form the desired layer.

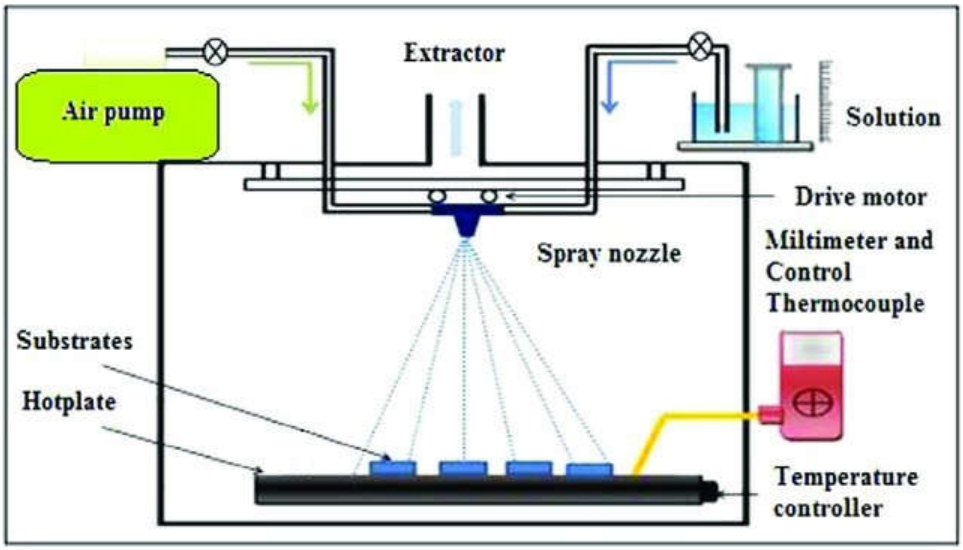

Figure I. 9 Schematic of spray pyrolysis technique.

The parameters that influence the properties of the thin layers prepared by spray pyrolysis are [53-55]:

• The temperature of the substrate.

• The precursor solution (the type of solvent, the viscosity of the solution, the concentration of the compound in the solution).

• The distance between the nozzle and the substrate.

• The carrier gas and the rate at which the aerosol passes through.

• The size and opening time of the nozzle.

• The number of sprays.

The advantages of depositing by the spray pyrolysis method are the low consumption of the material, the low cost of the material used and the possibility of deposition on large

surfaces with high speed. Despite this, the spray method has some disadvantages such as the materials to be deposited must be soluble, Edge effects (greater thickness on the edges of the substrate) and the problem of cleaning the laborious device [54, 56].

I.5.2.3 Sol-Gel

The term sol-gel corresponds to the abbreviation "solution-gelation". The sol-gel method, figure I.10, used to manufacture various materials such as ceramics, powders, fibers, and thin films and is particularly well suited for producing coatings such as thin layers of oxides [57, 58]. Its principle is based on chemical reactions of a chemical precursor consisting of metal atoms of the material that we want to deposit in a solution (solvent) to form an oxide network at an infinite viscosity called "gel", depending on the nature of the precursors used. We distinguish two synthetic voices [59]:

Inorganic route: obtained from metal salts such as nitrates, sulfates, chlorides, or acetates; dissolved in an aqueous solution.

Organometallic route: The most frequently used precursor is metal alkoxides in organic solutions.

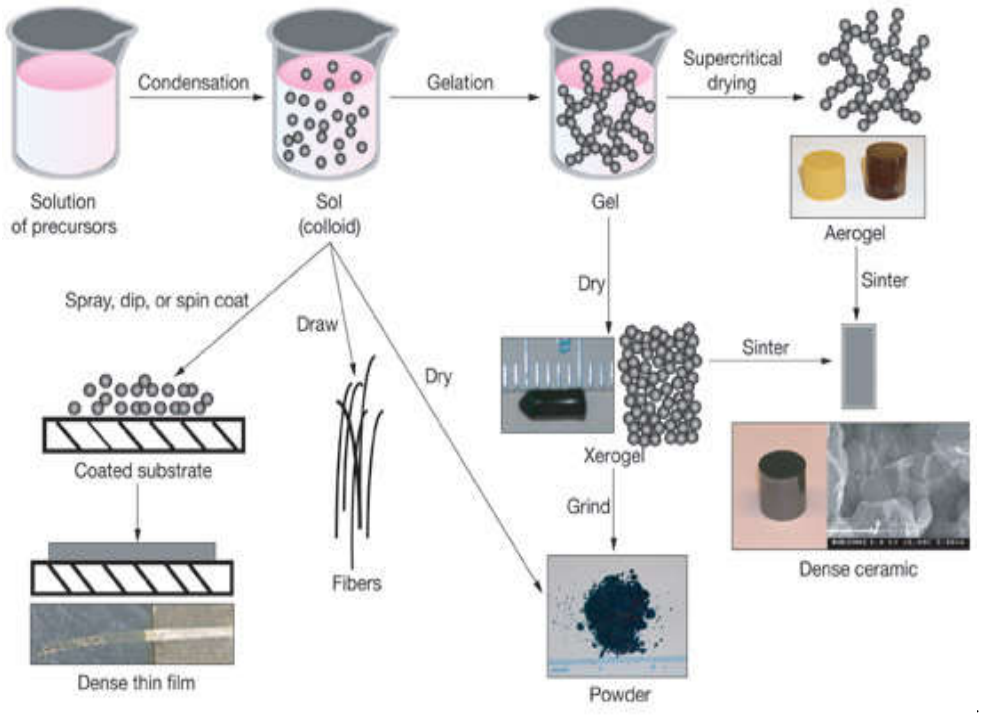

Figure I. 10 Synthesis of various forms of materials by the sol-gel method [60].

I.5.2.3.1 Chemical reactions

In the sol-gel method, the chemical mechanism usually decomposes in two stages hydrolysis and condensation. Each obtained gel is linked to chosen appropriate materials.

I.5.2.3.1.1 Hydrolysis

It is a reaction between a molecule of water and an alkoxide, allowing the releasing of a molecule of alcohol in three stages illustrated in figure I.11:

- The fixing of a molecule of water on the metal atom M.
- Transfer of proton from the water molecule.
- The departure of an R-OH group carried out by a balanced reaction process.

In a neutral condition, the reaction is written [61-62]:

$M\text{-}(OR)_n + H2O \rightarrow OH\text{-}M\text{-}(OR)_{n-1} + R\text{-}OH$

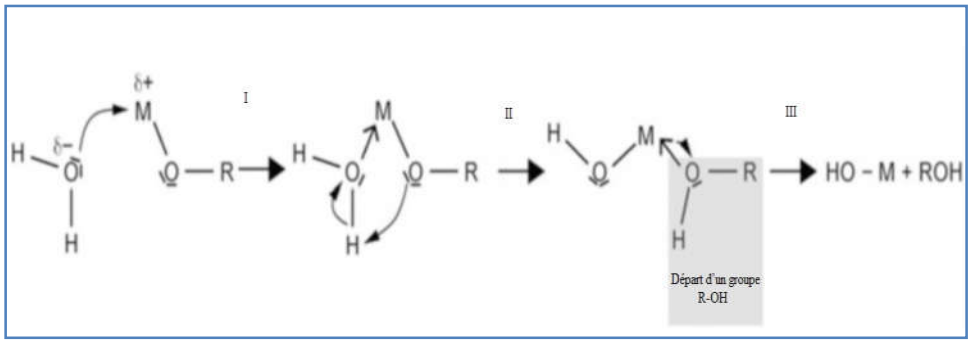

Figure I. 11 Hydrolysis Mechanism of alkoxides M-(OR)n [62].

This reaction can be influenced by the following parameters:

- The catalyst: acidic or basic.
- The nature of the solvent.
- The amount of water relative to the alkoxide ([H2O] / [alkoxide]).
- The temperature.

I.5.2.3.1.2 Condensation

The condensation reactions begin after the appearance of the hydroxyl groups and lead to the formation of bonds or metalloxane bridge "M-O-M". The condensation reaction can take place between the different groups. The reaction of the groups (OH-M- (OR) n-1) between them gives a molecule of water (it is the oxolation), the reaction is written:

$OH\text{-}M\text{-}(OR)_{n-1} + OH\text{-}M\text{-}(OR)_{n-1} \rightarrow (OR)_{n-1}\text{-}M\text{-}O\text{-}M\text{-}(OR)_{n-1} + H2O$

The reaction of the groups (OH-M- (OR) n-1) with remaining non-hydrolyzed groups M-OR giving an alcohol molecule R-OH (it is the alkoxolation) follows the reaction:

$OH\text{-}M\text{-}(OR)_{n-1} + M\text{-}(OR)n \rightarrow (OR)_{n-1}\text{-}M\text{-}O\text{-}M\text{-}(OR)_{n-1} + R\text{-}OH$

The condensation reaction mechanism is related to the hydrolysis reaction and therefore the parameters which influence the hydrolysis are also influencing the mechanism and the kinetics of the condensation reaction and consequently the characteristics of the obtained gel.

I.5.2.3.1.3 The sol-gel transition

The reactions above (hydrolysis and condensation) lead to the formation of a gel consisting of M-O-M chains (or M-OH-M) and polymeric clumps, the size of which increases with time. The sol-gel transition point is achieved when the viscosity becomes infinite [61].

I.5.2.3.2 Sol-gel deposition techniques

In the field of research, the thin layers prepared by the sol-gel process are widely known and are used in various applications. The most used techniques are dip-coating and spin-coating.

I.5.2.3.2.1 Spin-coating

This method consists of centrifuging a solution deposited in excess on a substrate. It has the advantage of being easily implemented and also it gives very good results on flat substrates of small areas (a few cm^2) for moderate investments. We can distinguish four main steps in this technique, as shown in figure I.12.

1) The deposition of the solution.

2) At the start of the rotation, the acceleration phase causes the liquid to flow towards the outside of the support.

3) The constant speed rotation allows the ejection of excess liquid in the form of droplets and the reduction of the thickness of the film uniformly.

4) Evaporation of the more volatile solvents which enhances the reduction in the thickness of the deposited film.

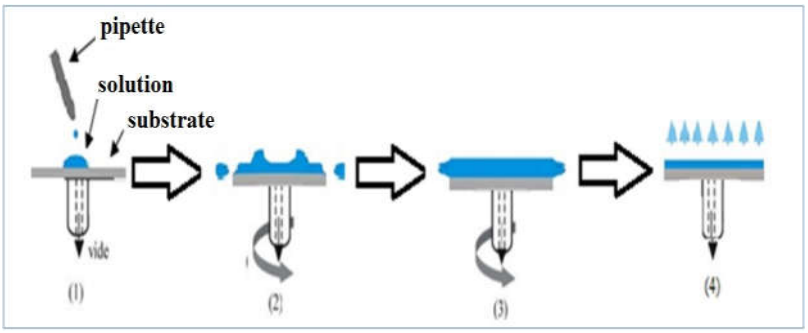

Figure I. 12 The four deposition steps by the spin-coating technique [63].

The properties of the films prepared by this technique depend on the intrinsic parameters of the solution (viscosity, density, etc.) and the deposition parameters (speed and duration of rotation, acceleration, etc.)

I.5.2.3.2.2 Dip-coating

This technique used in this work consists of immersing the substrate in the solution containing the "sol" and removing it under very controlled and stable conditions to obtain a film of a regular thickness (fig I.13). In general, the process can be separated into three important steps:

Immersion & dwell time: the substrate is dipped in the precursor solution at a constant speed and followed by a certain dwell time to allow sufficient interaction time of the substrate with the solution.

Deposition: the substrate is pulled upwards at a constant speed (film deposition: Excess liquid will drain from the surface).

Evaporation: the solvent evaporates by hot drying to form the thin films which can also be treated by annealing at a high temperature to improve their crystallization.

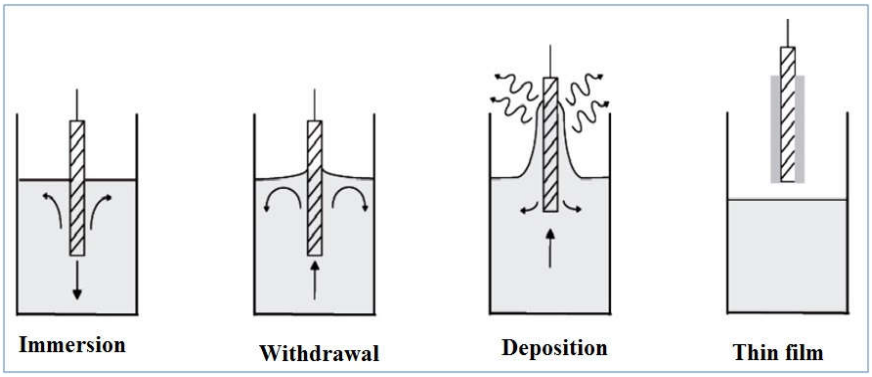

Figure I. 13 The different stages of the dip-coating technique [64].

I.5.2.3.3 Advantages and disadvantages of the sol-gel process

The sol-gel process has many advantages, including:

• The possibility of deposition of thin layers of oxides at low temperatures

• The possibility of doping (relatively simple during the preparation of the sol)

• The ability of deposition on large substrates

• High purity and homogeneity thin film

• It also allows for multi-component coatings

• Deposition of thin layers on both sides of the substrate (dip-coating).

The disadvantages of the sol-gel process:

• The very high cost of some precursors

• Certain chemicals are dangerous to human health.

• Often a long process time.

I.6 References

[1] https://www.embedded.com/print/4391796, (Nov 10th 2018).

[2] http://events.nace.org/TCCNews/2ndquarter_2014/teg474x.asp, (Apr 19th 2019).

[3] A. N. Banerjee and K. K. Chattopadhyay, "Recent developments in the emerging field of crystalline p-type transparent conducting oxide thin films," Progress in Crystal Growth and Characterization of materials, vol. 50, pp.52-105, 2005.

[4] K. Badeker, "Uber die elektrische Leitfahigkeit und die thermoelektrische Kraft einiger Schwermetallverbindungen", Annals of Physics, Vol. 22, pp. 749-766, 1907.

[5] F. Wang, X. Zhao, L. Duan, Y. Wang, H. Niu, and A. Ali, "Structural , optical and electrical properties of Hf-doped ZnO transparent conducting films prepared by sol – gel method," J. Alloys Compd, vol. 623, pp. 290–297, 2015.

[6] A. Klein and K. Christoph, "Transparent Conducting Oxides for Photovoltaics: Manipulation of Fermi Level, Work Function and Energy Band Alignment," Materials, vol. 3.11, pp. 4892–4914, 2010.

[7] Sylvie Faÿ, thèse de Doctorat, l'oxyde de zinc par dépôt chimique en phase vapeur comme contact électrique transparent et diffuseur de lumière pour les cellules solaires, école polytechnique fédérale de Lausanne, 2003.

[8] S. Salam, M. Islam, and A. Akram, "Sol – gel synthesis of intrinsic and aluminum-doped zinc oxide thin films as transparent conducting oxides for thin film solar cells," Thin Solid Films, vol. 529, pp. 242–247, 2013.

[9] Messai Zitouni , thèse de Magister ,« Elaboration sur wafer si (100) et (111) de couches sensibles de (ZnO) par electrocristallisation en vue d'application dans les domaines de l'optoelectronique et des capteurs » ,Université de Batna, 2003.

[10] Bedia Fatima Zohra, thèse de Doctorat, caractérisations et optimisations des dépôts des couches minces d'oxyde de zinc (ZnO) en vue d'applications dans les énergies renouvelables, Université Aboubakr Belkaïd – Tlemcen, 2015.

[11] G. J. Exarhos and X. Zhou, "Discovery-based design of transparent conducting oxide films," Thin Solid Films, vol. 515, pp. 7025–7052, 2007.

[12] R. G. Gordon, "Criteria for Choosing Transparent Conductors," MRS bulletin, vol. 25.8, pp. 52–57, 2000.

[13] KHERCHAOUI née GHOMRANI Fatima-Zohra, thèse de Doctorat, Elaboration et caractérisation de couches minces de ZnO :Al et ZnO :Al/TiO2, Universite M'hamed Bougara-Boumerdes, 2012.

[14] S. O'Brien, Mehmet Çopuroglu, Paul Tassie *et al.*, "The effect of dopants on the morphology , microstructure and electrical properties of transparent zinc oxide films prepared by the sol-gel method," Thin Solid Films, vol. 520, pp. 1174–1177, 2011.

[15] H. Hosono, "Recent progress in transparent oxide semiconductors : Materials and device application," Thin Solid Films, vol. 515, pp. 6000–6014, 2007.

[16] H. Sato, T. Minami, S. Takata, and T. Yamada, "Transparent conducting p-type NiO thin films prepared by magnetron sputtering," Thin Solid Films, vol. 236, no. 1–2, pp. 27–31, 1993.

[17] M. Wang *et al*., "Sol-gel derived transparent conducting ZnO : Al thin films : Effect of crystallite orientation on conductivity and self-assembled network texture," Mater. Chem. Phys, vol. 134, no. 2–3, pp. 845–850, 2012.

[18] H. Mahdhi, Z. Ben Ayadi, S. Alaya, J. L. Gauffier, and K. Djessas, "Superlattices and Microstructures The effects of dopant concentration and deposition temperature on the structural , optical and electrical properties of Ga-doped ZnO thin films," Superlattices Microstruct, vol. 72, pp. 60–71, 2014.

[19] X. Liu, K. Pan, W. Li, D. Hu, S. Liu, and Y. Wang, "Optical and gas sensing properties of Al-doped ZnO transparent conducting fi lms prepared by sol – gel method under different heat treatments," Ceram. Int, vol. 40, no. 7, pp. 9931–9939, 2014.

[20] M. S. Kim *et al*., "Growth and Characterization of Indium-Doped Zinc Oxide Thin Films Prepared by Sol – Gel Method," Acta Physica Polonica-Series A General Physics,vol. 121.1, pp. 3–6, 2012.

[21] R. Hamid, G. Trimmel *et al*., "Highly transparent and conductive indium-doped zinc oxide films deposited at low substrate temperature by spray pyrolysis from water-based solutions," Journal of Materials Science,vol. 52.14, pp. 8591–8602, 2017.

[22] K. H. Kim, C. Takahashi, Y. Abe, and M. Kawamura, "Optik Effects of Cu doping on nickel oxide thin film prepared by sol – gel solution process," Opt. - Int. J. Light Electron Opt., vol. 125, no. 12, pp. 2899–2901, 2014.

[23] S. Layek and H. C. Verma, "Journal of Magnetism and Magnetic Materials Room temperature ferromagnetism in Mn-doped NiO nanoparticles," J. Magn. Magn. Mater, vol. 397, pp. 73–78, 2016.

[24] X. Lou, X. Zhao, J. Feng, and X. Zhou, "Electrochromic properties of Al doped B-subsituted NiO films prepared by sol – gel," Progress in Organic Coatings, vol. 64, pp. 300–303, 2009.

[25] I. Sta, M. Jlassi, M. Hajji, and H. Ezzaouia, “Structural, optical and electrical properties of undoped and Li-doped NiO thin fi lms prepared by sol – gel spin coating method,” Thin Solid Films, vol. 555, pp.131-137, 2013.

[26] E. Burstein, "Anomalous optical absorption limit in InSb." Physical Review, vol. 93, pp. 632–633, 1954.

[27] G. J. Exarhos and X. Zhou, “Discovery-based design of transparent conducting oxide films,” Thin solid films, vol. 515, pp. 7025–7052, 2007.

[28] Pacchioni, Gianfranco, and Sergio Valeri, eds. Oxide ultrathin films: science and technology. John Wiley & Sons, 2012.

[29] Y, Wang, Q.Wang, X.Zhan, F.Wang, M.Safdar, & J. He, "Visible light driven type II heterostructures and their enhanced photocatalysis properties: a review." Nanoscale, vol. 5.18, pp.8326-8339, 2013.

[30] M.A. Carpenter, S. Mathur, and A. Kolmakov, eds. "Metal oxide nanomaterials for chemical sensors", Springer Science & Business Media, 2012.

[31] Abdullah, Eshraq Ahmed. "Band edge positions as a key parameter to a systematic design of heterogeneous photocatalyst." European Journal of Chemistry, Vol. 10.1,pp 82-94, 2019.

[32] S. Xu, D. Xiong, P. Yang, and L. Wang, “Gas sensing properties of NiO/SnO2 heterojunction thin film,” Sensors And Actuators B. Chem, vol. 252, pp.1163-1168, 2017.

[33] Y. Zhao, H. Wang, C. Wu, W. Li, F. Gao, and G. Wu, “Study on the electroluminescence properties of diodes based on n-ZnO / p-NiO / p-Si heterojunction,” Opt. Commun, vol. 336, pp. 3–6, 2014.

[34] F. Tian and Y. Liu, “Synthesis of p-type NiO/n-type ZnO heterostructure and its enhanced photocatalytic activity,” Scr. Mater., vol. 69, no. 5, pp. 417–419, 2013.

[35] A. Echresh, C. O. Chey, M. Zargar Shoushtari, V. Khranovskyy, O. Nur, and M. Willander, “UV photo-detector based on p-NiO thin film/n-ZnO nanorods

heterojunction prepared by a simple process," J. Alloys Compd, vol. 632, pp. 165–171, 2015.

[36] X. Wang, Y. Sang, D. Wang, S. Ji, and H. Liu, "Enhanced gas sensing property of SnO 2 nanoparticles by constructing the SnO 2 – TiO 2 nanobelt heterostructure," J. Alloys Compd, vol. 639, pp. 571–576, 2015.

[37] B. Sun, G. Zhou, T. Gao, H. Zhang, and H. Yu, "Applied Surface Science NiO nanosheet / TiO 2 nanorod-constructed p – n heterostructures for improved photocatalytic activity," Appl. Surf. Sci., vol. 364, pp. 322–331, 2016.

[38] S. H. Yan *et al*., "Chemical Synthesis of SnO 2 – ZnO heterostructured nanofibers for enhanced ethanol gas-sensing performance," Sensors and Actuators B, vol. 221, pp. 88–95, 2015.

[39] H. Wang, Y. Zhao, C. Wu, X. Dong, B. Zhang, and G. Wu, "Ultraviolet electroluminescence from n-ZnO / NiO / p-GaN light-emitting diode fabricated by MOCVD," J. Lumin., vol. 158, pp. 6–10, 2015.

[40] A. Hamrouni, N. Moussa, F. Parrino, A. Di, A. Houas, and L. Palmisano, "Chemical Sol – gel synthesis and photocatalytic activity of ZnO – SnO 2 nanocomposites," Journal of Molecular Catalysis A , vol. 390, pp. 133–141, 2014.

[41] Y. Luo *et al*., "Applied Surface Science Piezoelectric effect enhancing decay time of p-NiO / n-ZnO ultraviolet photodetector," Appl. Surf. Sci., vol. 361, pp. 157–161, 2016.

[42] P. Wu, Z. Liu, D. Chen, M. Zhou, and J. Wei, "Flake-like NiO/WO3p-n heterojunction photocathode for photoelectrochemical water splitting," Appl. Surf. Sci., vol. 440, pp. 1101–1106, 2018.

[43] M. R. Hasan, Md Rezaul, T. Xie *et al.* "Self-powered p-NiO/n-ZnO heterojunction ultraviolet photodetectors fabricated on plastic substrates." APL materials, vol. 3.10, pp. 106101, 2015.

[44] Saâd Rahmane, thèse de Doctorat, Elaboration et caractérisation de couches minces par spray pyrolyse et pulverisation magnetron, Universite Mohamed Kheider– Biskra ,2008.

[45] Khachab Hamid, thèse de Doctorat, Modélisation de la croissance épitaxiale par jets moléculaires (MBE) avec la méthode de Monte Carlo Cinétique (KMC), Université Abou-Bekr Belkaid -Tlemcen, 2010.

[46] Gabriel Tourbot, thèse de Doctorat, Croissance par épitaxie par jets moléculaires et détermination des propriétés structurales et optiques de nanofils InGaN/GaN, Université de Grenoble ,2012.

[47] Esteban Martinez-Guerrero, thèse de Doctorat, Elaboration en Epitaxie par Jets Moléculaires des Nitrures d'éléments III en Phase Cubique, Institut National des Sciences Appliquees de Lyon, 2002.

[48] Taabouche Adel, thèse de Doctorat, Etude structurale et optique de films minces ZnO élaboréspar voie physique et/ou chimique, Université Frères Mentouri Constantine I, 2015.

[49] Kefif Kheira, thèse de Doctorat, Elaboration et caractérisation optique des semiconducteurs amorphes et nanocristallins de silicium (a-Si :H, nc-Si :H) et de carbure de silicium (a-SiC :H, nc-SiC :H), Université d'Oran 1, 2015

[50] Maria Magdalena Şovar, thèse de Doctorat, du tri-isopropoxyde aux oxydes d'aluminium par dépôt chimique en phase vapeur : procédé, composition et propriétés des revêtements obtenus, INP Toulouse et Université Polytechnique de Bucarest, 2006.

[51] A. Mennad, "Les techniques de dépôt de couches minces et leurs applications," Revue des Energies Renouvelables, vol. 18, pp. 713–719, 2015.

[52] Ammar Mosbah, thèse de Doctorat, Elaboration et caractérisation de couches minces d'oxyde de zinc, Université Mentouri Constantine , 2009

[53] Lilia Baghriche , thèse de Doctorat, Elaboration et caracterisation des couches mincesd'oxyde de zinc et sulfure de zinc preparees par sprayultrasonique , Universite Freres Mentouri , 2015.

[54] Thomas Caron , thèse de Doctorat ,Développement de capteurs chimiquesd'explosifs basés sur la détection par fluorescence , Ecole Nationale Superieure de Chimie de Montpellier , 2010.

[55] Ibrahima Soumahoro , thèse de Doctorat ,Elaboration et caractérisation des couches mincesde ZnO dopées au molybdène et à l'ytterbium,pour des applications photovoltaïques , Université Mohammed V , 2012.

[56] Gahtar Abdelouahab, thèse de Magister , Elaboration et caractérisation de couches minces ZnO dopées en aluminium déposées par spray ultrasonique , Universitaire el Oued , 2010.

[57] Bachelet, Romain, thèse de Doctorat, Couches minces d'oxydes élaborées par voie sol-gel, épitaxiées et nanostructurées par traitements thermiques post-dépôt, Limoges, 2006.

[58] Gaudon Alexandre, thèse de Doctorat, Matériaux composites nanostructurés par séparation de phases dans le système silice-zircone, Limoges, 2005.

[59] J. Livage, Sol-gel synthesis of solids, Encyclopaedia of Inorganic Chemistry, R. Bruce King and. John Wiley edition, NewYork, 3836-3851, 1994.

[60] https://str.llnl.gov/str/May05/Satcher.html, Novel Materials from Sol-gel Chemistry, Lawrence Livermore National Laboratory, 2005.

[61] F. Collignon, Techniques de l'ingenieur : Cahier technologique Sol-Gel, certech asbl, B-7180 Seneffe – Belgium, 2008.

[62] T. Schneller and R. Waser, Chemical Solution Deposition of Functional Oxide Thin Films, London: Springer, 2013.

[63] Chahra Boukaous , thèse de Doctorat ,Etude et caractérisation des nanomatériaux à base d'oxyde métallique "ZnO" pour l'analyse d'humidité , Université Frères Mentouri I, 2014.

[64] Abbas Fouzia , thèse de Doctorat , étude de l'influence des effets des éléments lourds sur les propriétés physiques des couches minces de TiO_2 , Université Frères Mentouri I, 2015.

CHAPTER 2

Bibliographic on ZnO and NiO and their applications

II Introduction

The following chapter gives a bibliographic overview of zinc oxide (ZnO) and nickel oxide (NiO) by introducing their structural, optical and electrical properties. We will also present a general outline of the potential applications of metal oxides including gas sensors, solar cells, photodetectors and the photocatalysis application.

II.1 Zinc oxide

II.1.1 Crystallographic properties of ZnO

Zinc oxide (ZnO) is found in the natural state under the name of Zincite, it can crystallize in three crystallographic phases as shown in, fig II.1, according to the conditions of elaboration: the cubic rocksalt structure (NaCl), the hexagonal Wurtzite structure and the structure zinc blende.

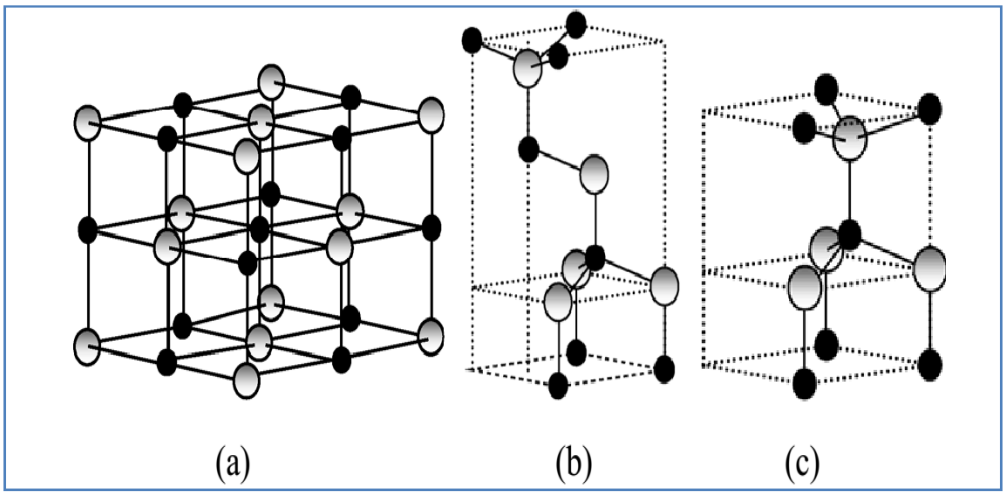

Figure II. 1 ZnO crystal structures: (a) Cubic rocksalt. (b) Cubic zinc blende. (c) Hexagonal wurtzite (Zinc atoms in gray and oxygen in black) [1].

The Blende structure is obtained when ZnO is deposited on certain substrates of cubic symmetry, the Rocksalt structure is observed under very high pressures [~ 10 GPa], the thermodynamically stable structure at room temperature is the hexagonal Wurtzite structure with the lattice parameters a = b = 3,249 Å, c = 5, 204Å. In this structure, each Zn ion is surrounded by tetrahedra of O ions, and vice-versa, the zinc atom is not exactly in the center of the tetrahedron but displaced by 0.11 Å in a direction parallel to the c axis [2]. Table II.1 illustrates some properties of the Wurtzite structure of ZnO.

Table II. 1 Some properties of ZnO in the wurtzite structure [3-5].

Properties	Parameters (Value) at 300 K
Crystalline structure	Wurtzite
Lattice parameters	a=3.249 Å c=5.2042 Å
Refractive index	2.008- 2.029
band gap energy	3.37 eV, direct
Melting point	1975 ^{o}C
Density (g/cm^3)	5.606
Electron effective mass	0.28 m_0
Exciton binding energy	60 meV

II.1.2 Electrical properties

Zinc oxide is an II-VI semiconductor with a wide direct band gap of 3.3 eV at room temperature. Generally, undoped zinc oxide is considered an n-type semiconductor. Table II.2 presents some electrical properties of ZnO.

The electrical properties of ZnO thin films such as electrical resistivity, charge carrier concentration, and mobility are determined by Hall Effect measurements. The electrical resistivity (ρ) of an n-type thin film depends on the electron density (n) in the conduction band and their mobility (μ):

$$\sigma = \frac{1}{\rho} = en\mu_n$$

σ: conductivity. n: the density of electrons. μ_n: electron mobility.

It is possible to modify the electrical resistivity of the zinc oxide by doping, by introducing excess zinc atoms in the interstitial position, or by creating oxygen vacancies. These zinc interstitials and oxygen vacancies thus created, behave like electron donors and lead to a decrease in the electrical resistivity of the material [6]. Interstitial hydrogen is also a shallow donor defect that may be responsible for the presence of free electrons [7].

It is important to mention that the electrical resistivity of zinc oxide depends on the deposition method and the preparation conditions, in particular, heat treatments. The n-type ZnO is obtained easily by substituting zinc atoms with Group III elements (Al, Ga, In and B) and Group IV (Si, Ge and Zr) or by replacing oxygen atoms with a group element VII (F, Cl), for p-type ZnO doping with group I elements (Li, Na and K) but it should be noted that type p is difficult to obtain compared to type n [8 -9].

ZnO is a semiconductor of the $A^{VI}B^{II}$ group. The electronic configurations of the oxygen and zinc atoms are as follows [10-11]:

O: $1s^2 2s^2 2p^4$,
Zn : $1s^2 2s^2 2p^6 3s^2 3p^6 3d^{10} 4s^2$.

Table II. 2 Some electrical properties of ZnO.

Properties	values
Nature of the band gap	direct
The band gap at 300 k (eV)	3.34 ± 0.02
Conductivity type	n et (p)
Electrical conductivity ($(\Omega.cm)^{-1}$)	10^{-6}-10^{2}
charge carrier density (cm^{-3})	10^{15}-10^{21}
Density of states in CB (cm^{-3})	3.71 10^{18}
Density of states in VB (cm^{-3})	1.16 10^{19}
Electrons mobility (cm^2/ V.s)	0.2-200
Holes mobility (cm^2/ V.s)	5-50

The effective mass of electrons:	$0.28\ m_0$
The effective mass of holes:	$0.60\ m_0$
Thermal velocity of electrons ($cm.s^{-1}$)	$2.2\ 10^7$
Thermal velocity of holes ($cm.s^{-1}$)	$1.5\ 10^7$
Relative dielectric constant $\varepsilon_r = \frac{\varepsilon}{\varepsilon_0}$	$\varepsilon_{//} = 8,7$ $\varepsilon_{\perp} = 7,8$

II.1.3 Optical properties

For the use of zinc oxide in various applications, its various optical properties such as transmission, absorption, optical gap and photoluminescence have been studied by several authors, the research results show that its optical property is related to several parameters that we quote: the thickness, the optical gap, the surface roughness, the doping, the crystalline quality of the film and the deposition method [13-17].

Zinc oxide typically is a transparent material in the visible range due to its wide gap, the zinc oxide refractive index in the massive form is equal to 2.0 [18] but in the case of thin films form, its refractive index and its absorption coefficient vary according to the conditions of elaboration. The index of refraction has a value which varies from 1.90 to 2.20 [19-20]. Table II.3 gives some optical properties of ZnO.

Table II. 3 Some optical properties of ZnO [21].

Properties	Values
Transmittance in the visible (%)	80-90
Refractive index at 560 nm	1.8–1.9
Refractive index at 590 nm	2.013–2.029
Absorption coefficient (cm^{-1})	10^4

The optical gap (eV)	3.3

II.2 Nickel oxide

II.2.1 Crystallographic properties

The nickel oxide (NiO) crystallizes in a cubic NaCl-type structure (rocksalt) as shown in fig II.2, with a lattice parameter equal to 0.417 nm.

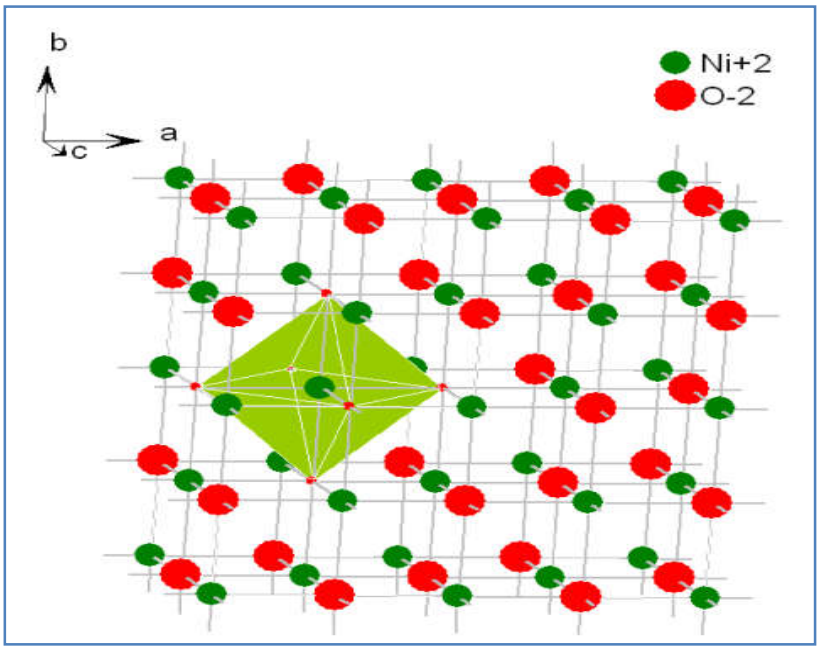

Figure II. 2 The crystalline structure of NiO [22].

II.2.2 Electrical properties of NiO

Nickel oxide is a promising candidate for transparent conductive oxide with p-type conductivity. Stoichiometric undoped NiO is an insulator having a resistivity of 10^{13} Ω cm at room temperature [23].

Substantial conductivity can be achieved in NiO by creating Ni vacancies, forming interstitial oxygen atoms or doping with other cations mainly with monovalent Li ions [24-26].

The electrical properties of NiO films are related to their microstructure and their composition, and the annealing atmosphere. Jlassi M. *et al.* [27] reported that the resistivity is

about 900 × 10^3 Ω cm for the treated samples in air and about 40 Ω cm for the samples treated under nitrogen. Table II.4, gave some electrical properties of NiO.

For the nickel oxide the electronic configurations of the oxygen and nickel atoms are as follows:

O: $1s^2 2s^2 2p^4$,
Ni: $1s^2 2s^2 2p^6 3s^2 3p^6 3d^8 4s^2$

The NiO has been under extensive investigation for decades due to its interesting electronic structure, strongly affected by Ni 3d electrons that are localized in space, but spread over a wide range of energy due to strong Coulomb repulsion between them [28-30].

Table II. 4 Some electrical properties of NiO [31-33].

Properties	Values
Conductivity type	P
Electrical conductivity ($(\Omega.cm)^{-1}$)	10^{-6}-10^{-1}
Hall coefficient (cm^3/C)	5-120
charge carrier density (cm^{-3})	10^{17}-10^{18}
Mobility (cm^2/ V.s)	0.1- 7.6

II.2.3 Optical properties of NiO

Nickel oxide is a transparent material in the visible with a wide optical gap of 3.6 to 4 eV [34]. The transmittance is varied between 40% - 80% and the refractive index is of the order of 2.18 [35]. Preparation conditions, deposition methods, and doping are the parameters that influence the optical properties of NiO. G. Turgut *et al.* [36] reported that the optical properties of thin films NiO prepared by spin-coating sol-gel are affected by the concentration of the precursor, the annealing temperature and the type of solvent. The better obtained optical properties is that corresponding to the 0.1M concentration films annealed at 550 ° C for the methanol solvent.

II.3 Applications of metal oxides

II.3.1 Gas sensors

II.3.1.1 Basics

Due to the increasing concerns about industrial safety, chemical control, and environmental pollution, Continuous efforts are being made in the development of gas sensors [37]. Applications of nanocrystalline metal oxide in gas sensors have attracted much attention due to their advantages such as low cost, easy synthesis, compact size, durable, easy tenability, low power consumption and small drift in signal over long. In addition and more importantly, high sensitivity, fast response, and low operation temperature are required for best candidate gas sensor [38, 40]. Recently, gas sensors based on the semiconducting metal-oxides such as SnO_2, CdO, Fe_2O_3, NiO and ZnO have been found to be very useful for detecting a wide variety of gases in ppm level.

The fundamental sensing mechanism of metal oxide based gas sensors relies on a change in electrical conductivity due to adsorption/desorption of target gas in a given ambient.

Typically, gases of interest include CO, H_2S, H_2, NH_3, SO_2, CO_2, CH_4 and other hydrocarbons. These gases can be harmful to human health if present beyond a certain concentration [41]. So an ideal gas sensor is considered to be sensitive, selective, fast active, and non-contaminating and lower operating temperatures.

A metal oxide sensor is generally composed of two elements as shown in figure II.3, a sensitive element (metal oxide layer) on which the reaction with the gaseous species takes place. The second is a transducer system that converts the interaction between the gas and the sensing element into a measurable (electrical) signal [42].

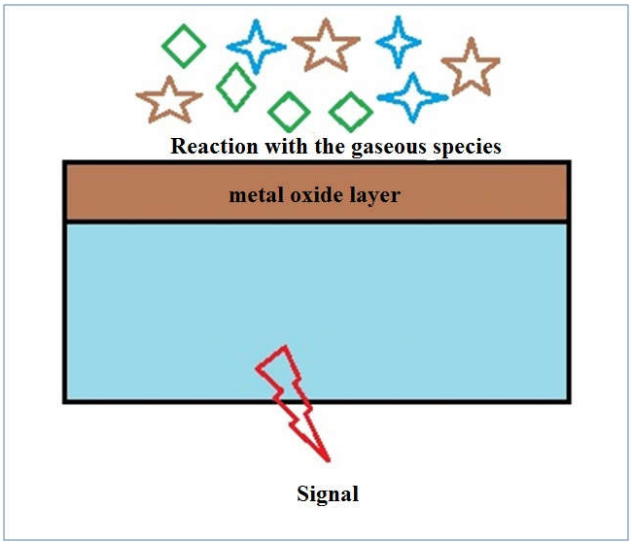

Figure II. 3 Schematic of a gas sensor based on metal oxide.

Gas sensors have been used at various locations, from indoor gas detection to monitoring of environmental pollution and industrial processes at different temperatures [39] such as:

Safety in the home environment: CO leak detection
Hygiene in the home environment: odor control
Safety in an industrial environment: solvent detection, the risk of explosion
Control of urban air pollution: CO detection in underground car parks and tunnels.

II.3.1.2 Performance of a gas sensor

The performance of a gas sensor is influenced by many parameters, the most important parameters and their definitions are given below:

Sensitivity

The sensitivity is defined by the variation or the change in resistance when the sensor is exposed to a certain concentration of gas.

Selectivity

This property is related to the ability of a sensor to detect a single gas in a gas mixture.

Stability

This property is defined as the stability of a sensor's measurements after long use.

Table II. 5 Parameters influencing the performance of a gas sensor [43].

Sensor performance	Some influence parameters
Gas Sensitivity	Nature of sensitive material
	The structure (0D, 1D, 2D, 3D ...)
	Doping
	Operating temperature
Stability / Repeatability	Stability of the structure of the sensitive material (morphological evolution)
	Operating temperature
	Measurement conditions (influence of variations in flow, temperature, and humidity, etc.)
selectivity	Selective filters
	Doping
	Operating mode (variable T)
Reversibility	Nature of the sensitive material vis-à-vis the gas to be detected
	Structure, morphology
	Operating and desorption temperature

As we can see that operating temperature plays a critical role in the gas sensor performance, so it is important to fabricate high sensitive gas sensor but also must operating at lower temperatures to avoid the effect on the other characteristics.

There are other parameters that affect the performances of nanosize gas sensor; the using of different structural (quantum dots, nanowires, nanosheet or nanocomposite) [44], also by the change in structural quality (the grain size), the thickness [38], the surface morphology [45] and the conductivity (the doping) [46]. The creation of heterostructure by using two metal oxides [47] is also another method which is interesting in other applications such as photocatalysis.

II.3.2 Solar cells and photodetectors

In general metal oxides (MO) are mostly non-toxic with obvious chemical stabilization and important abundance in nature, also manufactured using inexpensive methods under ambient conditions. MO-based devices are inexpensive, very stable, and environmentally safe. 10 years ago, it was difficult to use these materials as semiconductors but nowadays a lot of companies sell products based on these materials [48]. Thus, MO-based semiconductors are promising for third generation solar cells.

II.3.2.1 Solar cells

Photovoltaic cells essentially work by utilizing the photovoltaic effect which defines by the ability of a p-n junction device to convert the incident sunlight into electricity. The p-n junction formatted when a p-type semiconductor material is brought into contact with an n-type semiconductor material [49].

Figure II.4 illustrates the operating principle of a conventional photovoltaic cell called the first generation.

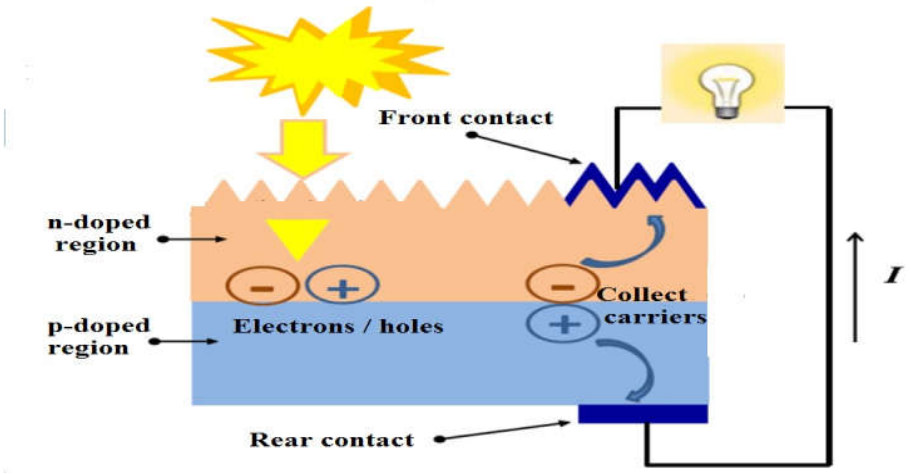

Figure II. 4 Operation principle of a photovoltaic cell (first generation) [50].

When photons of incident light with energies greater than or equal to the band gap of the semiconductor material are absorbed by the p-n junction, electron/hole pairs are created. Electrons are excited from the valence band into the conduction band leaving holes at valence band and by collecting those charges the electric energy will produce.

Cu_2O /ZnO is an example of a heterojunction solar cell, where the Cu_2O is spontaneously p-type and ZnO is n-type as shown in figure II.5. This junction is working well because the conduction band edges of Cu_2O and ZnO align well. Cu_2O is a good absorption layer material, and ZnO nanowires allow for good charge transport, high band gap and large interface, the latter allowing for thicker films and thus higher absorption [51]. Crystallographic orientation is important for achieving a good photoresponse for a p- Cu_2O /n-ZnO cell [52]. However, the efficiency is still very low.

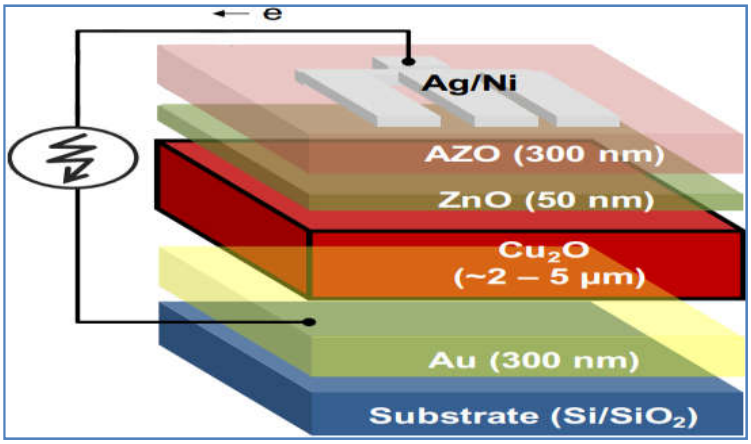

Figure II. 5 Representation of Cu_2O /ZnO heterojunction solar cell [53].

II.3.2.2 Photodetectors

Photodetectors are used in a variety of applications in many fields like compact disc players, optical-fiber communications, and surveillance of rockets or intercontinental ballistic missiles, remote sensing…. They are basically semiconductor devices that can detect an optical signal and convert it into an electrical signal. The operation of a general photodetector basically operates as a solar cell. Figure II.6 summarized the operating mechanism on three processes: first, carrier generation by incident light then second, carrier transport and/or multiplication then third, extraction of carriers as terminal current to provide the output signal [54]. Three main types of photodetectors are generally used: photoconductors, photodiodes, and phototransistors.

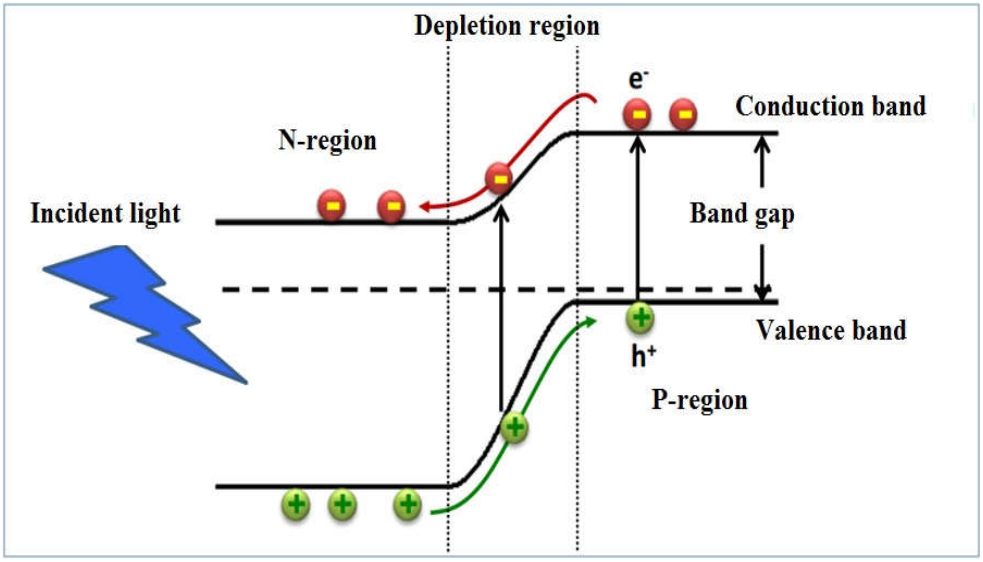

Figure II. 6 Operating Mechanism of the photodiode p-n junction

As mentioned before, ZnO has significant proprieties that allow it also to be regarded as one of the most promising candidates for UV photodetectors. The UV photoresponse in ZnO films was first observed by Mollow in the 1940s [55]. However, the research of ZnO based photodetectors flourished gradually since the 1980s [56]. In the beginning, the devices usually have a simple structure and the properties are not very good. With the improvement of the fabrication of the ZnO-based films using different techniques, many complex ZnO-based photodetectors such as doped ZnO, *p-n* junction, *p-i-n* junction, and Schottky junction, with high performance were reported [57-59].

As the photodetectors have practical applications in various fields, they have to satisfy appropriate requirements such as high sensitivity at the operating wavelength, good current response, and minimum noise. Table II.6 represent some results on photodetector properties of ZnO *p-n* heterojunction photodiodes,

Table II. 6 ZnO-based p-n heterojunction photodiodes [59].

Device structure	Fab Method	Detecting range	Forward threshold voltage	Dark current	Responsivity	Ref

p-NiO/ *i* ZnO/*n*-ITO	e-beam evaporation	UV	1 V	10 nA/cm^2 (-5 V)	-	[60]
n-ITO/ *i*-ZnO/ *p*-NiO			2 V	100 nA/cm^2 (-5 V)		
n-ZnO/*p*-Si	sol-gel	UV/Visible	1 V	7.6×10-5 A/cm^2 (-5 V)	-	[61]
nO:Al/*p*-Si	Sol-gel	UV/Visible	-	-	0.22 A/W at -5 V bias (420 nm)	[62]
n-ZnO/SiO2/*p* Si	Ultrasonic Spray pyrolysis	UV/Visible	-	4.98×10-10 A (-1 V)	0.225–0.297 A/W at -1 V bias	[63]
Si particles coated n ZnO/p-Si	RF Sputtering	UV/Visible	~4 V	4.7×10-6 A/cm^2 (-3 V)	-	[64]
n-ZnO/i-MgO/ *p*-Si	MBE	UV	~1.5 V	<1 nA (-2 V)	-	[65]
Ni/*n*-ZnO/*p*-Si	DC magnetron sputtering	UV/Visible	-	1 µA (-8 V)	210 A/W (390 nm) and 110 A/W (850 nm) at -5 V bias	[66]
n-ZnO/*p*-GaN	MBE	UV	4.6 V	-	~10-6 A/W (370 nm) at 0 V bias	[67]

II.3.3 Photocatalysis

The biggest challenges of the 21st century are the environmental and energy problems with the growth of the world population and the global industry. The environmental contaminations become a serious hazard, especially water pollution. Therefore, the development of new environmentally friendly technologies and methods for the cleanup of the environment has become an imperative task. On the other hand, limited the growing awareness of the availability of abundant fossil fuels on Earth has led many efforts to find sustainable alternatives with high efficiency of renewable energies. Various processes have frequently been used for water purification, including adsorption, biodegradation, electrocoagulation, nanofiltration, chlorination, ozonation and advanced oxidation [68, 69].

Among these methods, advanced oxidation processes (AOPs) are widely used as a simple and cost-effective way to mineralize polluting water without generating harmful secondary pollutants, heterogeneous photocatalysis is an advanced oxidative process, which is of particular interest because it can degrade a wide range of organic pollutants [70]. The heterogeneous photocatalysis process has many advantages over other conventional methods, Md. Tamez Uddin [71] has reported that: (i) the processes can be carried out under ambient conditions (temperature and pressure); (ii) the process uses atmospheric oxygen as an oxidant and no other expensive oxidative chemicals are required; (iii) the oxidant is powerful and less selective, leading to complete mineralization of almost all organic pollutants in the wastewater; (iv) this process is called green technology because the degradation products (carbon dioxide, water and mineral acids) have a moderate toxicity; (v) no residue of the original material remains and therefore no sludge requiring landfill disposal is produced during this process; (vi) photocatalysts are: cheap, non-hazardous, stable, biologically and chemically inert, insoluble under most conditions and reusable.

II.3.3.1 The basic principle of photocatalysis

In the photocatalytic oxidation process, the organic pollutants are destroyed by the semiconductor photocatalyst (e.g., TiO_2, ZnO) in the presence of a source of light energy and an oxidizing agent such as oxygen. In heterogeneous photocatalysis, the interaction of the semiconductor with the light results in the generation of electron-hole pairs. When the light-illuminated semiconductor with energy equal to or greater than the band gap, the electrons are moved from a valence band to a conduction band and left behind holes in the valence band. These electron-hole pairs play a role in the degradation of organic dyes, figure II.7.

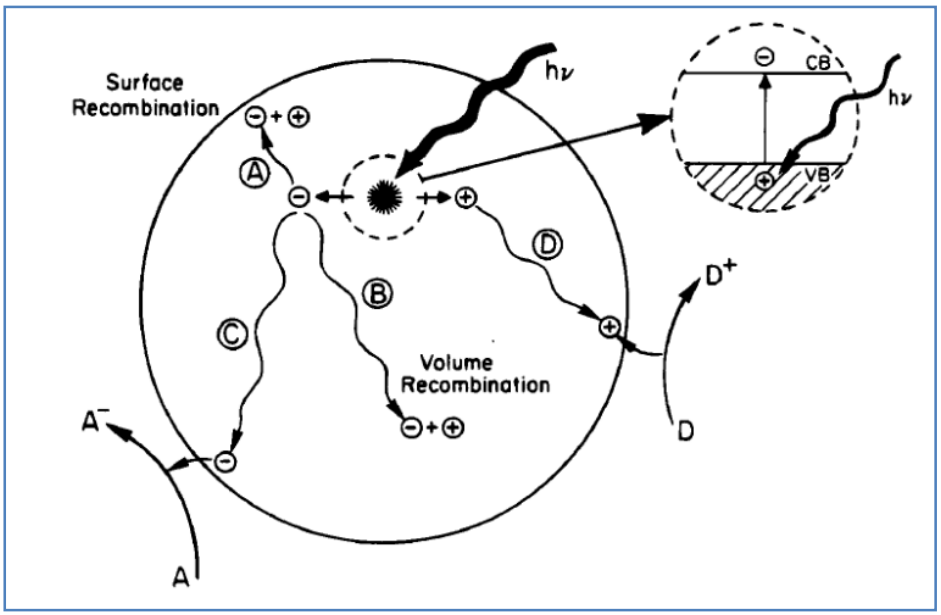

Figure II. 7 Diagram of photoexcitation in a semiconductor photocatalyst followed by excitation pathways

The electrons of the conduction band of the excited state and the holes of the valence band can then follow several paths [72]. The transfer of photoinduced electrons to adsorbed organic or inorganic species or to the solvent results from the migration of electrons and holes to the surface of the semiconductor. At the surface, the semiconductor can give electrons to reduce an electron acceptor (usual oxygen in an aerated solution) (pathway C), a hole can migrate to the surface where an electron from a donor species can be combined with the oxidizing surface hole of the donor species (pathway D).

The probability and rate of charge transfer processes for electrons and holes depend on the position of the band edges for the conduction and valence bands and the redox potential levels of the adsorbed species. The main challenge of charge transfer to adsorbed species is the recombination of electrons and holes. The recombination of the separated electron and hole may occur in the volume of the semiconductor particle (pathway B) or at the surface (pathway A) and be in the form of heat releasing.

In the heterogeneous photocatalytic process, the reaction itself takes place in the adsorbed phase and the overall process can be decomposed into five independent steps [71]:

(i) Mass transfer of reagents in the liquid phase to the catalyst surface.

(ii) Adsorbing the reagents on the surface of the photon-activated catalyst.

(iii) The photocatalytic reaction for the adsorbed phase at the catalyst surface.

(iv) Desorption of products from the catalyst surface.

(v) Desorption of the products from the surface of the catalysts.

Generally, in the presence of photocatalyst semiconductor and oxygen, a chain of reactions occurs. Reactive oxygen species such as H_2O_2, $O^{-\bullet}{}_2$ and the hydroxyl radical $OH^{\bullet}$ are produced using electromagnetic radiation, the deferent reactions to obtain these species are:

$(SC) + h\nu \rightarrow SC(e^- + h^+)$

$SC\ (h_) + H_2O_{ads} \rightarrow SC + OH^{\bullet}_{ads} + H^+$

$SC\ (h^+_) + HO^-_{ads} \rightarrow SC + OH^{\bullet}_{ads}$

$SC\ (e^-) + O_{2ads} \rightarrow SC + O^{\bullet-}{}_2$

$O^{\bullet-}{}_2 + H^+ \rightarrow H_2O^{\bullet}$

$SC\ (e^-) + O^{\bullet-}{}_2 + H^+ \rightarrow SC + H_2O_2$

$H_2O_2 + h\nu \rightarrow 2\ OH^{\bullet}$

$H_2O_2 + O^{\bullet}_2 \rightarrow OH^{\bullet} + O_2 + OH^-$

$SC\ (e^-) + H_2O_2 \rightarrow SC + OH^{\bullet} + OH^-$

It should be mentioned that the photocatalytic reaction cannot occur in the absence of water molecules [73], it also takes three electrons to produce one hydroxyl radical by the above pathway, but it suffices a hole to produce one hydroxyl radical from the adsorbed water or a hydroxyl group. As a result, most hydroxyl radicals are generated by hole reactions. Due to these species, photocatalytic processes will successfully intervene in the degradation of polluting substances and will lead to the formation of carbon dioxide, water, and inorganic ions.

II.3.3.2 Semiconductor photocatalysis

Since Fujishima and Honda reported in 1972 the water splitting into H_2 and O_2 using titanium dioxide (TiO2) electrode [74], semiconductor-based photocatalysis has garnered

considerable attention because of its application potential in wastewater treatment and the production of hydrogen fuel using solar or ultraviolet light. P-type semiconductors are rarely used in photocatalytic semiconductors and generally, only n-type semiconducting oxides are used. ZnO, CdS, Fe_2O_3, tungsten oxide (WO_3) are the best known of semiconductor photocatalysis but their photocatalytic activity is lower than that of titanium dioxide (TiO_2) which is the most useful photocatalyst for the environmental application.

Photocatalyst semiconductors are essentially wide bandgap semiconductors. Therefore, the photons must have high energies to generate electrons from the valence band to the conduction band. In general, these photons belong to the UV part. There are many approaches to obtain semiconductor with a photocatalytic activity under solar radiation and different photocatalytic systems were used. We intend to use the systems shown in figure II.8(b).

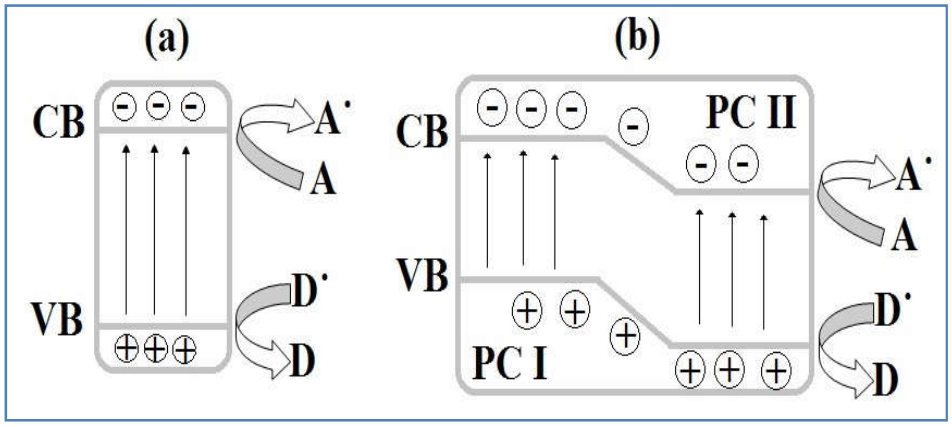

Figure II. 8 Schematic diagrams of photocatalytic systems we used a) Single photocatalyst, (b) type II heterojunction. (PC I: photocatalyst I, PC II: photocatalyst II).

In general, studies focus on the development of efficient photocatalytic materials and attempt to obtain the following characteristics [75]:

- High-efficiency photocatalysts which absorb a large amount of solar energy (ability to generate electron-hole pairs)
- High charge separation (electron-hole pairs).
- Less expensive and easier to produce, non-toxic and durable.

Mainly the position of the edge of the semiconductor band is one of the most important and useful parameters to be considered for use as a photocatalyst. Figure II.9 shows the positions of the band edge of several commonly used semiconductors. It should be noted a

certain important parameter such as; the position of VB must be lower than the oxidation potential of oxygen and CB must be greater than that of hydrogen, also the importance of the presence of grain boundaries and surface states on the semiconductor to allow the electrons/ holes pairs generated to reach the pollutant species.

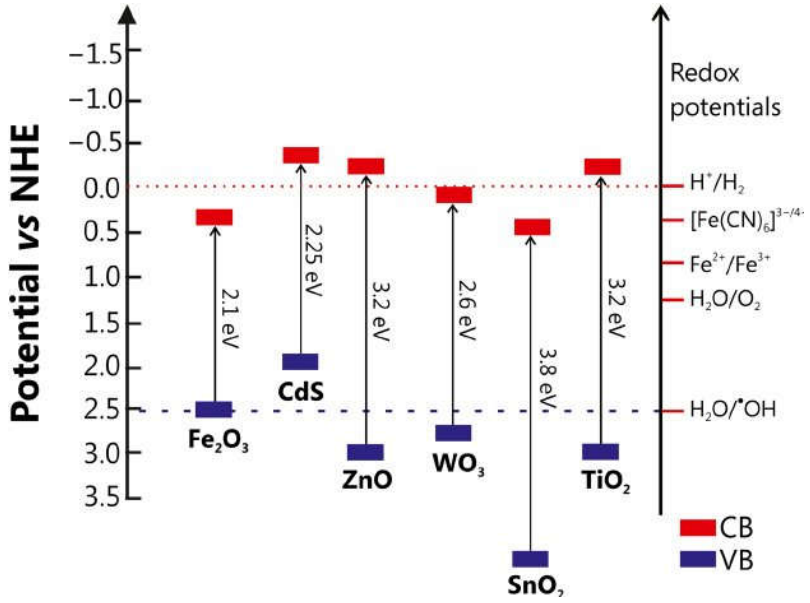

Figure II. 9 Band positions of commonly used semiconductors with respect to the redox potentials of oxidizing species [76].

In order to design an efficient photocatalyst, heterojunction systems are one of the approaches offering good charge separation, reduced charge recombination, and increased optical absorbance range, allowing for better photocatalyst performance. Photocatalysis of nanoscale semiconductors also provides a considerable amount of sites per volume/mass that promotes the reactions.

II.3.3.3 Hydrogen production

The production of H_2 from fossil fuels consumes enormous quantities and produces significant CO_2 emissions (natural gas, for example), therefore renewable energy sources such as hydropower, wind power, and solar energy are the best alternative energies for the H_2 gas production via water splitting reaction especially the solar energy. H_2 photocatalytically generated from water using solar radiation (water splitting) is a promising approach that is of great interest as a source of clean energy; in this process, the light energy is converted into chemical energy and the Gibbs free energy increases considerably by the following water splitting reaction [77]:

$H_2O + h\nu \rightarrow H_2 + 1/2\ O_2 \qquad \Delta G^o = 238\ kJ\ mol^{-1}$

Photocatalysis consists of three main steps: light absorption, separation and charge transfer, and surface reactions. The decomposition of water based on wide bandgap semiconductor materials most often requires ultraviolet (UV) light (<400 nm). The decomposition of water under visible light was an ambitious goal, as we have already mentioned. The heterogeneous semiconductor photocatalyst for the water splitting must be stable in aqueous solutions under photoradiation and must have the bottom of the conduction band more negative than the reduction potential of water to produce H_2, and the top of the valence band is more positive than the oxidation potential of water to produce O_2 [78].

Figure II.10 shows the simplest method of decomposing water using a powder photocatalyst. It can easily break down water into H_2 and O_2 by dispersing a photocatalyst powder into water and using solar energy.

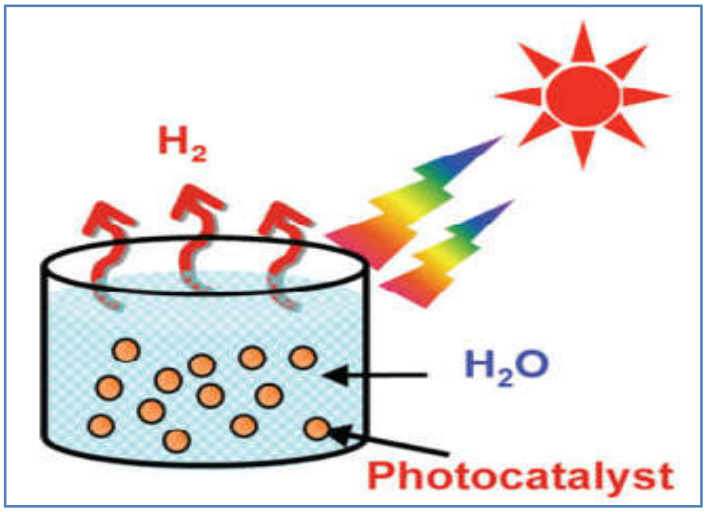

Figure II. 10 Production of hydrogen from water using a powder photocatalyst [71].

II.4 References

[1] Maache Mostefa, thèse de Doctorat, Elaboration de films minces d'oxydes semiconducteurs par voie Sol-Gel, Université Mohamed Khider-Biskra, 2014.

[2] Noua Bouhssira, thèse de Doctorat, Elaboration des films minces d'oxyde de zinc par évaporation et par pulvérisation magnétron et étude de leurs propriétés, Université Constantine 1, 2013.

[3] Bedia Fatima Zohra, thèse de Doctorat, caractérisations et optimisations des dépôts des couches minces d'oxyde de zinc (ZnO) en vue d'applications dans les énergies renouvelables, Université Abou Bakr Belkaïd – Tlemcen, 2015.

[4] Hafdallah Abdelkader, thèse de Doctorat, Dépôt et Caractérisation des Electrodes en Couches Minces Transparentes et Conductrices, Université des Frères Mentouri-Constantine, 2016.

[5] Elkaiem Abdellah, Mémoire de Magister, Contribution au Développement des Matériaux Nano-Composites à Base de ZnO et Polymère Etude Structural et Optique, Université des Frères Mentouri-Constantine, 2015.

[6] Abdellah Moustaghfir. Elaboration et caractérisation de couches minces d'oxyde de zinc. Application à la photoprotection du polycarbonate. Matériaux. Université Blaise Pascal - Clermont-Ferrand II, 2004.

[7] Van de Walle, Chris G. "Hydrogen as a cause of doping in zinc oxide." Physical review letters, vol. 85. 5, pp. 1012, 2000.

[8] S. Tu, "Principal issues in producing new ultraviolet light emitters based on transparent semiconductor zinc oxide," Optical Materials, vol. 30, pp. 292–310, 2007.

[9] M. Zaharescu *et al*., "ZnO based transparent conductive oxide films with controlled type of conduction," Thin Solid Films, vol. 571, pp. 727–734, 2014.

[10] L. Herissi, Mémoire de magister, Élaboration par pulvérisation pyrolytique et caractérisation de couches minces semiconductrices et transparentes d'oxyde de zinc : Perfectionnement du système de dépôt, Université Larbi Ben M'hidi - Oum El Bouaghi, 2008.

[11] C. Badre, thèse de doctorat, Étude de la réactivité de surface par mesure d'angle de contact: Influence de la fonctionnalisation et de la structure Applications aux films d'oxyde de zinc électrodéposés, Université Pierre et Marie Curie, 2007.

[12] V. Kumar, N. Singh, R. M. Mehra, A. Kapoor, L. P. Purohit, and H. C. Swart, "Role of film thickness on the properties of ZnO thin films grown by sol-gel method," Thin Solid Films, vol. 539, pp. 161–165, 2013.

[13] C. Tsay, C. Wu, C. Lei, F. Chen, and C. Lin, "Microstructural and optical properties of Ga-doped ZnO semiconductor thin films prepared by sol – gel process," Thin Solid Films, vol. 519, no. 5, pp. 1516–1520, 2010.

[14] S. Singh and P. Chakrabarti, "Superlattices and Microstructures Comparison of the structural and optical properties of ZnO thin films deposited by three different methods for optoelectronic applications," Superlattices Microstruct, vol. 64, pp. 283–293, 2013.

[15] C. Tsay and W. Lee, "Effect of dopants on the structural, optical and electrical properties of sol-gel derived ZnO semiconductor thin films," Curr. Appl. Phys , vol. 13, no. 1, pp. 60–65, 2013.

[16] Chen, Cheng-Ying, Ming-Wei Chen, Jr-Jian Ke, Chin-An Lin, José RD Retamal, and Jr-Hau He. "Surface effects on optical and electrical properties of ZnO nanostructures." Pure and Appl Chemistry, vol. 82. 11, pp. 2055-2073, 2010.

[17] David R. Lide, ed., CRC Handbook of Chemistry and Physics, Internet Version 2005.

[18] E. M. Bachari, G. Baud, S. Ben Amor, and M. Jacquet. "Structural and optical properties of sputtered ZnO films," Thin Solid Films, vol. 348.1-2, pp. 165-172, 1999.

[19] T. K. Subramanyam, B. S. Naidu, and S. Uthanna, "Characterisation of DC Reactive Magnetron Sputtered ZnO Films Prepared at Different Oxygen Pressures," physica status solidi (a), vol. 425, pp. 425–436, 1999.

[20] C. Gümü, O. M. Ozkendir, H. Kavak, and Y. Ufuktepe, "Structural and optical properties of zinc oxide thin films prepared by spray pyrolysis method," J. Optoelectron. Adv. Mat., vol. 8. 1, pp. 299–303, 2006.

[21] M. Maache, thèse de doctorat, Elaboration de films minces d'oxydes semiconducteurs par voie Sol-Gel, Université Mohamed Khider-Biskra (2014).

[22] Benoit Chavillon, thèse de doctorat, Synthèse et caractérisation d'oxydes transparents conducteurs de type p pour application en cellules solaires à colorant matériaux. Université de Nantes, 2011.

[23] M. Krunks, J. Soon, T. Unt, A. Mere, and V. Mikli, "Deposition of p-type NiO films by chemical spray pyrolysis," Vacuum, vol. 107, pp. 242–246, 2014.

[24] A. N. Banerjee and K. K. Chattopadhyay, "Recent developments in the emerging field of crystalline p-type transparent conducting oxide thin films," Prog. Cryst. Growth Ch., vol. 50, pp.52-105, 2005.

[25] I. Sta, M. Jlassi, M. Hajji, and H. Ezzaouia, "Structural , optical and electrical properties of undoped and Li-doped NiO thin films prepared by sol-gel spin coating method," Thin Solid Films, vol. 555, pp. 131–137, 2014.

[26] S. Kerli, U. Alver, and H. Yaykas, "Applied Surface Science Investigation of the properties of In doped NiO films," Appl Surf Sci, vol. 318, pp. 164–167, 2014.

[27] M. Jlassi, I. Sta, M. Hajji, and H. Ezzaouia, "Optical and electrical properties of nickel oxide thin films synthesized by sol-gel spin coating," Mater. Sci. Semicond. Process., vol. 21, no. 1, pp. 7–13, 2014.

[28] Y. R. Park, K. J. Kim, Sol-gel preparation and optical characterization of NiO and $Ni_{1-x}Zn_xO$ thin films, " J. Cryst. Growth, vol. 258, pp. 380–384, 2003.

[29] W. Nolting, L. Haunert, G. Borstel, "Temperature-dependent electronic structure and magnetic behavior of Mott insulators, " Phys. Rev. B, vol. 46, pp. 4426–4445, 1992.

[30] O. Bengone, M. Alouani, P. Bl. Ochl, J. Hugel, "Implementation of the projector augmented-wave LDA+U method: Application to the electronic structure of NiO, " Phys. Review B, vol. 62, pp. 16392–16401, 2000.

[31] A. Madhavi, Ch. Seshendra Reddy, N.V. Ravindra, P. Lokeshand, P. Sreedhara Reddy, "Effect of substrate temperature on the structural, optical and properties of electron beam evaporated NiO thin films, " Int. J. Adv. Res. Phys. Sci, vol. 1, pp. 16–20, 2014.

[32] H.-L. Chen, Y.-M. Lu, W.-S. Hwang, "Characterization of sputtered NiO thin films, " Surf. Coat. Technol, vol. 198, pp. 138–142, 2005.

[33] B. Chavillon, thèse de doctorat, Synthèse et caractérisation d'oxydes transparents conducteurs de type p pour application en cellules solaires à colorant, Université de Nantes 2011.

[34] H. Sato, T. Minami, S. Takata, and T. Yamada, "Transparent conducting p-type NiO thin films prepared by magnetron sputtering," Thin Solid Films, vol. 236, no. 1–2, pp. 27–31, 1993.

[35] N. Talebian and M. Kheiri, "Sol-gel derived nanostructured nickel oxide films: Effect of solvent on crystallographic orientations," Solid State Sci., vol. 27, pp. 79–83, 2014.

[36] G. Turgut, E. Sonmez, and S. Duman, "Determination of certain sol-gel growth parameters of nickel oxide films," Ceram. Int., vol. 41, no. 2, pp. 2976–2989, 2015.

[37] Y. Hou and A. H. Jayatissa, "Sensors and Actuators B : Chemical Low resistive gallium doped nanocrystalline zinc oxide for gas sensor application via sol – gel process," Sensors And Actuators B: Chem., vol. 204, pp. 310–318, 2014.

[38] A. M. Soleimanpour, Y. Hou, and A. H. Jayatissa, "Evolution of hydrogen gas sensing properties of sol-gel derived nickel oxide thin film," Sensors And Actuators B : Chem., vol. 182, pp. 125–133, 2013.

[39] H. Sefardjella, thèse de doctorat, Propriétés opto-électriques des films minces du dioxyde d'étain, Université 20 aout 1955- Skikda, 2015.

[40] V. V. Ganbavle, S. I. Inamdar, G. L. Agawane, J. H. Kim, and K. Y. Rajpure, "Synthesis of fast response, highly sensitive and selective Ni:ZnO based NO_2 sensor," Chem. Eng. J., vol. 286, pp. 36–47, 2016.

[41] M. K. Deore, "Synthesis, characterisation and gas sensing application of nano ZnO material," Inter. J. of Nanoparticles, vol. 7. 1, pp. 57–72, 2014.

[42] D. Ju, H. Xu, Z. Qiu, J. Guo, J. Zhang, and B. Cao, "Highly sensitive and selective triethylamine-sensing properties of nanosheets directly grown on ceramic tube by forming NiO/ZnO PN heterojunction," Sensors And Actuators: B Chem., vol. 200, pp. 288–296, 2014.

[43] Philippe Menini, thèse de doctorat, Du capteur de gaz à oxydes métalliques vers les nez électroniques sans fl. Micro et nanotechnologies/Microélectronique, Université Paul Sabatier - Toulouse III, 2011.

[44] Y. Shen *et al*., "Highly sensitive hydrogen sensors based on SnO2 nanomaterials with different morphologies," Int. J. Hydrogen Energy, vol. 40, no. 45, pp. 15773–15779, 2015.

[45] A. Arfaoui, S. Touihri, A. Mhamdi, A. Labidi, and T. Manoubi, "Applied Surface Science Structural , morphological , gas sensing and photocatalytic characterization of MoO_3 and WO_3 thin films prepared by the thermal vacuum evaporation technique," Appl. Surf. Sci., vol. 357, pp. 1089–1096, 2015.

[46] K. Sankarasubramanian, P. Soundarrajan, K. Sethuraman, and K. Ramamurthi, "Materials Science in Semiconductor Processing Chemical spray pyrolysis deposition of transparent and conducting Fe doped CdO thin films for ethanol sensor," Mater. Sci. Semicond. Process., vol. 40, pp. 879–884, 2015.

[47] S. Xu, D. Xiong, P. Yang, and L. Wang, "Gas sensing properties of NiO/SnO2 heterojunction thin film," Sensors Actuators B: Chem, vol.252, pp. 1163-1168, 2017.

[48] Francisco Anderson de Sousa Lima, thèse de doctorat, Application of transition-metal-oxide-based nanostructured thin films on third generation solar cells, Universidade Federal do Ceará , 2015.

[49] Bhachu D, thèse de doctorat, The synthesis and characterisation of metal oxide thin films. University College London, 2013.

[50] Fellahi Ouarda, thèse de doctorat, Élaboration de nanofils de silicium par gravure chimique assistée par un métal: caractérisation et application en photocatalyse hétérogène de l'oxyde de graphène, du chrome (VI) et de la rhodamine B, Université Sétif 1, 2014.

[51] Yuhas, D. Benjamin, and Peidong Yang. "Nanowire-based all-oxide solar cells." Journal of the American Chemical Society, vol.131.10, pp. 3756-3761, 2009.

[52] K. Akimoto, S. Ishizuka *et al*. "Thin film deposition of Cu2O and application for solar cells." Solar energy, vol.80.6, pp. 715-722, 2006.

[53] Tran Man Hieu, Jae Yu Cho, Soumyadeep Sinha, Myeng Gil Gang, and Jaeyeong Heo. "Cu_2O/ZnO heterojunction thin-film solar cells: the effect of electrodeposition condition and thickness of Cu_2O," Thin Solid Films, vol. 661, pp. 132-136, 2018.

[54] Sze, Simon M., and Kwok K. Ng. Physics of semiconductor devices. John wiley & sons, 2006.

[55] Mollow, E. Proceedings of the Photoconductivity Conference, Breckenridge, R.G., Ed.; Wiley, New York, NY- USA, p. 509, 1954.

[56] Fabricius, H.; Skettrup, T.; Bisgaard, P. Ultraviolet Detectors in Thin Sputtered ZnO Films. Appl. Opt, vol.25, pp. 2764-2767, 1986.

[57] Y. Luo, B. Yin *et al*., "Piezoelectric effect enhancing decay time of p-NiO / n-ZnO ultraviolet photodetector," Appl. Surf. Sci, vol. 361, pp. 157–161, 2016.

[58] C. Tsay and S. Yu, "Optoelectronic characteristics of UV photodetectors based on sol – gel synthesized GZO semiconductor thin films," J. Alloys Compd., vol. 596, pp. 145–150, 2014.

[59] K. Liu, M. Sakurai, and M. Aono. "ZnO-based ultraviolet photodetectors." Sensors, vol. 10.9, pp. 8604-8634, 2010.

[60] Wang, Kai, Yuriy Vygranenko, and Arokia Nathan. "ZnO-based p-i-n and n-i-p heterostructure ultraviolet sensors: a comparative study." Journal of applied physics, vol. 101.11, pp. 114508, 2007.

[61] S. Mridha, and Durga Basak. "Ultraviolet and visible photoresponse properties of n-Zn O⁄ p-Si heterojunction." journal of Applied Physics, vol. 101.8, pp. 083102, 2007.

[62] Gupta Babita, Anubha Jain, and R. M. Mehra. "Development and characterization of sol-gel derived Al doped ZnO/p-Si photodiode." Journal of materials science & technology, vol. 26.3, pp. 223-227, 2010.

[63] L-C.Chen, and C-N. Pan. "Photoresponsivity enhancement of ZnO/Si photodiodes through use of an ultrathin oxide interlayer." The European Physical Journal-Applied Physics, vol. 44.1, pp. 43-46, 2008.

[64] C. P. Chen, P. H. Lin *et al*. "Nanoparticle-coated n-ZnO/p-Si photodiodes with improved photoresponsivities and acceptance angles for potential solar cell applications," Nanotechnology, vol. 20.24, pp. 245204, 2009.

[65] T. C.Zhang, Y. Guo, *et al*. "Visible-blind ultraviolet photodetector based on double heterojunction of n-Zn O/insulator-Mg O/ p-Si," Applied Physics Letters, vol. 94.11, pp. 113508, 2009.

[66] L. A. Kosyachenko, G. V. Lashkarev, *et al*. "ZnO-based photodetector with internal photocurrent gain," Physica status solidi (a), vol. 207.8, pp. 1972-1977, 2010.

[67] H. Zhu, C. X. Shan, *et al*. "High spectrum selectivity ultraviolet photodetector fabricated from an n-ZnO/p-GaN heterojunction," The Journal of Physical Chemistry C, vol. 112.51, pp. 20546-20548, 2008.

[68] Pawar, Rajendra, and Caroline Sunyong Lee. Heterogeneous Nanocomposite-Photocatalysis for Water Purification, William Andrew, 2015.

[69] Y. Wang, Q. Wang, *et al*. "Visible light driven type II heterostructures and their enhanced photocatalysis properties: a review." Nanoscale vol.5.18, pp. 8326-8339, 2013.

[70] M. M. Sajid, S. B. Khan, N. A. Shad, N. Amin, and Z. Zhang, "RSC Advances crystal violet dye and electrochemical detection of," RSC Advances, vol. 8.42, pp. 23489–23498, 2018.

[71] Md. Tamez Uddin, thèse de doctorat, Metal Oxide Heterostructures for Efficient Photocatalysts, Technical University of Darmstadt- Germany, 2013.

[72] Lahcène Djafer, thèse de doctorat, etude d'un systeme autonome pour le traitement des eaux usees par les techniques membranaires.membranes a effet photocatalytique a base de TiO_2, Université Hassiba Ben Bouali Chlef, 2011.

[73] Chong, Meng Nan, *et al*. "Recent developments in photocatalytic water treatment technology: a review." Water research, vol. 44.10, pp. 2997-3027, 2010.

[74] Fujishima, Akira, and Kenichi Honda. "Electrochemical photolysis of water at a semiconductor electrode." Nature, vol. 238. 5358, pp. 37, 1972.

[75] Mathew Robert Waugh, thèse de doctorat, The Synthesis, Characterisation and Application of Transparent Conducting Thin Films, University College London, 2011.

[76] G.G. Bessegato, T. T. Guaraldo, J. F. Brito, M. F. Brugnera, and M. V. B. Zanoni. "Achievements and trends in photoelectrocatalysis: from environmental to energy applications," Electrocatalysis, vol. 6. 5, pp. 415-441, 2015.

[77] Ryu Abe, "Recent progress on photocatalytic and photoelectrochemical water splitting under visible light irradiation," J. Photochem. Photobiol. B, Biol C: Photochem. Rev, vol. 11.4, pp. 179-209, 2010.

[78] M. Xiao, Z. Wang, M. Lyu, B. Luo, S. Wang, and G. Liu, "Hollow Nanostructures for Photocatalysis : Advantages and Challenges Hollow Nanostructures for Photocatalysis : Advantages and Challenges," Advanced Materials, pp. 1801369, 2018.

CHAPTER III

Experimental details and characterization methods

III Introduction

In this chapter, we present the different parameters affecting the sol-gel deposition such as the precursor (nature and concentration), the nature of the solvent, aging time and the heat treatment, in addition to all experiment details and the conditions of preparations. The characterizations techniques basics are also given briefly to allow a better understanding of this work.

III.1 Parameters affecting the sol-gel deposition

The preparation of metal oxides by the sol-gel method is based on the dissolution of metal alkoxides in organic solvents [1], as we mentioned in Chapter I, the synthesis process involves two steps; hydrolysis and condensation to obtain the precursor solution that can be deposited by one of the sol-gel techniques (in our case, the dip-coating method), after the deposition, a heat treatment is applied on the thin films to obtain a better crystalline structure. The entire process can be affected by many parameters, including:

- ✓ The precursor (nature and concentration),
- ✓ The nature of the solvent,
- ✓ Aging time,
- ✓ The coating method (deposition rate),
- ✓ Heat treatment

However, the results related to the effect of a given parameter are certainly different from one author to another due to differences in experimental conditions. Therefore, we can not give a model on how a parameter can effect, but we give research results and references to examine the impact of these parameters.

III.1.1 Effect of the precursor (nature and concentration)

Various reports studying the effect of precursors and their concentration during the deposition of ZnO thin films. Precursors such as nitrate, chloride, and perchlorate are conceded as inorganic salts and zinc nitrate is the most widely used for the deposition of ZnO thin layers of. In addition, acetates and acetylacetonates are considered as organic salts and zinc acetate is most commonly used for the deposition of zinc oxide [2-4].

Precursors mainly affect all structural, optical and morphological properties. In the following example, we give the results of some studies on the effect of sol concentration on the properties of the ZnO thin film. L. Xu *et al.* [5] Prepared ZnO sols at different concentrations of 0.1, 0.3, 0.5, 0.7 and 1.0 mol / L using zinc acetate, ethanol and monoethanolamine (MEA) as a precursor, solvent and stabilizer, respectively. The films were deposited by spin-coating and the film thickness was maintained in the order of ~ 240 nm, the annealing process was carried out at 500 ° C for 60 minutes, the different results were as follows:

Thin ZnO films with a concentration of less than 0.5 mol / L have only one peak (0 0 2) but preferential orientation along the c-axis, in particular for a concentration of 0.3 mol / l. L, which is in good agreement with [6] and contrary to [7] who reported that the high concentration solution was favorable to the formation of thin films of ZnO with preferential orientation in the c-axis. However, when the sol concentration is greater than 0.5 mol / L, the other two peaks (1 0 0) and (1 0 1) also appear next to the peak (0 0 2). For morphological properties, the increase in sol concentration leads to an increase in ZnO grains and surface roughness due to solute increase per volume of the solution; when the concentration in the sol increases, which leads to the formation of larger particles of ZnO, as also indicated by [8]. The author indicated that the transmittance of ZnO thin films depends mainly on three factors: layer thickness, surface roughness and grain boundary density, and also indicated that the only factor that decreases the transmittance of the ZnO Thin layers deposited by the high-concentration sol in his study is the surface roughness and he concluded by suggesting that solutions with concentration of 0.3-0.5 mol / L can be the best to deposit ZnO thin films.

Generally, the optical transmittance decreases as the concentration increases in the sol, as indicated in [9-12], because of the increase in the film thickness or the increasing of optical scattering caused by grain boundaries or roughness of the surface.

III.1.2 Effect of solvents

The well-known solvents have a higher dielectric constant such as methanol (32.6), ethanol (24.3), 1-propanol (20.81) and 2-methoxyethanol (16.90). The dissolution of the salts depends on the higher dielectric constant [13]. Therefore, zinc acetate has a higher solubility in methanol (higher dielectric constant).

In addition to the dielectric constant of the solvent, the boiling point of the solvent also has a considerable impact on the properties of the films, C.Y. Tsay *et al.* [14] carried out a comparative study of ZnO thin films prepared from zinc acetate dissolved in a solvent composed of; 2-methoxyethanol (2-ME), ethanol (EtOH) and isopropyl alcohol (IPA) having boiling points of 124.6 ° C and 78.3 ° C and 97.2 ° C, respectively. X-ray results revealed that ZnO films synthesized with EtOH and IPA had a higher degree of orientation of the (0 0 2) plane than films synthesized with 2-ME. The films prepared from EtOH and IPA had average crystallite sizes about 20% lower than films synthesized with 2-ME. In addition, the average thickness of films synthesized with 2-ME, EtOH and IPA, respectively, were 170, 180 and 185 nm. Solvents used in the synthesis of thin films of ZnO have a significant influence on the surface roughness. Thin films synthesized using low-boiling solvents, such as EtOH and IPA, have reduced the average crystallite size in ZnO films, so their surfaces are smoother (Lower RMS) compared to 2-ME which shows a rough surface; unfortunately, this roughness causes scattering and reflection of the light and leads to minimal optical transmittance of the 2-ME sample (85.4%) compared to the EtOH and IPA samples (> 92.0%).

These results are in good agreement with those obtained by [15], other solvents such as acetone and water as well as ethanol were used [16], and a high degree of crystallinity of the phase hexagonal ZnO with the dominant (101) plane was reported.

III.1.3 Effect of stabilizers

Stabilizers have an important role to play in the deposition of ZnO nanostructures. They contribute to the dissolution of precursors and the formation of stable sols. The stabilizers frequently used in the sol-gel ZnO system are the amines. Of these, monoethanolamine and diethanolamine are the best choices for thin films with appropriate optical properties [17].

III.1.4 Effect of aging time

The aging time has a great influence on the properties of thin films prepared, [18] reported that thin films of undoped and aluminum-doped ZnO were polycrystalline and had a hexagonal wurtzite structure with c-axis preferred orientation. The aging time of 48h is the optimal condition for the aging time; the aging time shows no significant effect on the optical properties with the aging time. [19] Also reported that the crystallinity was improved by increasing the aging time in addition to minimal surface roughness, but the optical

transparency of the films was considerably improved by the aging of the solution for longer periods of time.

Based on other studies [20-23], we can say that the structural and optical properties of thin films of ZnO are improved by the increasing the aging time of the sol and the ideal aging time is between 24h and 48h.

III.1.5 Effect of the coating method (the deposit rate)

Among the various parameters that influence deposition by the sol-gel method, the deposition rate, whether in spin-coating or in dip-coating, plays an important role in the evolution of the properties of the films, we will discuss this in more detail in the next chapter by studying the effect of the withdrawal speed on the properties of NiO thin films.

III.1.6 Effect of heat treatment (drying and annealing)

Heat treatment is another factor affecting the properties of films. Typically, it consists of two stages of drying and annealing and can be classified into three stages: 1-evaporation, 2-decomposition of organic residues, 3-crystallization, if one of these steps is not completed before the beginning of the next step, crystal growth will be disturbed. Therefore, conceding drying is a crucial step as it contains steps 1 and 2, evaporation of the solvent and removal of organic compounds. The drying temperature cannot be defined as an absolute value because it depends on the boiling point of the solvent and the stabilizer, but it must be higher than the boiling point of the solvent and the additives for evaporating the solvent and the stabilizer and furthermore to eliminate the organic residues produced by the precursor, the boiling point is known for all the solvents (alcohol, stabilizer) and [24] reported that the Zn $(OAc)_2$ began to decompose at 190 ° C and the decomposition was complete at 310 ° C.

The last step is the crystallization carried out by the annealing process in order to obtain a better crystallinity; this step begins after the evaporation of the solvent and the elimination of all the organic substances by the drying process. The prepared films are subjected to a high temperature heat treatment (> 300 ° C) which gives the atoms a greater activation energy to the diffusion, which allows the atoms to move to the favorable energy site in the crystal lattice growth then grew in the preferred growth direction, which allowed to improve the crystallinity of the films [25, 26]. [25] The effect of annealing temperature from 100 ° C to 400 ° C (low-temperature annealing) on the properties of ZnO and AZO films prepared using

the spin-coating technique was investigated; as the annealing temperature increased, the films exhibited stronger preferential orientation along the c-axis with improved crystallinity, increased RMS roughness and improved optical transmittance.

For high temperature annealing, [27] reported that the degree of orientation of the crystals increased with the annealing temperature, the annealed film at 600 ° C was strongly oriented along the c-axis, in addition, the average transmittance films increases from 60% to 80% with increasing the annealing temperature; these results are in good agreement with [28, 29], but they go against [30, 31] which stated that high-temperature annealing leads to a decrease in transmittance in the visible range, this disagreement can be due to the difference in the conditions of preparation.

Based on previous studies and our results, we suggest that the annealing temperature range between 500 and 600 ° C seems to be the most appropriate (we used a 550 ° C annealing temperature for our films).

The parameters we mentioned earlier are the key factor of deposition via the sol-gel method and they change almost all the properties. Therefore, the preparation conditions must be controlled in order to generate a given result. In addition, other parameters have also affected the properties of ZnO thin films prepared by the sol-gel method, such as; the type of substrate [32, 33] and the thickness of the film [34, 35].

III.2 Experimental Details

III.2.1 Preparation of the precursor solution

The preparation of the precursor solution is the first step of the thin-film deposition process by the sol-gel method, as we have seen before, there are many parameters during the preparation phase that affect the quality films such as molarities, solvents, and precursors, in section below we present the different experiment details and conditions that we used in the preparation of our films

III.2.1.1 NiO

In this study, the NiO precursor solution was obtained by dissolving nickel (II) acetate tetrahydrate in 30 ml of methanol and adding monoethanolamine (MEA) as a stabilizing agent. The molar ratio of MEA to the nickel acetate was maintained at 1.0 and the nickel

acetate concentration was 0.1M. The solution was stirred at 70 ° C for one hour, resulting in the formation of a light green homogenous solution as shown in Figure III.1.

Figure III. 1 NiO precursor solution under stirring.

III.2.1.2 ZnO

The precursor solution of zinc oxide was obtained under the same conditions as the NiO precursor solution, with the exception of the use of zinc acetate as a precursor and ethanol as a solvent, the molar ratio of MEA to zinc acetate was maintained at 1.0. After stirring, we obtained a clear homogeneous solution which was kept for 24 hours at room temperature.

The various details of the compounds used for the preparation of ZnO and NiO thin films are given in Table III.1 below:

Table III. 1 Chemicals used in the preparation of solutions.

	Compound	Molecular formula	Molecular weight (Mol / L)
Precursor	nickel Acetate	$(Ni(CH_3CO_2)_2 \cdot 4\ H_2O)$	248.84
	zinc Acetate	(Zn (CH3COO)2, 2H2O)	219.49
Solvent	Methanol	CH_3OH	32.04
	Ethanol	C2H5OH	46.06

Stabilizer (catalyst)	Monoethanolamine (MEA)	$NH_2CH_2CH_2OH$	61.08

III.2.2 Preparation of substrates

III.2.2.1 Choice of the substrate

W. Chebil *et al.* [36], reported that the properties of ZnO thin films deposited by the spin-coating sol-gel technique are strongly influenced by the nature of the substrate, taking into account our subject to study TCO materials. The glass substrate is a perfect choice that allows us to obtain very transparent thin films.

Glass substrates of dimensions (3 × 2.5 cm 2) and about 2 mm thick were used for the preparation of our thin films (NiO and ZnO).

III.2.2.2 Cleaning of substrates

To obtain thin layers of good quality, the substrate must be free from scratches, grease, and dust, since the smallest impurity can lead to contamination and the ruin the deposited layers.

- The common cleaning procedures are as follows:
- Cleaning in an acetone bath in an ultrasonic bath for 15 min.
- Rinsing with distilled water in an ultrasonic bath for 15 min.
- Rinsing for 20 min in a bath of methanol ultrasonic.
- Drying the samples.

The ultrasonic apparatus used in the cleaning processes are shown in figure III.2, the beakers and glassware were also cleaned according to the same procedure as above.

Figure III. 2 The ultrasonic apparatus used for the cleaning process.

III.2.3 Deposition details by Dip-coating

The prepared samples were obtained by a computer-controlled KSV-DCx2 (Biolin Scientific) Dip-Coater device with "KSV NIMA DC" software (figure III.3) at the laboratory of active components and materials (Larbi Ben M'hidi University-Oum El Bouaghi). The principle of this process is very simple, it can be described as follows, the substrate is dipped in the coating solution and remains in the solution for a while then it removed from the solution at a controlled rate.

Figure III. 3 The Dip-coating equipment.

Sinem Aydemir [37] reported that the withdrawal speed (WS) has a significant impact on the properties of ZnO: Al thin films prepared by the sol-gel dip-coating technique, we also studied the effect of the withdrawal speed on the properties of NiO thin films and we used the speeds of 30, 50 and 70 mm / min.

III.2.4 Heat treatment

III.2.4.1 Drying

This process used to evaporate the solvent by conventional thermal, in our case using a BINDER oven brand that showed the figure III.4, after several minutes at 150 ° C in the oven we got dried layer, another layer can be applied on it with another dip-coating process until we obtain the desired thickness.

Figure III. 4 The oven used for drying.

III.2.4.2 Annealing

This is usually the most important process in the preparation of thin films, it allows a better crystallization (transition from amorphous to polycrystalline) and eliminates organic residues of precursors used in the solution, the prepared films was air-annealed for 2 hours in an oven (Figure III.5) at 550^{o}C. We chose this temperature because it gives the best degree of crystallization for the NiO thin films, as reported by [38], as well as for our use of the glass substrate.

Figure III. 5 The oven used for annealing.

The whole procedure for the preparation of ZnO and NiO thin films with the sol-gel method can be summarized as shown in Figure III.6.

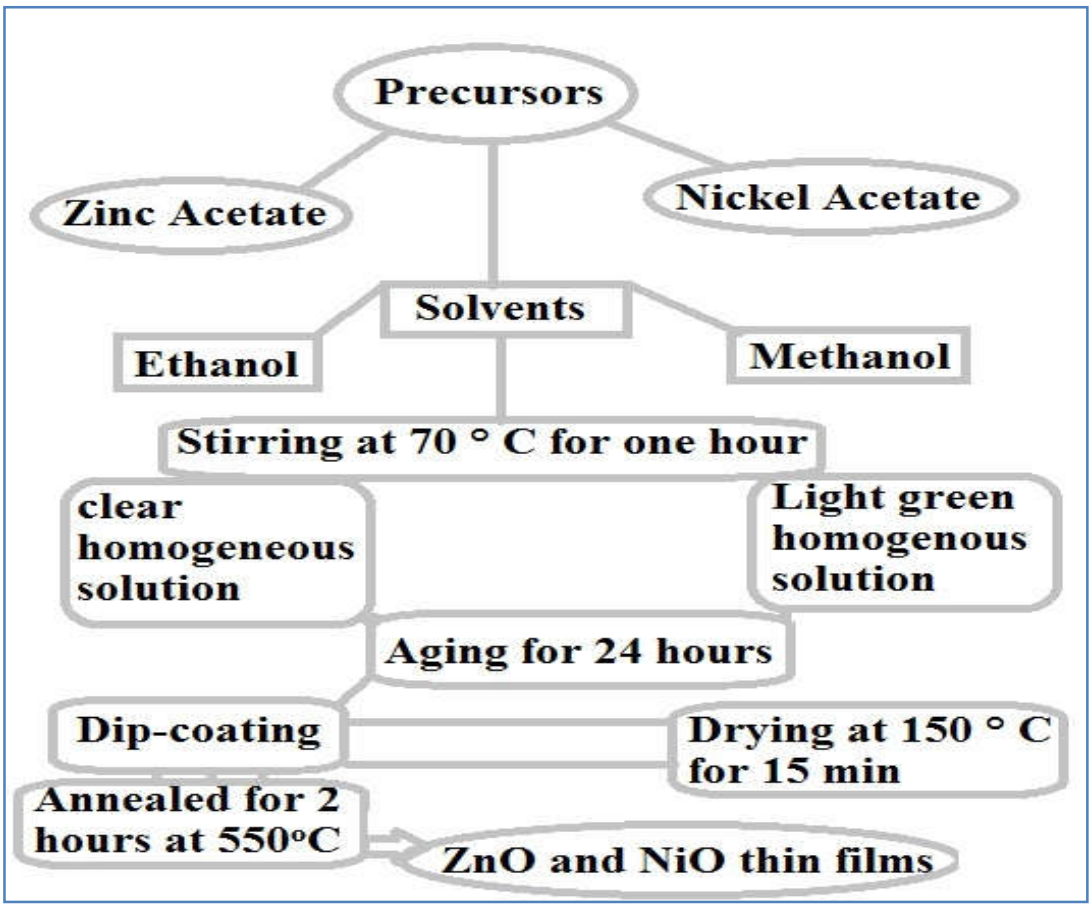

Figure III. 6 The preparation of ZnO and NiO thin films via the sol-gel method.

III.3 Characterization techniques

III.3.1 Structural characterization using X-Ray Diffraction (XRD)

The X-ray diffraction is a non-destructive structural analysis method for determining the crystal structure of materials in the form of bulk materials, powders or thin films. It is based on the Bragg law (figure III.7) which gives the relation between the distance d_{hkl} between the crystallographic planes, the wavelength λ of the X-rays and the diffraction angle θ:

$$2d.\sin\theta = n.\lambda \qquad \text{(III.1)}$$

Where:

d: the interplanar distance;

θ: X-ray incidence angle;

n: the order of diffraction;

λ: the wavelength of X-rays.

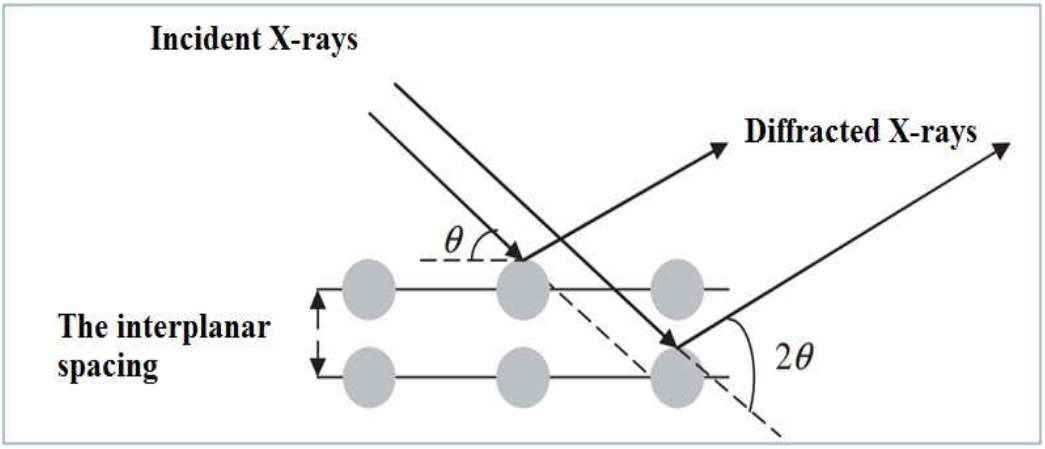

Figure III. 7 The Principle of Bragg Law [39].

In this technique, an X-ray beam is directed on the sample to be analyzed with an angle θ, and recorded the intensity of the ray beam diffracted by the sample depending on the 2θ angle it forms with the X-ray beam incidents as illustrated in Figure III .8 to identify compounds and/or phases is performed by comparing the results obtained with the reference values listed in the standard files JCPDS (Joint Committee for Powder Diffraction Standards).

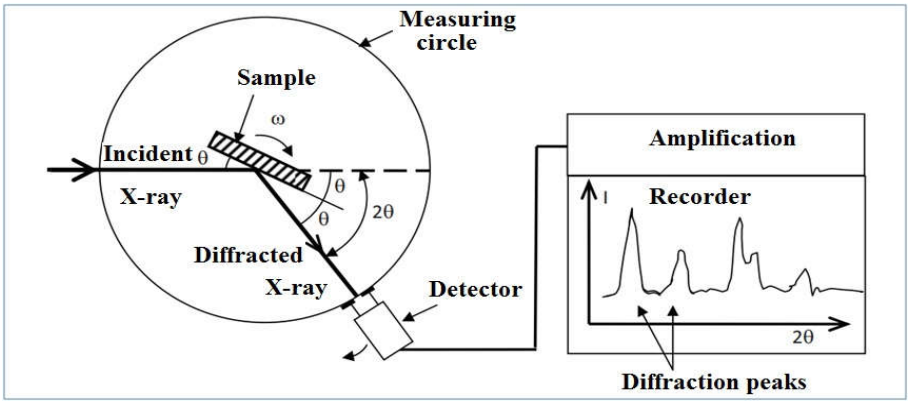

Figure III. 8 Schematic diagram of an X-ray diffractometer [40].

The spectrum of X-ray diffractions makes it possible to know the different characteristics of a crystallized material, the orientation of the crystallites, the crystalline phases (peak position), the strain, the size of the crystallites (D) which can calculated From the width at half height or FWHM (Full Width at Half Maximum) by the Scherrer formula [41]:

$$D = 0.9\lambda/\beta cos\theta \qquad \text{(III.2)}$$

Where: D: is the average crystallite size in nm.

β: is the width at half height (in radian).

θ: is the diffraction angle (in degrees).

λ: is the wavelength of the X-ray beam in Å.

In this work, we used a diffractometer BRUCKER-AX-type D8 (fig III. 9) with a source of Cu-Kα1 radiation has a wavelength of 0.15406 nm, an acceleration voltage of 40 kV and a current of 40 mA.

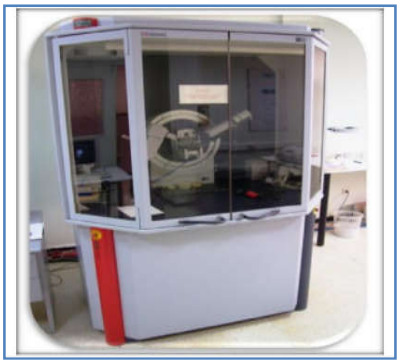

Figure III. 10 Bruckers D8 Advance diffractometer.

III.3.2 Morphological characterization by Atomic Force Microscopy (AFM):

Atomic force microscopy (AFM) is a method that allows us to study topography and physical properties of our samples at the nanoscale, this technique appeared in the 1980s. It is composed as shown in the figure III.10, a flexible lever (cantilever) with a fine tip at the end that scans the surface using a piezoelectric ceramic, a laser diode and a detector for measured cantilever deflection by atomic force however scanning the surface. With this technique, we can obtain images of the surface morphology, roughness and determine the grain size of our samples.

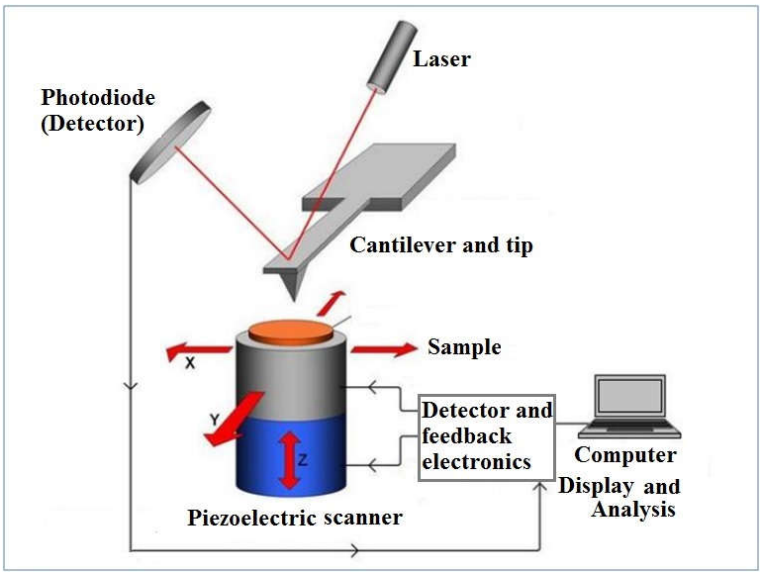

Figure III. 11 Schematic explaining the principle of an atomic force microscope [42].

In AFM we can distinguish three different operating modes:

The contact mode: in this mode, the tip and the surface of the sample are in direct contact and the interaction forces between them are repulsive forces. The disadvantage of this mode is damage to the tip or sample observed because of the increase in frictional forces.

Non-contact mode: this is the case where the tip is at a distance from the surface and the cantilever oscillates at its resonant frequency. In this mode, the interaction forces are only attractive forces.

The tapping mode (or intermittent contact): to avoid the friction forces the tip is located at a distance closer to the surface of the sample and the cantilever oscillates at a frequency close

to the resonance frequency, the interaction between the tip and the surface of the sample vary the characteristics of the oscillation and by measuring this variation we can get the topographic image.

In this work, the morphological properties of the samples were investigated by an atomic force microscope figure III.11 using a silicon nitride tip (Si3N4) under ambient conditions.

Figure III. 12 Photography of the atomic force microscope used.

III.3.3 Optical characterization

UV-Visible spectrophotometry is based on the interaction of electromagnetic radiation and matter in the following spectral domains: Ultraviolet-Visible and Infrared. With this technique, we can obtain certain optical properties of our samples as the curve of the transmittance or absorbance versus wavelengths of the UV-visible spectrum, the determination of the band gap energy (Eg), the optical absorption threshold, the absorption coefficient, the refractive index, and the extinction coefficient...Etc, in our work, we used a double-beam recording spectrophotometer, whose operating principle is shown in Figure III.12.

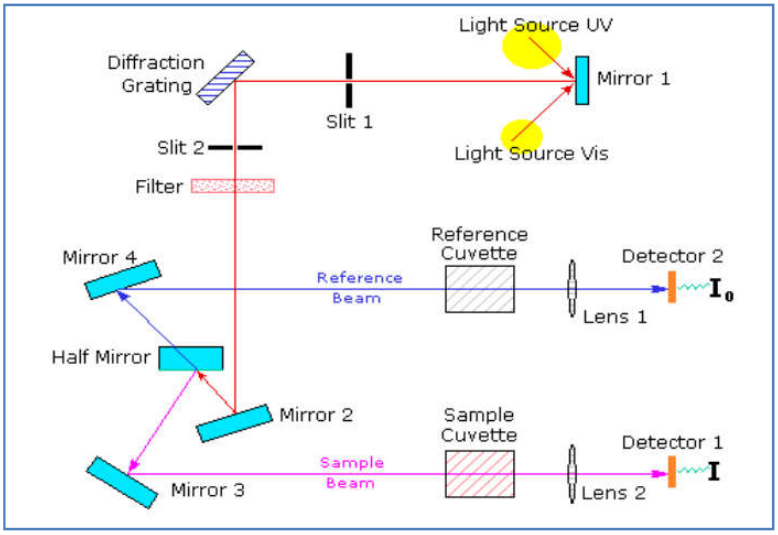

Figure III. 13 Schematic representation of the UV-Visible spectrophotometer.

The optical gap (Eg) is determined by using the Tauc equation [43]:

$$(\propto h\nu) = A(h\nu - Eg)^n \qquad \text{(III.3)}$$

A is a constant, α is the absorption coefficient, hν the energy of a photon and n is a number depends on the nature of optical transition, can obtain the values 1/2, 2, 3 and 3/2 for direct allowed, indirect allowed, direct forbidden and indirect forbidden transitions, respectively. From the plot of $(\propto h\nu)^2$ versus hν, we can estimate the value of optical band gap by extrapolating the linear region to meet hν axis.

If we have a spectrum of transmittance and the thickness d of a thin layer we can determine the absorption coefficient by using the Bouguer-Lambert-Beer formula [44]:

$$T = e^{-\alpha d} \qquad \text{(III.4)}$$

In the case where the transmittance T is expressed in (%), the absorption coefficient is given by:

$$\alpha = \frac{1}{d}\ln\left(\frac{100}{T(\%)}\right) \qquad \text{(III.5)}$$

Where: T is the transmittance, d: the thickness of the layer, α is the absorption coefficient.

In this work, the experimental measurements are carried out using a Visible UV spectrophotometer of the type (JASCO V-630) which shows on the figure III.13.

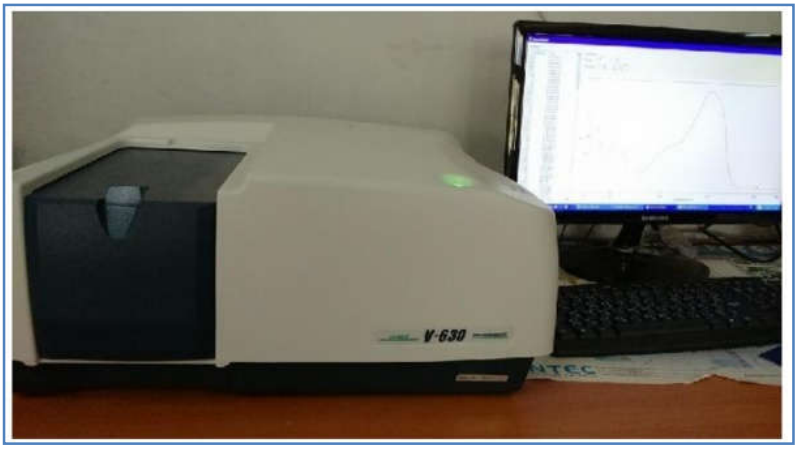

Figure III. 14 UV Visible spectrophotometer (JASCO V-630).

III.4 Photocatalytic, methylene blue dye

The photocatalytic activity of the thin films prepared was evaluated by studying the photodegradation of methylene blue (MB, Figure III.14) as a model pollutant, Table III.2 presented some properties of methylene blue.

Table III. 2 Some Properties of Methylene Blue.

Properties	Chemical Names	Molecular Formula	Molecular Weight (g/mol)	Solubility in water (g / l) at 20 ° C	Melting point (° C)
	Methylene blue, Methylthioninium chloride	C16H18N3ClS	319,85	40	190

Photocatalytic experiments were performed at room temperature, under solar irradiation, in sunny days of November from 9 AM to 2 PM at the Laboratory of active components and materials (Larbi Ben M'hidi University, Oum El Bouaghi, Algeria).

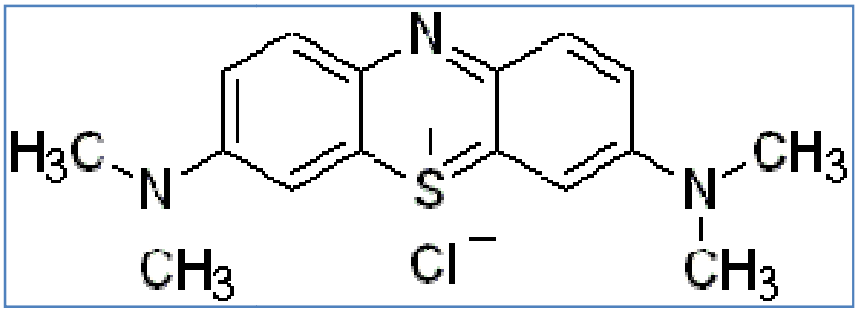

Figure III. 15 Chemical structure of methylene blue.

An aqueous solution of MB (8 mg /l) prepared by dissolving BM dye in water, the suspension was stirred in the dark for 30 minutes to achieve adsorption equilibrium, each sample was immersed in 30 ml of aqueous solution of BM and after each irradiation time interval, 3 ml of solution was extracted for measuring the concentration of MB by a spectrophotometer, the absorbance measurements were carried out at the using a UV-visible spectrophotometer type JASCO V-750 by measuring the absorbance peak of the dye at 662 nm.

The degradation efficiency was calculated using the following equation:

$$\text{Degradation rate (\%)} = \frac{C_0 - C_t}{C_0} \times 100 \qquad \text{(III.6)}$$

Where: C_0 is the initial concentration of MB (mg/l) and C_t is the concentration of MB after time t of irradiation (mg/l).

III.5 References

[1] J. Livage and D. Ganguli, “Sol-gel electrochromic coatings and devices : A review,” Solar Energy Materials and Solar Cells, vol. 68. 3-4, pp. 365-381, 2001.

[2] Znaidi, Lamia. "Sol–gel-deposited ZnO thin films: A review." Materials Science and Engineering: B, vol. 174.1-3, pp. 18-30, 2010.

[3] T. Saidani, , M. Zaabat, M. S. Aida, R. Barille, M. Rasheed, and Y. Almohamed. "Influence of precursor source on sol–gel deposited ZnO thin films properties." Journal of Materials Science: Materials in Electronics, vol. 28. 13, pp. 9252-9257, 2017.

[4] M. Soylu, , and M. Coskun. "Controlling the properties of ZnO thin films by varying precursor concentration." Journal of Alloys and Compounds, vol. 741,pp. 957-968, 2018.

[5] L. Xu, G. Zheng, J. Miao, and F. Xian, "Applied Surface Science Dependence of structural and optical properties of sol – gel derived ZnO thin films on sol concentration," Appl. Surf. Sci., vol. 258. 19, pp. 7760–7765, 2012.

[6] M. Dutta, S. Mridha, and D. Basak. "Effect of sol concentration on the properties of ZnO thin films prepared by sol–gel technique." Applied Surface Science, vol. 254.9, pp. 2743-2747, 2008.

[7] J. Liu, X. Zhao, and L. Duan, "Effect of solution concentration on the structural , optical and conductive properties of ZnO thin films prepared by sol – gel method," Journal of Materials Science: Materials in Electronics, vol. 24.12, pp. 4932–4937, 2013.

[8] S. Ashikin, K. K. Chan, H. Y. Mohd, Z. Sahdan, H. Saim, and D. Knipp, "Zinc oxide films prepared by sol – gel spin coating technique," Applied Physics A, vol. 104.1, pp. 263–268, 2011.

[9] Xu, Dong, Qian Yu, Taiyun Chen, Sujuan Zhong, Jia Ma, Li Bao, Lei Zhang, Feiwen Zhao, and Sanming Du. "Effects of PEG1000 and Sol Concentration on the Structural and Optical Properties of Sol–Gel ZnO Porous Thin Films." Materials, vol. 11.10, pp. 1840, 2018.

[10] N. Nagayasamy, S. Gandhimathination, and V. Veerasamy, "The Effect of ZnO Thin Film and Its Structural and Optical Properties Prepared by Sol-Gel Spin Coating Method," Open Journal of Metal, vol. 3.02, pp. 8–11, 2013.

[11] Aryanto, D., W. N. Jannah, T. Sudiro, A. S. Wismogroho, P. Sebayang, and P. Marwoto. "Preparation and structural characterization of ZnO thin films by sol-gel method." In Journal of Physics: Conference Series, vol. 817.1, pp. 012025, 2017.

[12] R. Amari, A. Mahroug, A. Boukhari, B. Deghfel, and N. Selmi, "Structural , Optical and Luminescence Properties of ZnO Thin Films Prepared by Sol-Gel Spin-Coating

Method : Effect of Precursor Concentration," Chinese Physics Letters , vol. 35.1, pp. 1–5, 2018.

[13] E. Hosono, S. Fujihara, T. Kimura, and H. Imai, "Non-Basic Solution Routes to Prepare ZnO Nanoparticles," Journal of Sol-Gel Science and Technology, vol. 4, pp. 71–79, 2004.

[14] C. Tsay, K. Fan, Y. Wang, C. Chang, Y. Tseng, and C. Lin, "Transparent semiconductor zinc oxide thin films deposited on glass substrates by sol – gel process," Ceram. Int., vol. 36, no. 6, pp. 1791–1795, 2010.

[15] C. Boukaous, A. Telia, D. Horwat, M. S. Aida, and B. Boudine, "Effect of Solvents on the Properties of ZnO Thin Layers Obtained by Sol Gel Influence of solvent on humidity sensing of sol-gel deposited ZnO thin films," Journal of New Technology and Materials, vol. 277.1747, pp. 1-5, 2014.

[16] P. B. Khoza, M. J. Moloto, and L. M. Sikhwivhilu, "The Effect of Solvents , Acetone , Water , and Ethanol , on the Morphological and Optical Properties of ZnO Nanoparticles Prepared by Microwave," Journal of Nanotechnology, 2012.

[17] P. H. Vajargah, H. Abdizadeh, R. Ebrahimifard, and M. R. Golobostanfard, "Applied Surface Science Sol – gel derived ZnO thin films : Effect of amino-additives," Appl. Surf. Sci., vol. 285, pp. 732–743, 2013.

[18] G. El Hallani, N. Fazouan, A. Liba, and M. Khuili, "The effect of sol aging time on Structural and Optical properties of sol gel ZnO doped Al," In Journal of Physics: Conference Series, vol. 758.1, pp. 012021, 2016.

[19] Marouf Sara, Abdelkrim Beniaiche, Hocine Guessas, and Amor Azizi. "Morphological, structural and optical properties of ZnO thin films deposited by dip coating method." Materials Research, vol. 20.1, pp. 88-95, 2017.

[20] Y. Li, L. Xu, X. Li, X. Shen, and A. Wang, "Effect of aging time of ZnO sol on the structural and optical properties of ZnO thin films prepared by sol–gel method," Appl. Surf. Sci., vol. 256, pp. 4543–4547, 2010.

[21] N. Kaneva, A. Bojinova, and K. Papazova, "Effect of Precursors Aging Time on the Photocatalytic Activity of ZnO Thin Films," World Academy of Science, Engineering

and Technology, International Journal of Chemical, Molecular, Nuclear, Materials and Metallurgical Engineering, vol. 9.3, pp. 406–411, 2015.

[22] F. J. Serrao, S. M. Dharmaprakash, F. J. Serrao, and S. M. Dharmaprakash, "Sol ageing effect on the structural , optical and electrical properties of Ga-doped ZnO thin films," Materials Technology, vol. 31.8, pp. 443-447, 2016.

[23] El Hallani Ghizlan, Nejma Fazouan, Ahmed Liba, and Larbi Laanab. "Structural and optical properties of ZnO thin films prepared by spin coating method." 2014 International Renewable and Sustainable Energy Conference (IRSEC), pp. 82-84. IEEE, 2014.

[24] S. Ong, C. Li, Y. Li, Y. Wu, and R. Loutfy, "Stable , solution-processed , high-mobility zno thin-film transistors," Journal of the American Chemical Society, vol. 129.10, pp. 2750-2751, 2007.

[25] Z. Ng, K. Chan, and T. Tohsophon, "Effects of annealing temperature on ZnO and AZO films prepared by sol – gel technique Applied Surface Science Effects of annealing temperature on ZnO and AZO films prepared by sol – gel technique," Appl. Surf. Sci, vol. 258, no. 24, pp. 9604–9609, 2012.

[26] J. Sengupta, R. K. Sahoo, K. K. Bardhan, and C. D. Mukherjee, "Influence of annealing temperature on the structural , topographical and optical properties of sol – gel derived ZnO thin films," Materials Letters, vol. 65, pp. 2572–2574, 2011.

[27] Li, Hongxia, Jiyang Wang, Hong Liu, Huaijin Zhang, and Xia Li. "Zinc oxide films prepared by sol–gel method." Journal of Crystal Growth, vol. 275.1-2, pp. e943-e946, 2005.

[28] M. Jun and J. Koh, "Effects of annealing temperature on properties of al-doped zno thin films prepared by sol-gel dip-coating," Journal of Electrical Engineering and Technology, vol. 8.1, pp. 163–167, 2013.

[29] E. M., S. Benramache, B. Benhaoua, N. Khechai, and F. Chabane, "Matériaux Elaboration and characterisation of ZnO thin films," Nanomaterials, vol. 580, pp. 573–580, 2012.

[30] T. Ivanova, A. Harizanova, T. Koutzarova, and B. Vertruyen, “Study of ZnO sol – gel fi lms : Effect of annealing,” Materials letters, vol. 64, pp. 1147–1149, 2010.

[31] M. Saleem, L. Fang, Q. L. Huang, D. C. Li, F. Wu, H. B. Ruan, and C. Y. Kong. "Annealing treatment of ZnO thin films deposited by sol–gel method." Surface Review and Letters, vol. 19.05, pp. 1250055, 2012.

[32] E. Bingöl, F. Bozali, E. F. Keskenler, and V. Nevruzoğlu, “Influence of substrate type on morphology and photoluminescence properties of ZnO thin films prepared by ultrasonic spray pyrolysis method,” J. Mater, vol.1, pp. 19-24, 2016.

[33] R. A. Kadir, N. M. Taib, W. Rosmaria, and W. Ahmad, “Effect of substrates on Zinc Oxide thin films fabrication using sol-gel method Effect of substrates on Zinc Oxide thin films fabrication using sol-gel method,” In IOP Conference Series: Mater. Sci. and Eng., vol. 340.1, p. 012002, 2018.

[34] S. D. L. Z. Nanoparticles, “Effect of film thickness on structural , electrical , and optical properties of sol-gel deposited layer-by-layer zno nanoparticles,” Transactions on Electrical and Electronic Materials, vol. 13.2, pp. 102-105, 2012.

[35] T. Ganesh, , K. Perumal, R. Kumar, and N. Bhaskar. "Effect of thickness on micro-structural and optical properties of al-doped zno films prepared by sol-gel spin coating," In Nano Hybrids and Composites, vol. 17, pp. 171-178. Trans Tech Publications, 2017.

[36] W. Chebil *et al*., “Comparison of ZnO thin films on different substrates obtained by sol-gel process and deposited by spin-coating technique,” Indian Journal of Pure & Applied Physics (IJPAP), vol. 53, pp. 521–529, 2015.

[37] S. Aydemir, “Effects of withdrawal speed on the microstructural and optical properties of sol-gel grown ZnO:Al thin films,” Vacuum, vol. 120, pp. 51–58, 2015.

[38] G. Turgut, E. Sonmez, and S. Duman, “Determination of certain sol-gel growth parameters of nickel oxide films,” Ceram. Int., vol. 41, no. 2, pp. 2976–2989, 2015.

[39] Liu YANG , thèse de Doctorat , Caractérisation de couches minces de ZnO élaborées par la pulvérisation cathodique en continu , Université du Littoral côte d’Opale , 2012.

[40] Tayeb Brouri, thèse de Doctorat, Élaboration et étude des propriétés électriques de couches minces et de nanofils de ZnO, Université Paris-Est , 2011.

[41] A. Hamrouni, N. Moussa, F. Parrino, A. Di, A. Houas, and L. Palmisano, "Sol – gel synthesis and photocatalytic activity of ZnO – SnO_2 nanocomposites," Journal of Molecular Catalysis A: Chemical, vol. 390, pp. 133–141, 2014.

[42] Younes Mouchaal, thèse de Doctorat, Elaboration et étude de nouvelles électrodes transparentes substituts de l'ITO dans les dispositifs optoélectroniques, Université d'Oran 1 Ahmed Ben Bella, 2016.

[43] A. A. Al-Ghamdi, M. S. Abdel-Wahab, A. A. Farghali, and P. M. Z. Hasan, "Structural, optical and photo-catalytic activity of nanocrystalline NiO thin films," Mater. Res. Bull, vol. 75, pp. 71–77, 2016.

[44] L. Herissi, L. Hadjeris, M. S. Aida, and J. Bougdira, "Properties of (NiO)1- x (ZnO) x thin films deposited by spray pyrolysis," Thin Solid Films , vol. 605, pp. 116–120, 2016.

CHAPTER 4
Results and discussion

IV Introduction

TCOs properties can be enhanced by different parameters as mentioned in chapter 1, in this chapter we will discuss the results of three parameters that affect the properties of TCOs thin films. The first section is the effect of withdrawal speed on the properties of NiO thin films (effect of deposition method), the second section is the effect of silver doping on the properties of ZnO thin films (the effect of doping), the last section is about the fabrication of NiO/ZnO heterostructure (coupling two materials). The different properties in the three sections were investigated in addition to the photocatalysis application of the NiO/ZnO heterostructure.

IV.1 Effect of withdrawal speed on the properties of NiO thin films

In order to study the effect of withdrawal speed which is one of the main parameters that affect the quality of the thin films prepared via dip-coating method, NiO thin films were prepared as described in the previous chapter with different withdrawal speeds 30, 50 and 70 mm/min. Their structural, optical and morphological properties were investigated using X-ray diffraction (XRD), spectrophotometer and atomic force microscopy, respectively.

IV.1.1 Structural properties

Figure IV.1 shows the X-ray diffraction patterns of NiO thin films deposited on glass substrates by the sol-gel dip-coating method with different withdrawal speeds (30, 50, 70 mm/min). The main characteristic peaks observed are related to the planes (111), (200) and (220). These diffraction peaks are in good agreement with the JCPDS card (04-0835) and showed that all the films have a single-phase NiO with a cubic structure (bunsenite, NaCl-type structure) with (200) plane as the preferred orientation without the existence of any impurities.

From the diffraction patterns, we can observe that the peaks became broader and their intensity decrease when the withdrawal speed increase. This observation indicates that the crystallinity is deteriorated with the increase of withdrawal speed.

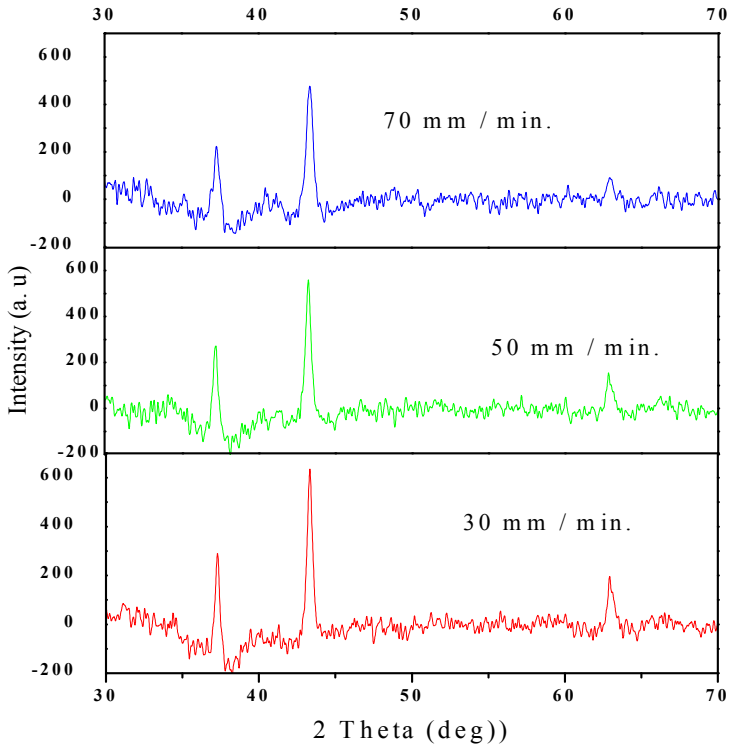

Figure IV. 1 X-ray diffraction patterns of NiO thin films prepared with different withdrawal speeds.

The crystallite size (D) of the prepared films was calculated from the full width at half maximum (FWHM) of the diffraction peaks using Scherrer's formula (III.2). The calculated structural parameters are given in Table IV.1.

Table IV. 1 Calculated structural parameters of NiO films prepared with different withdrawal speeds.

Withdrawal speed (mm/min)	FWHM (200) (rad)	Position 2θ (200) (degree)	Crystallite size (D) (nm)	Intensity (a. u)
30	0.006120	43.326	24	815.16
50	0.006415	43.280	22.98	674.54
70	0.007159	43.361	20.59	534.73

As can be seen from in Table IV.1, the withdrawal speed has a significant impact on the structural properties of the prepared films; this impact can be noticed by the decrease in the intensity of the (200) peak and the increase of the FWHM as the withdrawal speed increased and that's why the grain size was observed to decrease. The reasonable explanation might be that the films became thicker at higher withdrawal speed because the solvent on the substrate has less time to draw back into the beaker unlike the low withdrawal speeds, hence the drying stage may not be complete in the case of thicker films because it became more difficult to evaporate all the solvent. Adding another coating layer on a not well-dried layer could also disturb the oriented crystal growth. However, Sajilal *et al.* [1] reported that an increase in thickness may improve the crystallinity but to a given value (0.483 µm). Further increase of the thickness at about of 0.513 µm leads to a decrease in the film crystallinity and the films became totally amorphous.

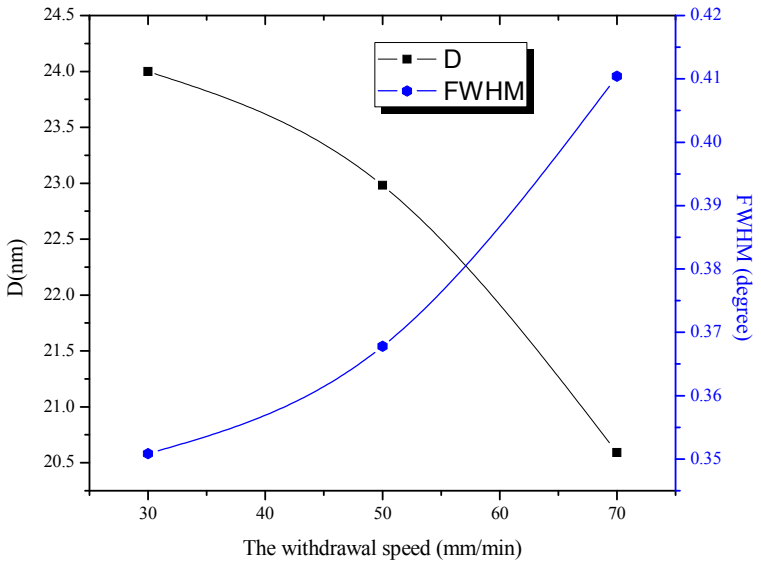

Figure IV. 2 The variation of crystallite size (D) and the full width at half maximum (FWHM) as a function of withdrawal speed.

Figure IV.2 shows the variation of crystallite size (D) and the full width at half maximum (FWHM) as a function of withdrawal speed for the (200) peak. It was clearly seen that the grain size was influenced by the withdrawal speed, the grain sizes of the films decrease from 24.0 to 20.6 nm when the withdrawal speeds increase from 30 to 70 mm/min, this decreasing

of the grain size proves the presumption above and it can be said that increasing the withdrawal speed deteriorates the quality of film crystallization.

The interplanar spacing (d_{hkl}) values and lattice parameter "a" of NiO films prepared with different withdrawal speeds are calculated for (200) plan using the equations (1) and (2):

$$2d_{hkl} \sin \theta = n\lambda \quad \text{(IV.1)}$$

$$a = d\,(h^2+k^2+l^2)^{1/2} \quad \text{(IV.2)}$$

Where n is the order of diffraction (usually n=1) and λ is the X-ray wavelength, θ is the diffraction angle and d is the interplanar spacing of the atomic planes whose Miller indices are (hkl). The unit cell volume is calculated by $V = (a)^3$ $Å^3$. Furthermore, other microstructural parameters such as strain and dislocation density are listed in table IV.2.

Table IV. 2 Microstructural parameters of NiO films prepared with different withdrawal speeds.

WS (mm/min)	d_{200} (Å)	a (Å)	Volume of unit cell ($Å^3$)	ε (10^{-4})	Dislocation density (lines/m^2)*10^{14}
30	2.0866	4.1733	72.6840	14.2210	17.3611
50	2.0887	4.1775	72.9048	14.9092	18.9365
70	2.0850	4.1700	72.5166	16.6326	23.5877

As shown in table IV.2, the interplanar spacing (d) and lattice parameter (a) are in a good agreement with cubic NiO (JCPDS Card No. 04-0835) (fig IV.3). In addition, Table IV.2 clearly shows that with increasing the withdrawal speed, an increase in strain is associated with an increase in dislocation density. These results confirm the deterioration of crystalline quality as said before. The strain in NiO thin films is mainly due to the difference between lattice constant of the films and the substrate and also to the combined effect of thickness and dynamics of the deposition [2].

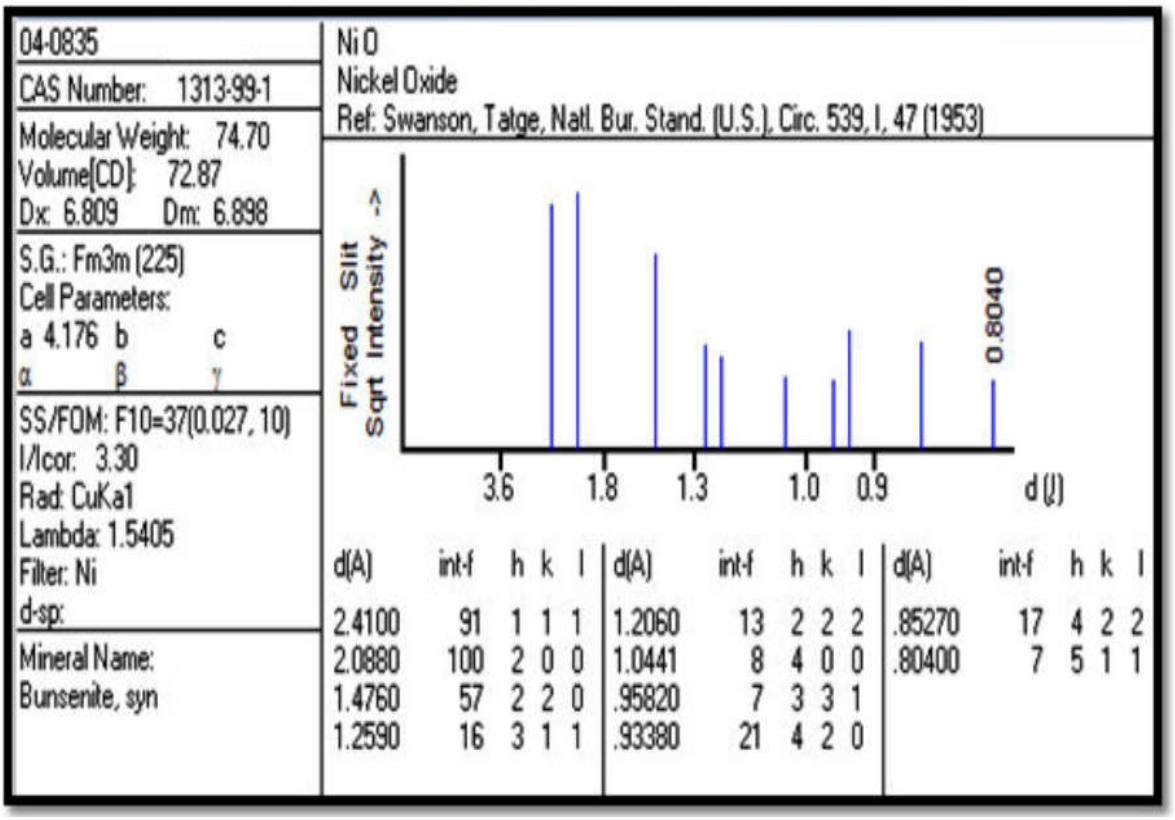

Figure IV. 3 (JCPDS) card number 04-0835.

IV.1.2 Morphological Analysis by Atomic Force Microscope (AFM)

The morphological properties of the films were examined by atomic force microscopy. Figure IV.4 shows two-dimensional (2D) atomic force microscopy images of NiO thin films prepared with different withdrawal speeds. It is clearly observed that all films have a uniform and dense NiO grains. Thin NiO layers became denser as the withdrawal speed increased. This is logical because the particle size decrease in this case.

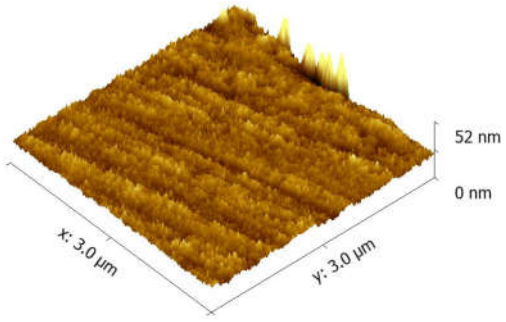

30mm/min

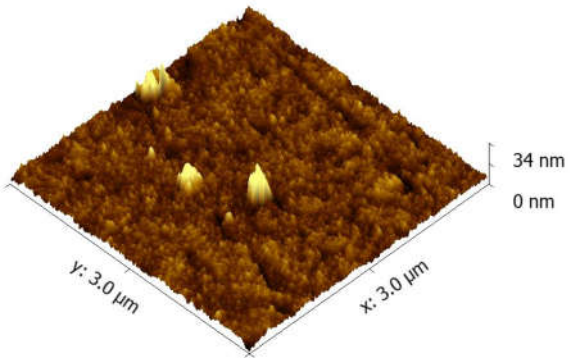

50mm/min

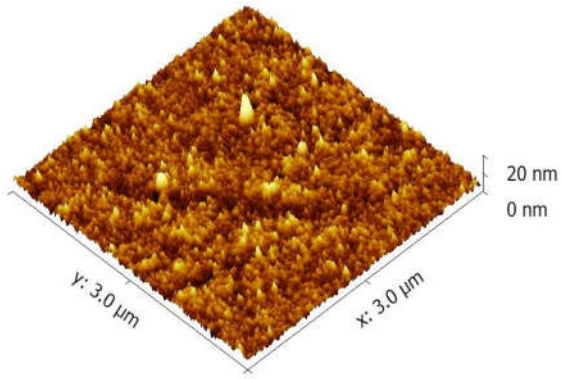

70mm/min

Figure IV. 4 AFM image of NiO thin film deposited with different withdrawal speeds.

In order to know the effect of withdrawal speed on the surface morphology of the films, Gwyddion analysis software was used to calculate the root mean square. RMS was found to increase due to the increase in withdrawal speed. It was found to be 3.78, 10.02 and 15 nm for withdrawal speeds of 30, 50 and 70 mm / min, respectively. This can be attributed to the effect of withdrawal speed on film thickness.

IV.1.3 Estimation of films thickness

The thickness of the deposited films is calculated by the weight difference method. In this method, we measure the mass of the film (we weigh the substrate before applying the film and its weight after application) and use the formula.

$$d = m/A\rho \qquad \text{(IV.3)}$$

Where m: the mass of the film; A: the film surface; ρ: density of the film material.

The obtained estimated thickness using this formula is not very accurate because the density of the bulk material and the thin film is different.

The thickness of the samples was found to be at about 154, 170 and 250 nm for withdrawal speeds of 30, 50 and 70 mm/min, respectively. In fact, the relationship between thickness and withdrawal speed is a direct relationship. As the withdrawal speed increases, the film thickness also increases because a faster withdrawal speed causes more liquid to rise onto the surface of the substrate before it has time to draw back to the solution. Thickness is also affected by fluid viscosity, fluid density, and surface tension.

IV.1.4 Optical properties

The Spectra of optical transmission in the 200-1000 nm wavelength range of nickel oxide thin films prepared by different withdrawal speeds of 30, 50 and 70 mm/min is shown in figure IV.5. As can be seen, the thin films have high transparency and no interference fringes because of their small thickness.

The curves showed that the transmittance of thin layers decreases with increasing withdrawal speeds. This decrease in the transmittance of thin films can be due to an increase in the thickness of the thin layers and by the increase of the surface roughness which leads to more optical scattering.

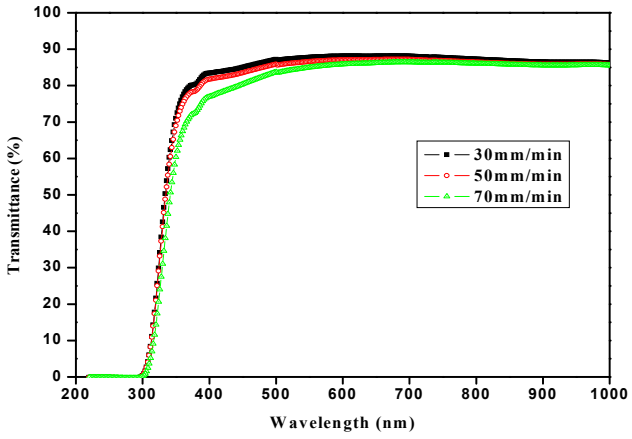

Figure IV. 5 Transmittance spectra of NiO thin film prepared with different withdrawal speeds.

The optical band gap for the prepared films was obtained using the Tauc equation (eq. III.3), Eg was estimated from the plot of the curve $(\propto h\nu)^2$as a function of hν and then extrapolated to $\propto h\nu = 0$ (fig IV.6).

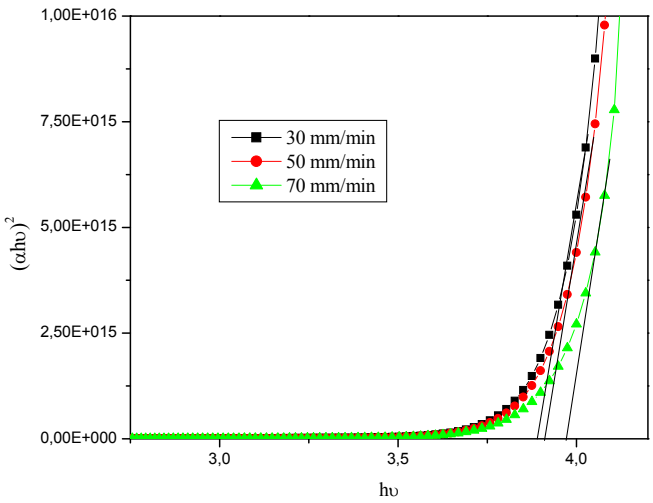

Figure IV. 6 Determination of the optical band gap for NiO thin film deposited with different withdrawal speeds.

The obtained values of the optical band gap are 3.88, 3.91 and 3.97 eV for the withdrawal speeds 30, 50 and 70 mm/min, respectively. This increase in Eg is mainly due to the increase in carrier concentration.

IV.1.5 Comparison of the withdrawal effect on ZnO and NiO

Table IV. 3 Comparison between our thin layers of NiO and ZnO: Al [3] prepared by sol-gel dip-coating at different withdrawal speeds:

	NiO thin films (200)			ZnO:Al thin films (101)		
Withdrawal speed (WS) mm/min	30	50	70	20	40	80
FWHM (degree)	0.35087	0.36779	0.41042	0.271	0.158	0.183
Position 2θ (degree)	43.326	43.280	43.361	31.84	34.63	36.37

Crystallite size(D) (nm)	24.00	22.98	20.59	26	16	10
RMS (nm)	3.78	10.02	15	25	47	56
film thickness (nm) ±5%	154	170	250	90	115	210
Optical band gap Eg (eV)	3.88	3.91	3.97	3.20	3.25	3.27

As we can see in the table IV.3, when the WS has been increased, the crystallite size of ZnO:Al and NiO has decreased, indicating that WS decreases crystalline quality, we also notice that the position of peaks is slightly shifted towards a higher angle in the case of ZnO:Al. However, NiO remains the same and that indicates that the WS affects the preferred orientation in ZnO:Al and not in NiO.

For the morphological and optical properties, it can be said that the WS affects in the same way either ZnO:Al or NiO when WS increases; roughness, film thickness and the optical gap are all observed to be increased.

IV.2 Ag-doped ZnO thin films prepared by sol-gel dip-coating method

Pure and Ag-doped ZnO thin films were prepared by sol-gel dip-coating method using zinc acetate dehydrate ($Zn(CH_3COO)_2 \cdot 2H_2O$), silver nitrate ($AgNO_3$), ethanol and monoethanolamine (MEA) as a precursor, doping source, solvent, and stabilizer, respectively.

The mixtures of a 0.1 M of ZnO solution with different Ag concentration (0, 1, 3, and 5 wt %) were vigorously stirred at 60 °C for 2 h. After stirring the solution for about 15 min, monoethanolamine (MEA) was added dropwise into the solution, this process ending by achieving a transparent and homogenous solution which was aged at room temperature for 24 h prior the deposition process.

Clean glass slides were used as substrates, the thin films were deposited at a withdrawal speed of 100 mm/min using dip-coating method. After each deposited layer, the samples were dried at 250 °C for 5 min to evaporate the solvent and organic residuals, This process was repeated 15 times in order to obtain the desired thickness. Afterward, the obtained thin films were annealed in air at 500 °C for 2 h.

The properties of the prepared thin films were investigated using different characterization instruments such as; Bruker diffractometer (XRD), spectrophotometer, atomic force microscopy and FTIR spectrophotometer.

IV.2.1 Structural properties

The XRD patterns of Ag-doped ZnO thin films with different Ag contents (0, 1, 3, 5) fabricated by sol-gel dip-coating method on glass substrates are shown in fig IV.7. As can be seen, all the film show eight pronounced diffraction peaks corresponding to the reflections of the (100), (002), (101), (102), (110), (103), (112) and (201) planes and that depicts the clear presence of crystalline ZnO with the hexagonal wurtzite structure with (101) as preferential orientation, no other crystallized phases are observed which indicating the incorporation of Ag in the ZnO lattice.

Despite the fact that the diffraction peaks became higher and sharper with the increase of the Ag content, as shown in table IV.4, the crystallinity of the thin films was found to be deteriorated with the increase of Ag doping and that attributed to the shift of diffraction peak (101) toward higher 2θ, fig IV.8. This shift was suggested by previous report to the substitution incorporation of Ag species into the ZnO lattice [4].

Table IV. 4 Different structural parameters of pure and Ag-doped ZnO thin films for (101) peak

	2θ (^{o})	Int (a. u)	FWHM (rad)	D (nm)
Pure	36.16	46.43	0.01167	12.49767
1Ag-ZnO	36.21	47.90	0.01223	11.92886
3Ag-ZnO	36.25	51.71	0.01212	12.03322
5Ag-ZnO	36.22	52.40	0.01266	11.51842

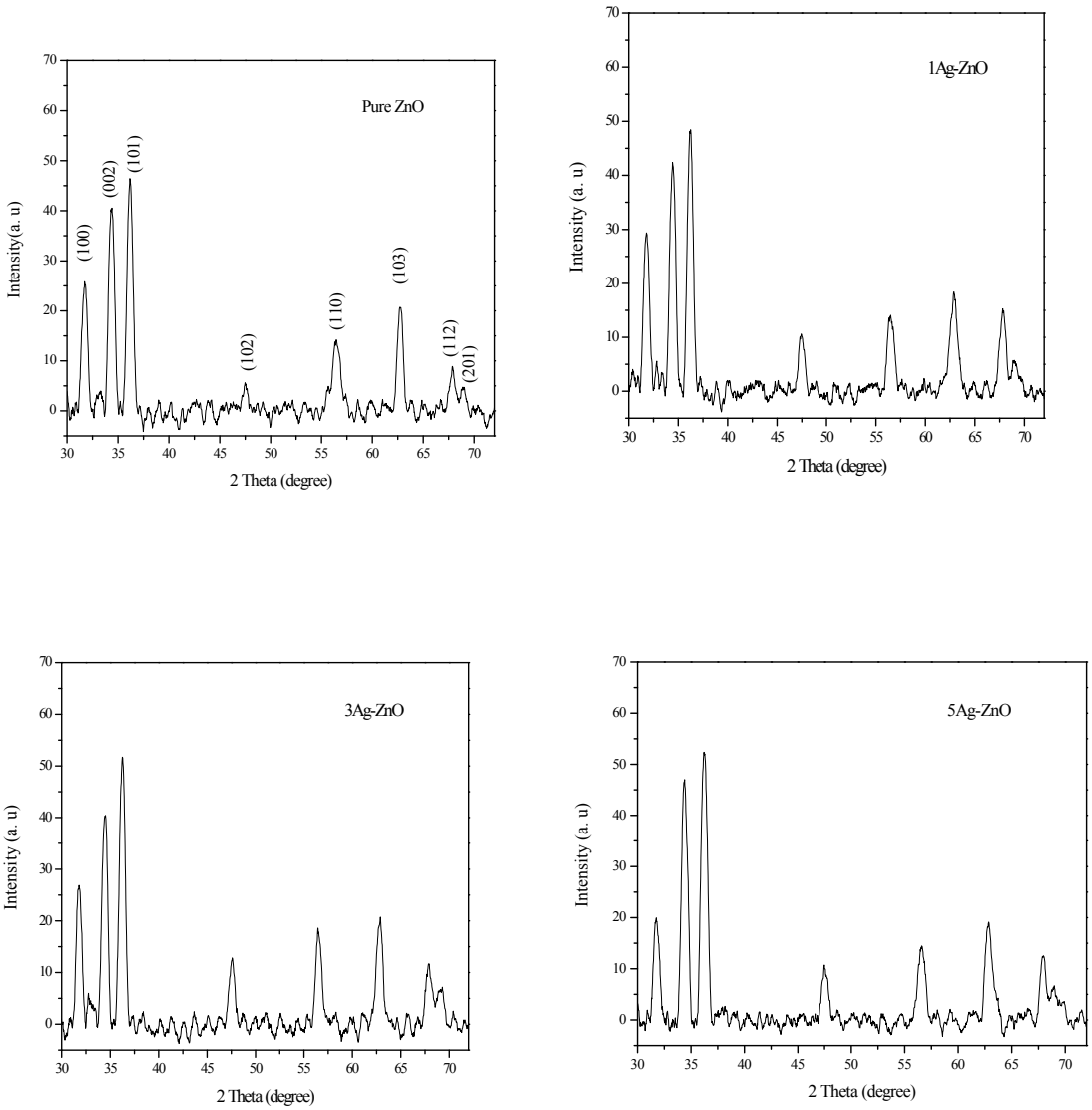

Figure IV. 7 XRD patterns of Ag-doped ZnO thin films (0, 1, 3, 5) prepared by sol-gel method

The crystallite size of pure and Ag-doped ZnO thin films was determined using the (FWHM) of the (1 0 1) diffraction peak using Debye–Scherrer's formula:

$$D=0.94\lambda/\beta\cos\theta \qquad \text{(IV.4)}$$

Where:

λ: the X-ray wavelength of 1.54 Å, β: the full width at half maximum (FWHM), θ : the Bragg diffraction angle.

The different structural parameters are given in table IV.4. It can be said that the crystallite size decreased by increasing of the silver amount, which confirms the deterioration of the crystallinity, this decreasing is linked to the lattice strain between the crystallite of the Ag-doped ZnO thin films and glass substrate [5].

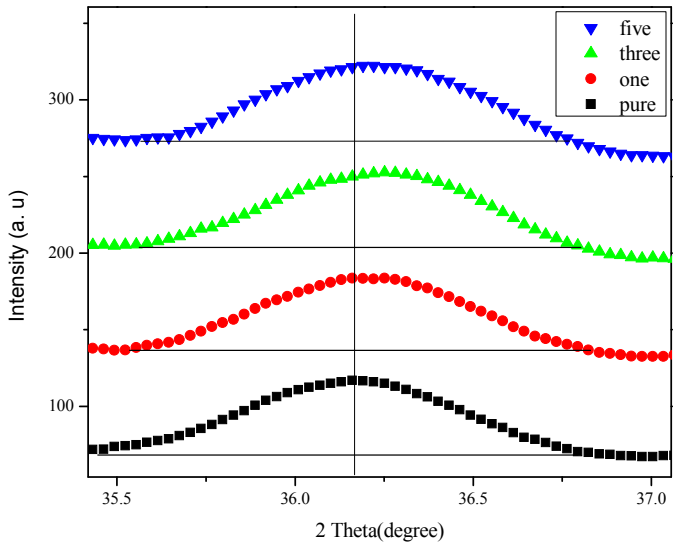

Figure IV. 8 Magnified the region of (101) peak showing the shift to higher 2θ as the Ag content increase

Figure IV.9 shows the variation of crystallite size (D) and the full width at half maximum (FWHM) as function of Ag doping content for the (101) peak, we can observe that the crystallite size decrease from 12.49 to 11.51 nm with the increase of Ag amount from 0 to 5 wt%. The absence of any Ag-related peak indicating that the silver ions occupy its position in ZnO lattice by substitution Zn^{2+} ions sites and that resulting in the disturbing of the crystal structure because of high difference in ionic radii between Ag^{+} and Zn^{2+}.

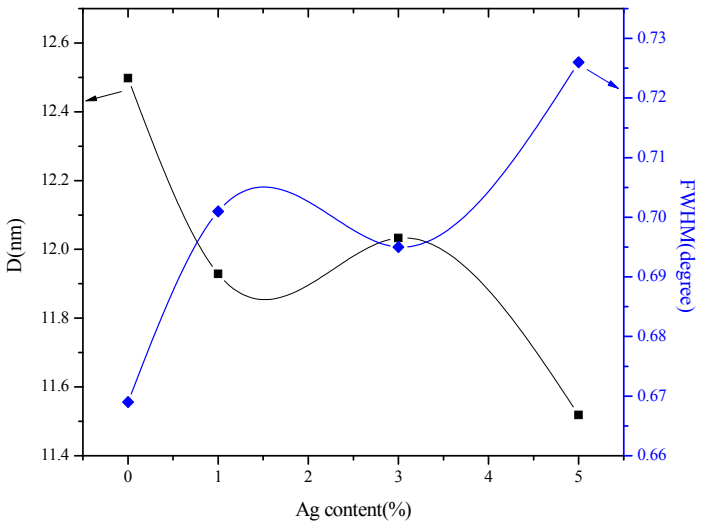

Figure IV. 9 The variation of crystallite size (D) and the full width at half maximum (FWHM) as a function of Ag doping content.

The interplanar spacing (d_{hkl}) values of pure and Ag-doped ZnO thin films were also calculated by using the Bragg equation as follows:

$$2d_{hkl} \sin\theta = n\lambda \qquad \text{(IV.1)}$$

Where n is the order of diffraction (usually n=1) and λ is the X-ray wavelength. In the ZnO hexagonal structure, the plane spacing is related to the lattice constants a, c and the Miller indices by the following equation:

$$\frac{1}{d^2} = \frac{4}{3}\left[\frac{h^2+hk+k^2}{a^2}\right] + \frac{l^2}{c^2} \qquad \text{(IV.5)}$$

The lattice parameters (a and c) for the hexagonal pure and Ag-doped ZnO are calculated via (002) and (101) orientations and presented in table IV.5 which also summarizes the calculated values of the interplanar spacing d_{hkl} of the thin films.

Table IV. 5 Interplanar spacing d_{hkl} and lattice parameters of pure and Ag-doped ZnO thin films.

	d_{002} (Å)	d_{101} (Å)	a (Å)	c (Å)	c/a (Å)
Pure ZnO	2.61002	2.48202	3.25781	5.22004	1.60231
1Ag-ZnO	2.6034	2.4787	3.25461	5.2068	1.59982
3Ag-ZnO	2.6012	2.47606	3.25093	5.2024	1.60028
5Ag-ZnO	2.60634	2.47804	3.25241	5.21267	1.60271

From table IV.5, it can be seen that the interplanar spacing (d_{hkl}) values decreases for film prepared using 3% then increase with Ag content. This phenomenon indicates that the Ag element is introduced into the ZnO matrix [6].

The dislocation density (δ), defined as the length of dislocation lines per unit volume, the dislocation density is evaluated using the equation:

$$\delta = 1/D^2 \quad \text{(IV.6)}$$

Due to the lattice mismatch between Ag-doped ZnO thin film and glass substrate, some stress and strain can be generated during deposition. Hence, the stress and strain modify the structural properties of Ag-doped ZnO thin films, the mean strain can be calculated by the following formula:

$$\varepsilon = \beta\cos\theta/4 \quad \text{(IV.7)}$$

Where: β is the full width at half maximum of (101) peak and θ is the Bragg angle. As can be seen from table IV.6, the microstrain increases from 27.73×10^{-4} to 30.03×10^{-4} when the silver concentration increase from 0 to 5Wt%, this increment may be the cause of the broadening of diffraction peaks [7]. In addition, the increase of the dislocation density with the increase of Ag concentration confirms the distortion of the crystalline structure and that match the results found above. Furthermore, the volume of ZnO unit cell decreases as Ag amount is added which implies that Ag is dissolved into the ZnO lattice as described by S.-T. Kuo *et al.* [8], however, they declared that the level of substitution of Zn^{2+} by Ag^{+} is expected to be quite low—about 0.08 mol% or slightly higher and that because of the difference

between Zn^{2+} and Ag^{+} ions radius and most of tend to segregate at the grain boundaries of ZnO.

Table IV. 6 Dislocation density, strain and volume of unit cell of pure and Ag-doped ZnO thin films.

	ε (10^{-4})	**Dislocation density (lines/m^2)*10^{14}**	**Volume of unit cell ($Å^3$)**
Pure	27.73525	64.02387	47.97807
1Ag-ZnO	29.05776	70.27517	47.76237
3Ag-ZnO	28.80675	69.06155	47.6141
5Ag-ZnO	30.0932	75.37274	47.75177

IV.2.2 Structural properties of Ag-doped ZnO nanopowders

Pure and Ag-doped Zinc oxide Nanopowders were synthesized by the sol-gel method by adding KOH to the previously prepared solution (after finish the dip-coating deposition), the resulting Nanopowders were treated in air at 500 °C for 2 h. Figure IV.10 shows the XRD patterns of pure and Ag-doped ZnO Nanopowders, it can be seen diffraction peaks corresponding to the reflections of the (100), (002), (101), (102), (110), (103),(200), (112) and (201) planes for pure and Ag-doped ZnO samples belonging to ZnO hexagonal wurtzite structure with (101) as a preferential orientation. In addition to Ag peaks (marked with *) corresponding to the reflection from (111), (200) and (202) crystal planes of the face-centered-cubic (fcc) metallic Ag. The XRD patterns of Ag-doped ZnO shows two peaks of Ag for the doping with 1 and 3Wt% and one more peak for doping with 5Wt%, the intensity of those peaks increase with doping which is logical because of the formation of much more Ag particles when doping increased.

Table IV. 7 Different structural parameters of pure and Ag-doped ZnO nanopowders.

	ZnO(101) 2θ (^{o})	2θAg (111) (^{o})	FWHM (rad) ZnO(101)	FWHM (rad) Ag(111)	D ZnO (nm)
Pure	36.55	- -	0.013400	- -	10.89597

1Ag-ZnO	36.49	38.26	0.011719	0.005353	12.45734
3Ag-ZnO	36.49	38.29	0.005353	0.007759	27.26895
5Ag-ZnO	36.55	38.48	0.005782	0.005545	25.24974

The shift of diffraction peak confirms the incorporation of Ag in the ZnO lattice which causes the improvement of crystallinity. However, it seems that only a small amount of Ag was introduced to the ZnO lattice and that clearly observed from table IV.7, the shift of *2*θ stopped at 36.49^{o} for 3Wt% doping and at 5Wt% the *2*θ became the same as pure ZnO value 36.55^{o}.

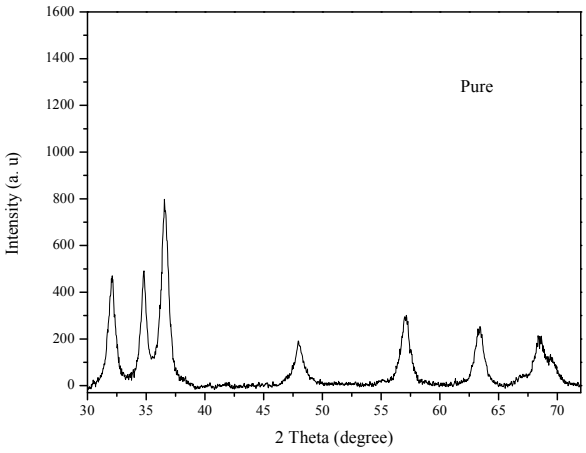

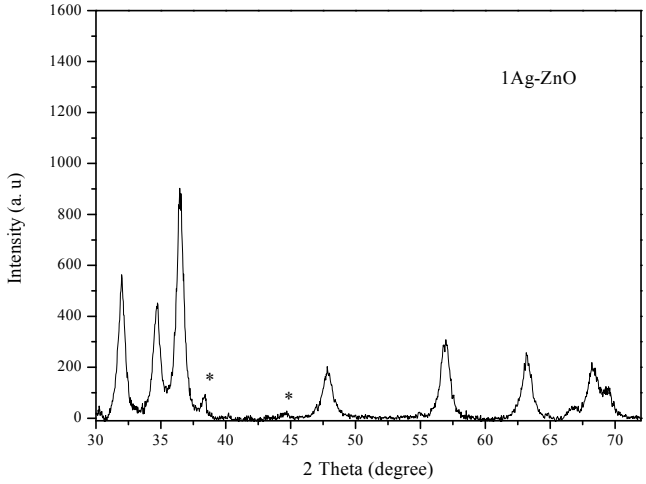

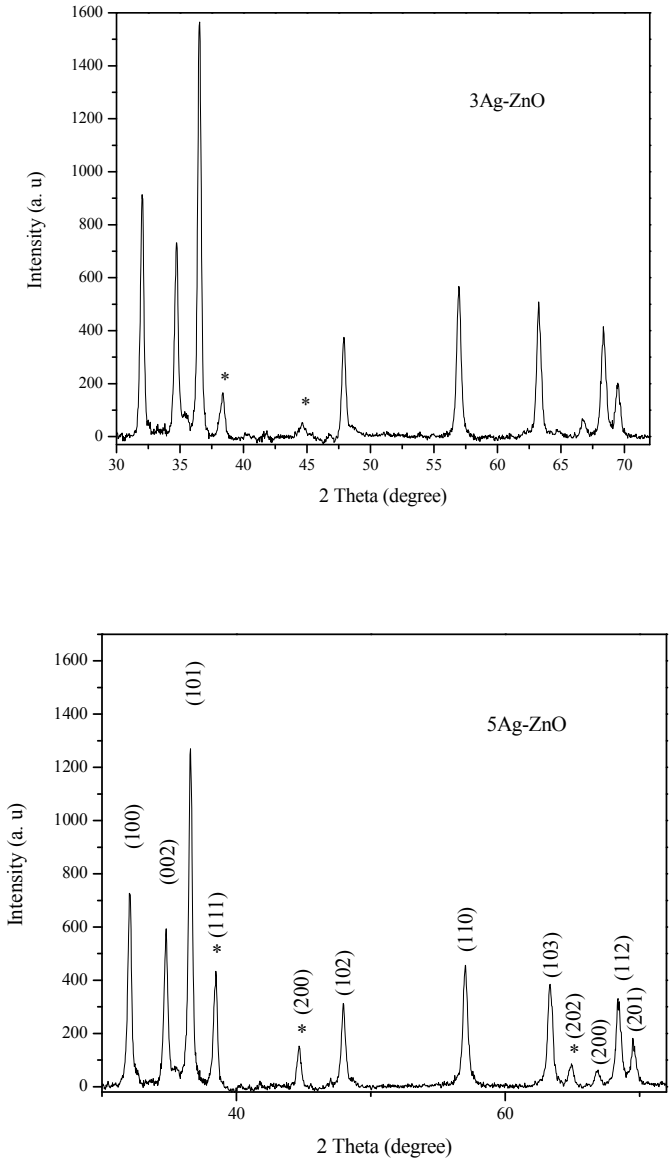

Figure IV. 10 XRD patterns of Ag-doped ZnO nanopowders prepared by sol-gel method.

The incorporation of Ag in the ZnO lattice can be interstitial or substitution incorporation, the interstitial incorporation leads to a peaks shift toward lower *2*θ contrary to the substitution incorporation where the peaks shift to higher *2*θ values [9-10]. As can be seen from table IV.7, our peaks shift to lower *2*θ values (unlike the Ag-doped ZnO thin films) which confirm the interstitial incorporation of Ag in the ZnO lattice.

Figure IV.11 shows the dependence of the calculated crystallite size and the full width at half maximum (FWHM) from (101) plan as a function of Ag content. The crystallite size was

found to be increased from 10.89 (pure ZnO) to a maximum value of 27.26 nm for 3Wt% Ag doping. However, the crystallite size was found to be decreased for higher Ag doping (5Wt %). Also, it can be seen that the FWHM decrease with the increasing of Ag doping (till 3Wt %) than slightly increase for 5Wt % doping. The incorporation of Ag in ZnO lattice caused the increase in the crystallite size and that because of the large ionic radii of Ag+ ion (0.129 nm), for such large ionic radii the solubility of Ag in ZnO is low and that is why the crystallite size starts decreasing at 5Wt%, we suggest that the Ag atoms are segregate at the vicinity of the grain boundaries leading to a reduction in the crystal grain size and a decrease in the intensity of the (101) diffraction peak (FWHM increase).

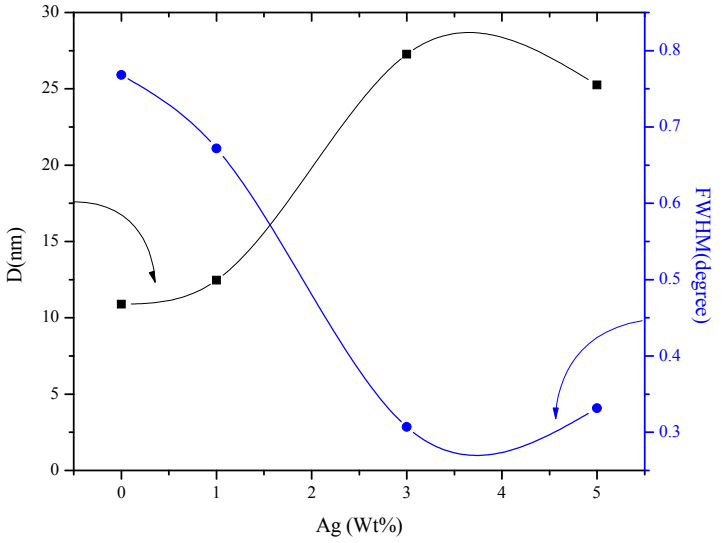

Figure IV. 11 The dependence of crystallite size (D) and the full width at half maximum (FWHM) as a function of Ag doping content.

The lattice parameters (a and c) for the hexagonal pure and Ag-doped ZnO are calculated via (002) and (101) orientations and presented in table IV.8 which also summarizes the lattice parameter (a) of Ag and the calculated values of the interplanar spacing d_{hkl}.

Table IV. 8 Interplanar spacing d_{hkl} and lattice parameters of pure and Ag-doped ZnO nanopowders.

	ZnO				Ag	
	d_{002} (Å)	d_{101} (Å)	a (Å)	c (Å)	d_{111} (Å)	a (Å)
Pure	2.5779	2.4563	3.22591	5.1558	--	--
1Ag-ZnO	2.5883	2.4603	3.22890	5.1766	2.3502	4.07066
3Ag-ZnO	2.5840	2.4603	3.23047	5.168	2.3484	4.06754
5Ag-ZnO	2.5886	2.4644	3.23574	5.1772	2.3451	4.06183

As shown in table IV.8, both lattice parameters a and c are increasing with Ag doping (this result is in a good match and confirming with the results above). This increase is due to the large ionic radii of the interstitial incorporation of Ag in the ZnO lattice, the increase in lattice parameters leads to the increase of the volume of unit cell as shown in table IV.9.

Table IV. 9 Dislocation density, strain, and volume of unit cell of pure and Ag-doped ZnO nanopowders.

	ε (10^{-4})	Dislocation density (lines/m^2)*10^{14}	Volume of unit cell (Å^3)
Pure	31.81229	84.23016	46.46434
1Ag-ZnO	27.82503	64.43904	46.73817
3Ag-ZnO	12.71137	13.44816	46.70592
5Ag-ZnO	13.72790	15.68505	46.94202

The decrease in strain and dislocation density when the Ag content increase indicates that the crystalline quality is improved, the best crystallinity is the one corresponding to 3Wt % Ag doping with minimum strain, dislocation density, and higher crystallite size.

IV.2.3 Morphological properties

The surface morphology of pure and Ag-doped ZnO thin film prepared by dip-coating on glass substrates are obtained by atomic force microscopy. Figure IV.12 shows 3D AFM images scan by contact mode over an area of 3 μm×3 μm, it can be clearly observed the influence of Ag doping on the surface morphology of the prepared films by the difference in the distribution of the grain size and their density, the root mean square (RMS) and the grain size were calculated from the AFM images using the Gwyddion analysis software, and the obtained results are presented in figure IV.13.

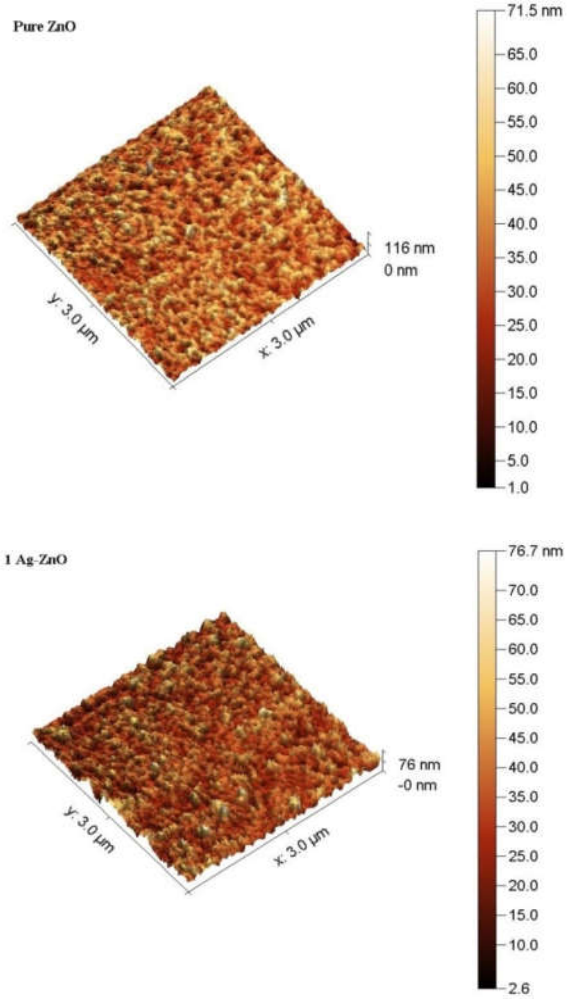

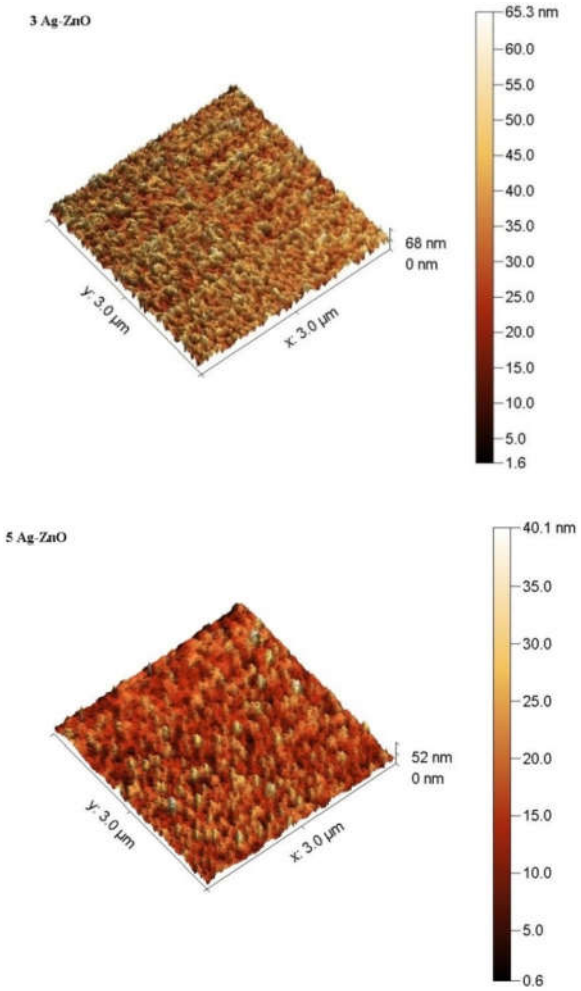

Figure IV. 12 AFM images of pure and Ag-doped ZnO thin films

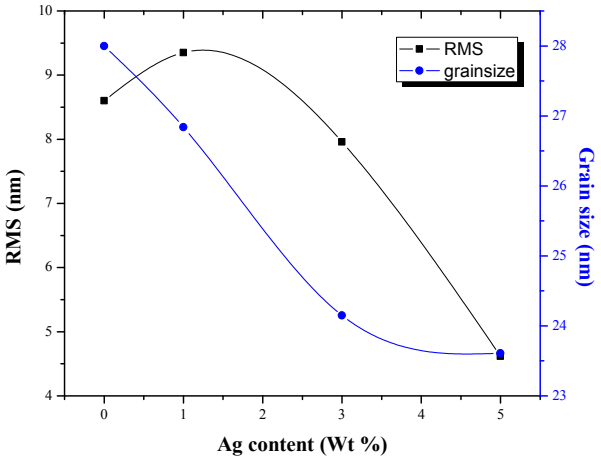

Figure IV. 13 The root mean square (RMS) and the grain size as a function of Ag contents.

It can be seen that the grain size was slightly decreased when the Ag concentration increase, these results are in a good agreement with the XRD finding. The surface roughness also was found to be dependent on the Ag doping, it increases from 8.60 nm for pure ZnO to 9.35 nm for 1Wt % Ag doping then slightly decrease to 7.96 and 4.62 nm for 3Wt % and 5Wt % Ag concentration, respectively. This decreasing in the surface roughness is may attribute to the decrease in the grain size.

IV.2.4 Optical properties

Figure IV.14 shows the optical transmittance spectra of pure and Ag-doped ZnO thin films prepared by sol-gel dip-coating method, It can be seen from figure IV.14 that all the samples exhibit high transparency within the visible range with a transmittance above 70 %, the optical transmittance increased with the increase in Ag doping concentration, similar results were reported by [11-12]. This increasing is may due to the decrease in the grain size and surface roughness because large grain size and rough surface can lead to higher dispersion of light.

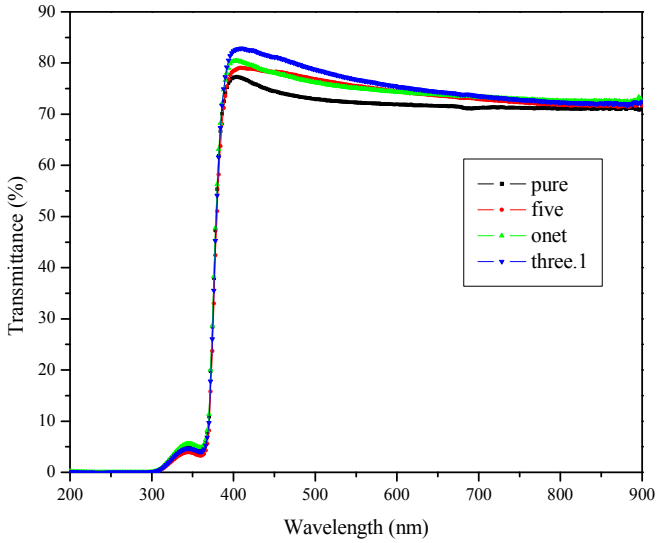

Figure IV. 14 The optical transmittance of pure and Ag-doped ZnO thin films

In order to calculate the optical band gap for pure and Ag-doped ZnO thin films, we plot $(\alpha h\nu)^2$ vs. photon energy $h\nu$ (Tauc's plot), then extrapolated the linear portion of the curve to zero to determine the optical band gap value as shown in figure IV.15.

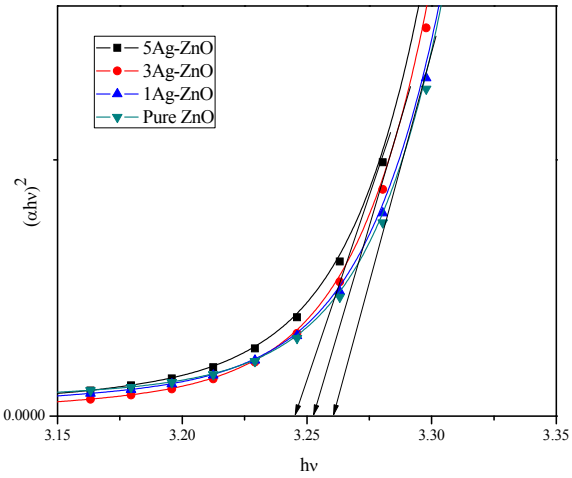

Figure IV. 15 Tauc's plot for calculation the optical band gap of pure and Ag-doped ZnO thin films.

The Eg values recorded are 3.26 eV for both pure ZnO and 1Wt% Ag-doped ZnO thin films which indicate that doping with small concentration has not much effect on the optical band gap. However, the Eg slightly decrease to 3.25 and 3,24 eV for 3Wt% and 5Wt% Ag doping, respectively. This decrease in the band gap with an increase in Ag dopant percentage is also observed by Nazir *et al.* and they suggest "that silver dopant is substituted into the zinc sites which imparts an energy acceptor level in the band gap" [5].

IV.2.5 FTIR analysis

The FTIR spectroscopy is a useful technique for the analysis of the molecular composition of compounds and to identify the functional groups of the films. Figure IV.16 shows the FTIR spectra of the pure and Ag-doped ZnO thin films.

The FTIR spectrum contains several bands, bands between 400 and 750 cm^{-1} correlated to metal oxide bond (ZnO) [13], Bands around 1400–1550 cm-1 are due to the oxygen stretching [14]and the absorption peaks appearing at 2359 cm^{-1} is due to the absorption of atmospheric of carbon dioxide (CO_2) by metallic cation [15-16], The broad peak in the range of 3700 to 3900 cm^{-1} is attributed to water molecule present in thin films [17]. It is evident from the FTIR data the successful synthesized of ZnO thin films which are already confirmed by XRD results.

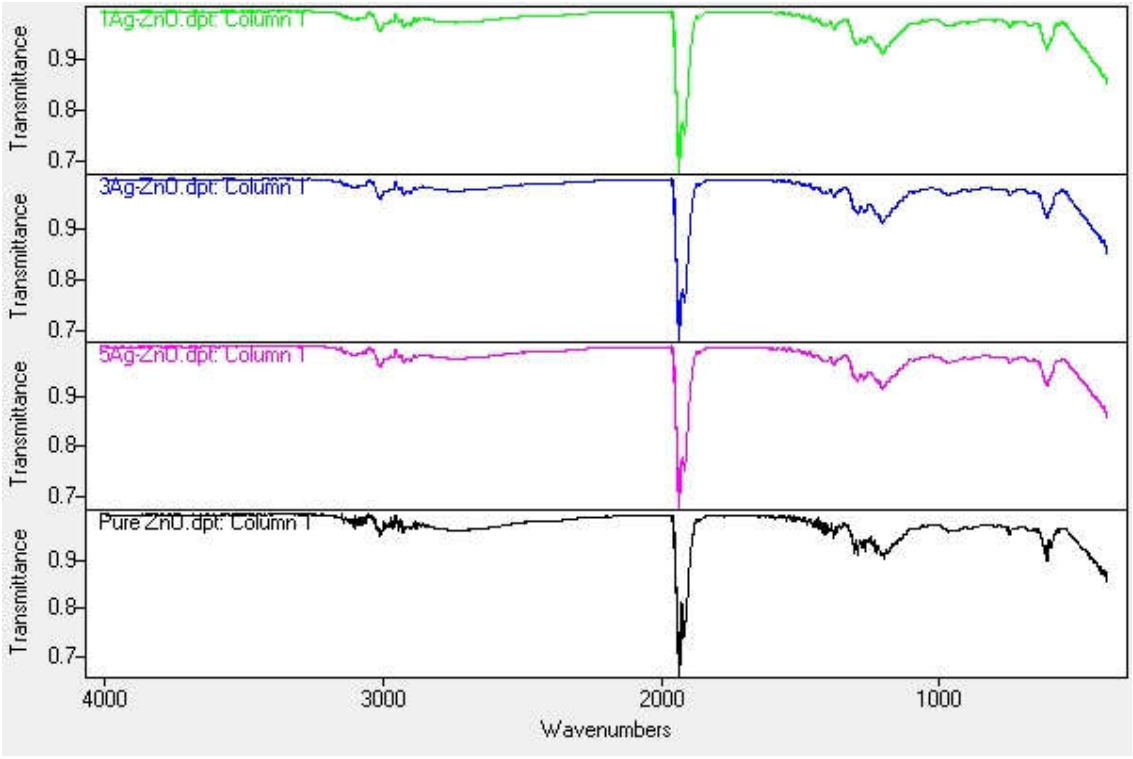

Figure IV. 16 FTIR spectrum of pure and Ag-doped ZnO thin film.

IV.3 n-ZnO/p-NiO heterostructure thin films

In recent years, researches have been focused on transparent conducting oxides (TCOs) materials due to their optical and electrical properties, in order to enhance the properties of many TCOs materials types (n-type or p-type) doping and co-doping were widely used, good results were achieved and huge enhancement in diverse applications were reported. However, introducing a dopant element has limits for the enhancement of properties than undesirables effects, begin to start such as the disturb of crystal structure, the decrease in conductivity…etc. Other approaches can be used among them is the coupling of n-type and p-type TCOs materials to form a P-N heterostructures materials such as p-CuO / n-ZnO [18], NiO/SnO_2 [19], NiO/ZnO [20-21], p-NiO / n-GaAs [22], P-N NiO/ZnO heterostructure is a promising choice because of their interesting properties and the closely match in band-gap energies [23].

In this study, NiO/ZnO thin films were prepared by sol-gel dip-coating method. NiO thin films were deposited onto clean glass substrates by dip-coating method at a withdrawal speed of 100mm/min. ZnO thin films were deposited on the prepared NiO thin films. ZnO precursor solution prepared by dissolving Zinc acetate dihydrate (Zn $(CH3COO)_2;2H_2O$) in ethanol and monoethanolamine (MEA) added as a stabilizer. The molar ratio of zinc acetate to MEA was maintained at 1:1 and the zinc acetate concentration was 0.1M. The obtained solution stirred for 2h at 60^{o}C to yield a homogeneous solution and then aged for 24h at room temperature.

At the withdrawal speed of 100 mm/min, a different number of ZnO layers (2, 6, 9, and 12) were deposited, now on we used S2, S6, S9, and S12 for the prepared samples according to their different coating number (2, 6, 9 and 12 ZnO coating number). To evaporate the solvent we dried the films at 230^{o}C for 5 min for each deposited layer. The obtained NiO/ZnO thin films were annealed at 550^{o}C for 2h. The structural, optical and Photocatalytic properties of the samples were investigated.

IV.3.1 Structural properties

Figure IV.17 shows the x-ray diffraction spectra of heterostructure ZnO/NiO samples (S2, S6, S9, and S12) prepared by sol-gel dip-coating method. From the results, we can see two sets of diffraction peaks (*refer to ZnO, #refer to NiO) belong to ZnO hexagonal wurtzite structure and to NiO cubic structure without the existence of any impurities which confirms the composition of NiO and ZnO in the heterostructure as reported in [24-25].

For S2, the two ZnO coating layers star to appear in the XRD pattern in the peak located at 31.76° corresponding to the (100) plan, by increasing the coating number from 2 to 6, we can see the change from the intense peak of NiO to the preferred (002) peak of the ZnO, this intensity keeps increasing when the coating number increase from 6 to12 due to the thickness increases indicating the improvement of ZnO crystallinity.

However, the change to the ZnO peak and the decrease in NiO peaks even the all samples have the same NiO film thickness is due to the x-ray that explores much more of the ZnO film because of its thickness increasing and did not penetrate much deeper inside the films as described by V. Sushmitha *et al.* [26].

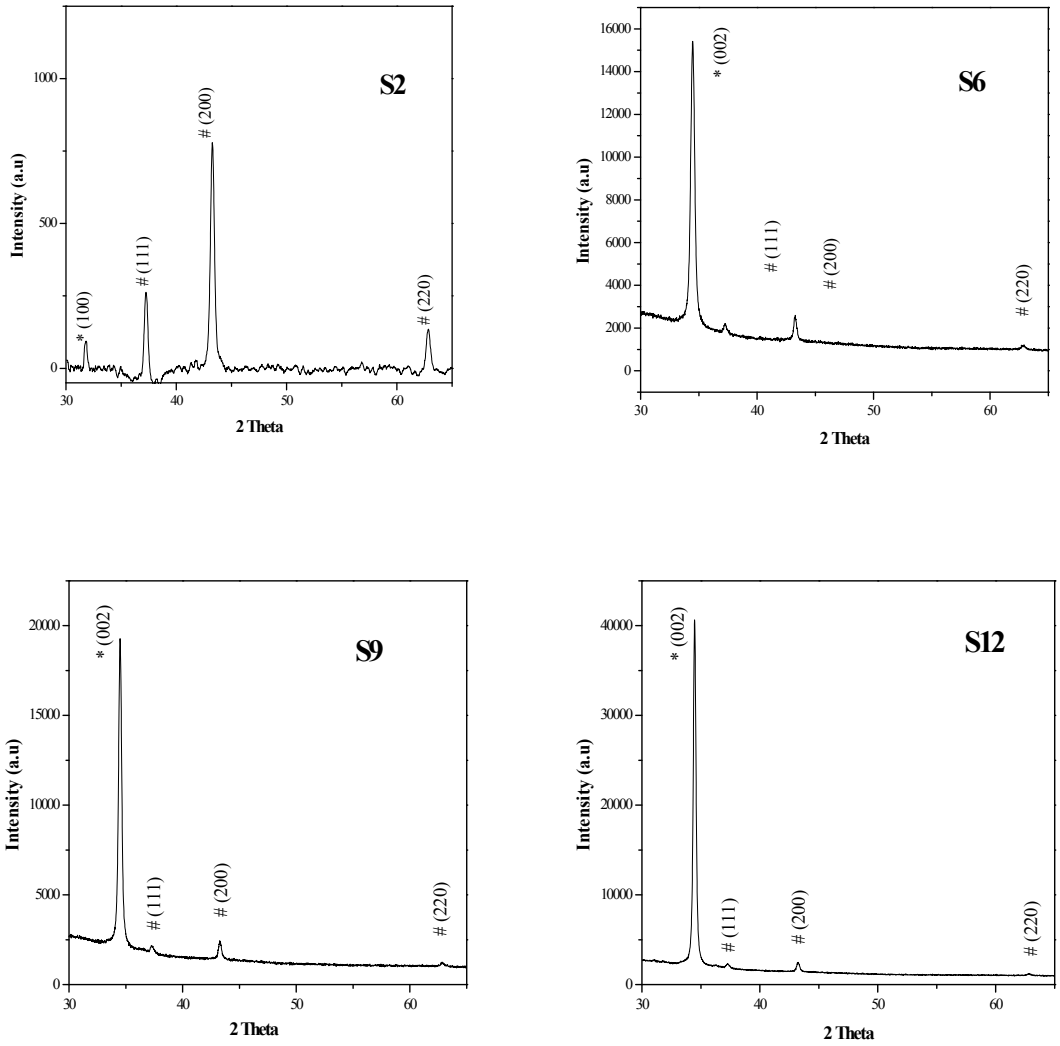

Figure IV. 17 X-ray diffraction pattern of NiO/ZnO heterostructure with different ZnO coating number (2, 6, 9, and 12) S2, S6, S9, and S12.

Table IV. 10 Structural parameters of NiO/ZnO heterostructure prepared by sol-gel method.

	FWHM (o)		Position 2θ (o)		Crystallite size (nm)		Intensity [%]	
	NiO (200)	ZnO (002)	NiO (200)	ZnO (002)	NiO (200)	ZnO (002)	NiO (200)	ZnO (002)
S2	0.2047	--	43.26	--	146	--	100	--
S6	0.2184	0.4110	43.23	34.47	137	71	7.75	100
S9	0.2558	0.3207	43.26	34.49	117	91	5.76	100
S12	0.2047	0.2563	43.21	34.46	146	113	2.56	100

The average crystallite size (D) is estimated from the peak width for half maximum intensity for both NiO and ZnO and it was calculated using Debye–Scherrer's formula, the grain size values of ZnO and NiO and other structural parameters are given in Table IV.10. We noticed that NiO intensity decrease with the increase of ZnO coating numbers which explain above as the x-ray explores much more of the ZnO film because of its thickness increasing. In addition, the (002) ZnO peak is clearly seen to be the highest in intensity for the three samples (S6, S9 andS12); this is revealed that the ZnO has a preferential orientation along the c-axis. Furthermore, figure IV.18 shows the variation of crystallite size (D) and the full width at half maximum (FWHM) as a function of ZnO coating number for the (002) peak. The crystallite size increase from 71 to 113 nm for S6, S9, and S12 respectively, we can notice that the crystallite size increase after the increase in the ZnO thickness (increase the coating number) indicating the enhancement in the crystallinity of ZnO.

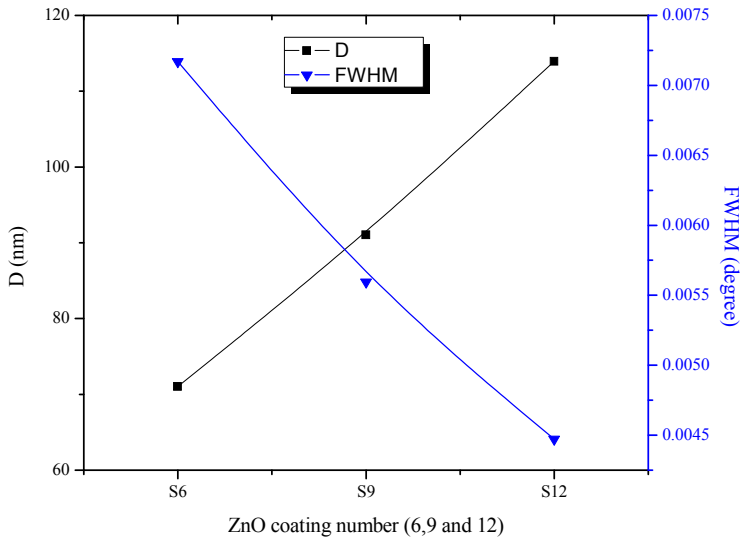

Figure IV. 18 The variation of crystallite size (D) and the full width at half maximum (FWHM) as a function of ZnO coating number.

As shown in table IV.11, other micro structural parameters such as the lattice parameters, interplanar spacing, strain and dislocation density were calculated for both NiO cubic and ZnO hexagonal phases for (200) and (002) plan, respectively.

Table IV. 11 Microstructural parameters: the lattice parameters, interplanar spacing, strain and dislocation density of NiO and ZnO.

	d(Å)		Lattice parameters (Å)		Strain ε (10^{-4})		Dislocation density (lines/m^2)*10^{14}	
	NiO (200)	ZnO (002)	NiO "a"	ZnO "c"	NiO	ZnO	NiO	ZnO
S2	2.09124	--	4.18248	--	8.29857	--	0.46554	--
S6	2.09085	2.59944	4.1817	5.19888	8.85489	17.11933	0.53005	1.98116
S9	2.09106	2.59833	4.18212	5.19666	10.37018	13.35735	0.72697	1.20611
S12	2.09353	2.60244	4.18706	5.20488	8.30001	10.67592	0.4657	0.77047

As presented in table IV.11, the lattice parameters and interplanar spacing of NiO are almost unchanged because all the samples have the same NiO thickness deposited at the same conditions. Furthermore, the strain and dislocation density of NiO also remains unchanged that much, the strain in NiO is due to the lattice mismatch between NiO and the substrate. The increase in the lattice parameters and interplanar spacing in addition to the decrease in strain and dislocation density of ZnO is due to the increase of thickness which also confirming the improvement of the crystallinity.

IV.3.2 Optical properties

The optical transmittance of the samples S2, S6, S9, and S12 of the heterostructure of p-NiO/n-ZnO prepared by dip-coating method is shown in figure IV.19, the transmittance spectra exhibit a shift toward low energies when the ZnO coating number increased and of course low transmittance due to the increased of the thickness of the film. [27] Report that when the film thickness increased the grain size also increased and film coverage improved which caused a higher dispersion of the incident light.

The optical band gap of the prepared films was calculated using Tauc's equation:

$$(\propto h\nu) = A(h\nu - Eg)^n \qquad \text{(IV.8)}$$

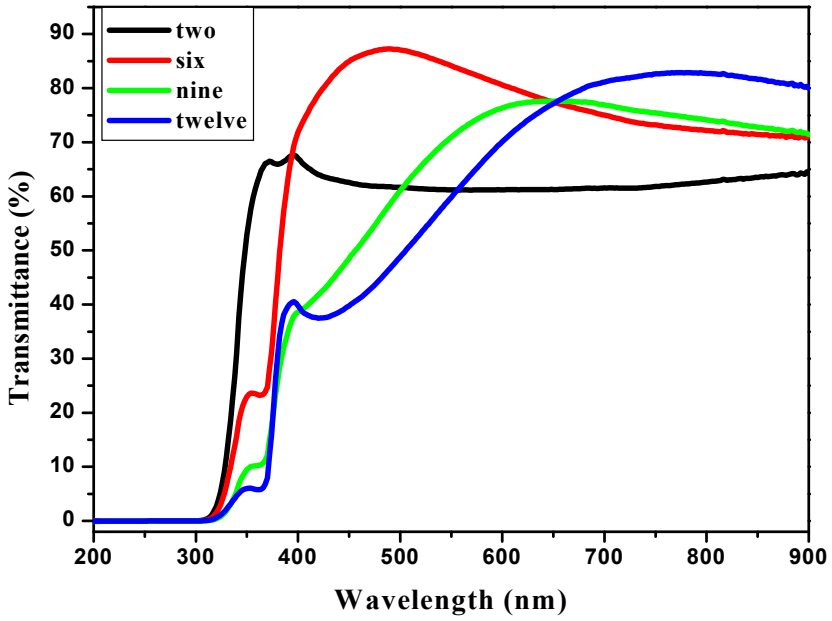

Figure IV. 19 Optical transmittance of the p-NiO/n-ZnO heterostructure.

Where A is a constant, ∝ is the absorption coefficient, hν is the photon energy and n is a number depends on the nature of the optical transition. It can take the values 0.5 and 2 for direct and indirect allowed transition respectively. From the plots of $(\propto h\nu)^2$ versus hν (figure IV.20) the optical band gap was determined; it is varying from 3.62, 3.54, 3.50 and 3.45 for the samples S2, S6, S9, and S12, respectively. In addition, there are other gap values belonging to ZnO as shown in table IV.12, which indicates the presence of two phases of ZnO and NiO as confirmed by XRD data. As can be seen, by the increasing of the ZnO thickness, the Eg deceased from energies that are close to NiO (S2) to energies that have belonged to ZnO (S12).

Table IV. 12 Bandgap values of the p-NiO/n-ZnO heterostructure

	SS2	S6	S9	S12
Eg1 (eV)	3.62	3.54	3.50	3.45
Eg2 (eV)	/	3.19	3.22	3.25

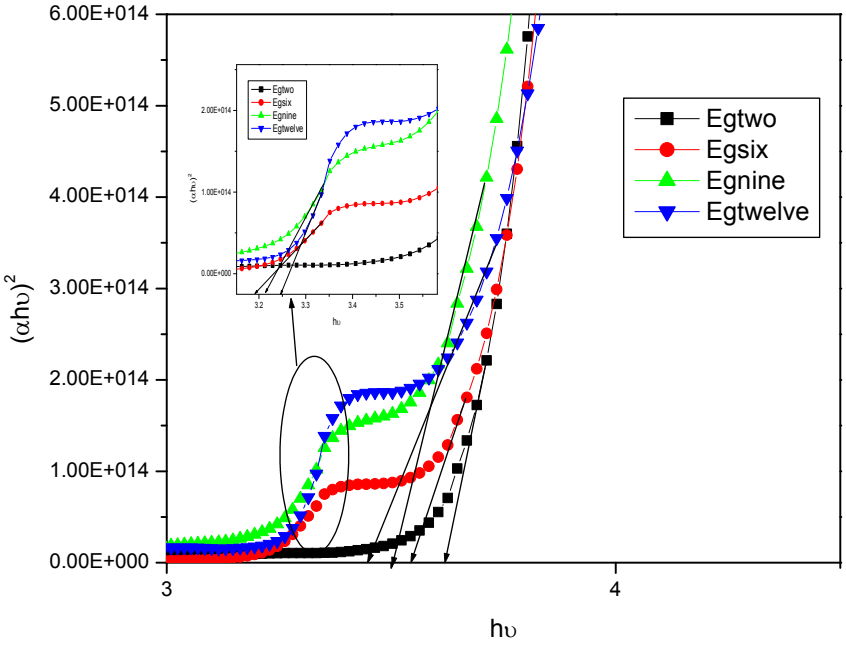

Figure IV. 20 Determination of the optic gap energies using the plot $(\propto \mathbf{h\nu})^{\mathbf{2}}$ versus $\mathbf{h\nu}$.

IV.3.3 Photocatalytic properties of NiO/ZnO heterostructure thin films

IV.3.3.1 Photocatalytic performance

Photocatalytic activity of the NiO/ZnO heterostructure thin films was investigated for the Methylene blue degradation under visible light irradiation, figure IV.21 represents the time-dependent absorption spectra of MB under solar light irradiation and figure IV.23 represents the degradation rate as a function of the time of irradiation. We can observe that the effect of thickness shown an increase to a certain value and then a slight decrease in photocatalytic activity. The sample S6 show the highest Photocatalytic activity compare to the other samples because it has the lowest Eg 3.19eV, the increase in ZnO thickness S9 and S12 by increasing the coating number leads to the decrease in the Photocatalytic activity but still show better results compared to small ZnO thickness S2 indicating the important role of ZnO (n-layer) in the heterojunction as source of photogenerated electrons and in the separation processes.

By take into account, that the enhancement in photocatalytic activity is attributed to the excellent electrical conductivity as reported by P. Zhang *et al.* [28], and based on Alzahrani *et*

al. who found that 200 nm is the optimal thickness of the ZnO for the NiO/ZnO heterojunction optimal properties [29]. We conclude that is why S6 presents the best photocatalytic activity because the thickness of S6 is the closest to 200 nm and that give the NiO/ZnO heterojunction the optimal electrical properties, N. Kaneva *et al.* [30] also reported that in the case of ZnO films with 7 coats have better photocatalytic efficiency compared to less coating number (1, 3 and 5).

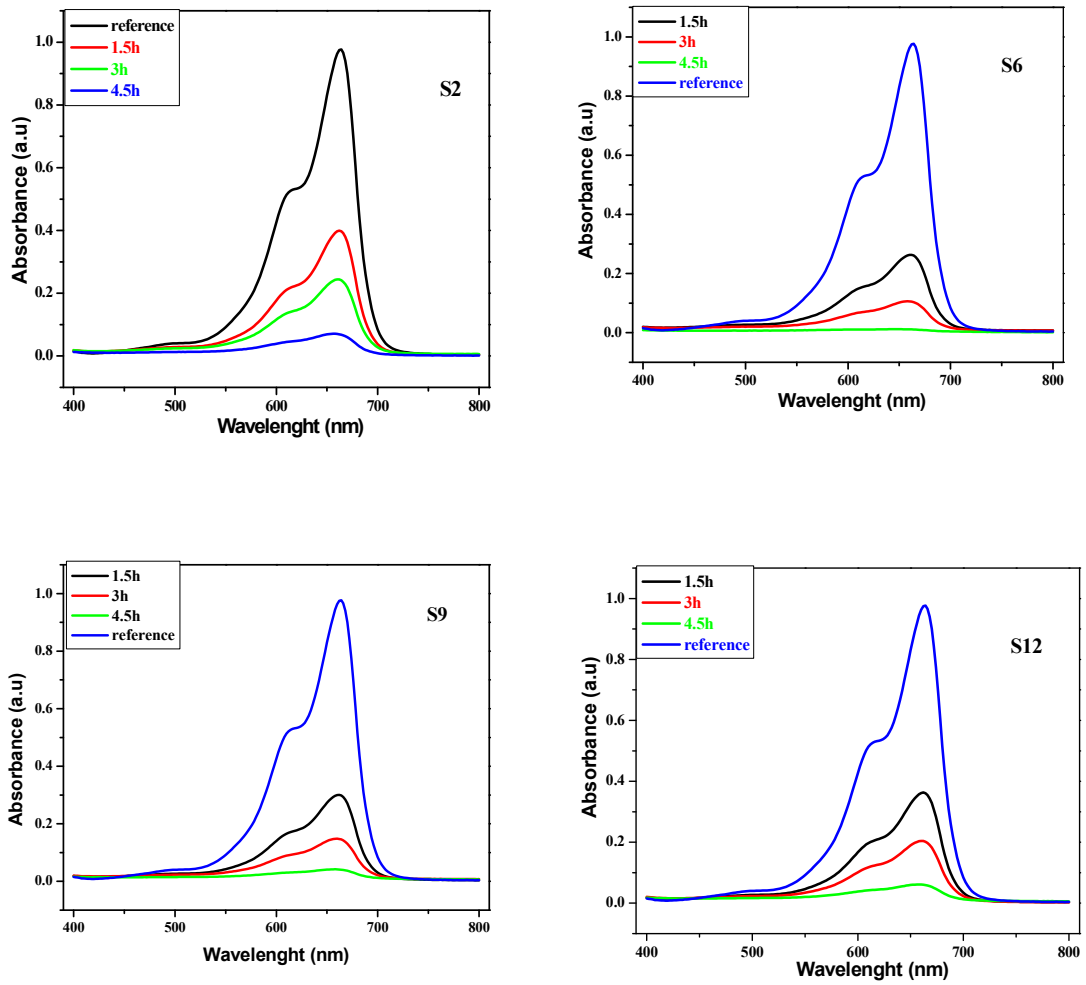

Figure IV. 21 The time-dependent absorption spectra of MB under solar light irradiation.

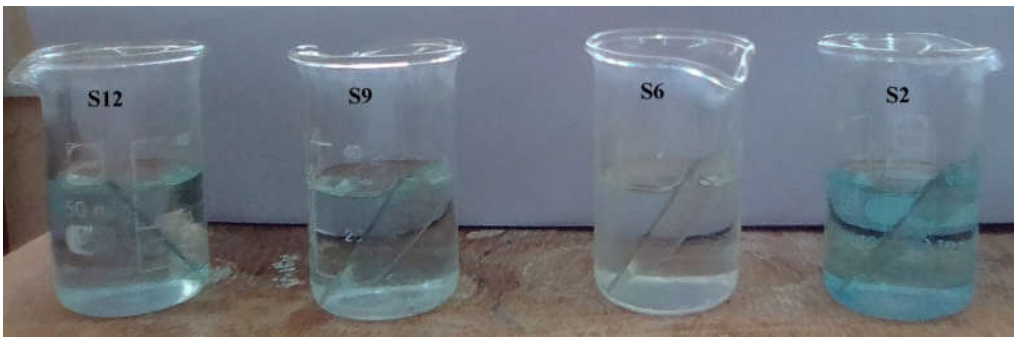

Figure IV. 22 MB solutions after 4.5h of solar irradiation exposure.

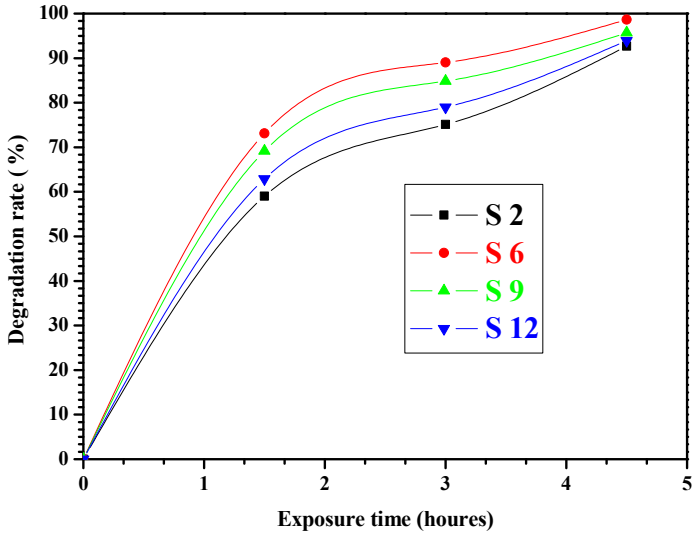

Figure IV. 23 The Degradation rate as a function of the time of irradiation

Figure IV.22 shows the resulting MB solutions after 4.5h of solar irradiation exposure. Compare to other solutions, it seems that S6 became totally transparent because the total degradation of methylene blue around 98.67 %. We can conclude that the ZnO film thickness plays an important role in the photocatalytic performance of ZnO/NiO heterostructure and the optimal thickness of 6 coats gives the highest degradation rate after 4.5h of solar irradiation exposure.

IV.3.3.2 Photocatalysis mechanism

The mechanism of methylene blue degradation using the ZnO/NiO heterostructure is illustrated in figure IV.24. Under visible light irradiation there are a photogenerated

electrons/holes pairs in the p-n heterostructure in both materials NiO and ZnO, the electrons excited from VBs to CBs and left holes in VBs, at this moment the heterostructure form take a place in the separation of electrons and holes, figure IV.24. The electrons from NiO CB migrate to the ZnO CB, in contrary the holes from ZnO VB migrate to NiO VB. In result, we have an effective and efficient way to separate the electrons/holes pairs, those free e/h pairs are able to participate in chemical reaction to produce (OH•, O2•-) radicals which are responsible for the degradation of the organic dye molecules (MB) and that caused the enhancement in the Photocatalytic activity.

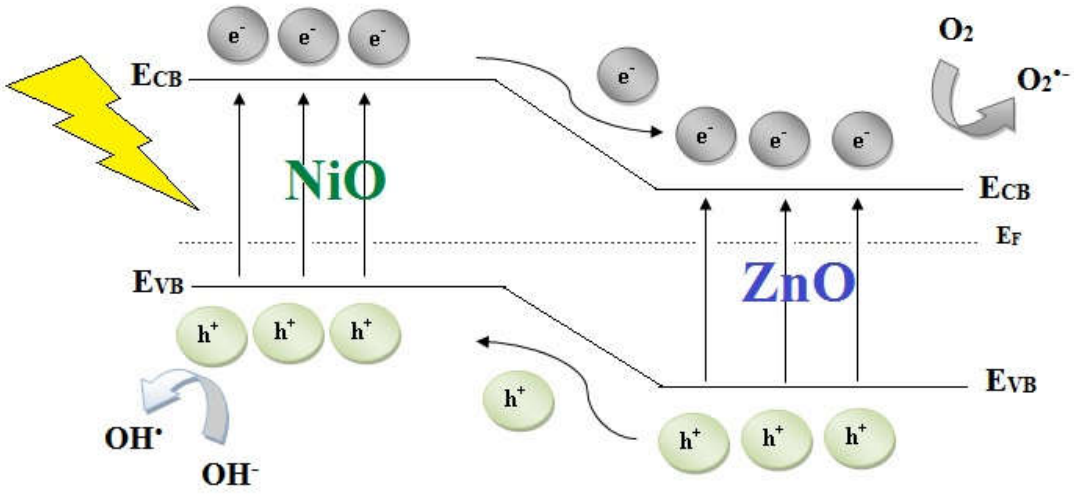

Figure IV. 24 The energy band structure and electron-hole pair separation process in the p-type NiO/n-type ZnO heterojunction.

IV.3.4 Conclusion

Nickel oxide (NiO), Zinc oxide (ZnO) and ZnO/NiO heterostructure thin films were successfully prepared by sol-gel dip-coating method. Firstly, the withdrawal speed affects the properties of NiO thin films, it was found that the crystallinity of the films deteriorated, the surface roughness increased and the optical transmittance decrease when the withdrawal increase. Secondly, the silver doping ZnO thin films enhanced the optical transmittance, decreased the surface roughness and deteriorate the crystalline structure compared to pure ZnO thin films. Finally, it was found that the thickness of the ZnO layer in the ZnO/NiO heterostructure enhances the photocatalytic properties under solar irradiation and optimal thickness is 6 coats which gives the highest degradation of MB dye.

IV.4 References

[1] K. Sajilal and A. M. Ezhil Raj, "Effect of thickness on structural and magnetic properties of NiO thin films prepared by chemical spray pyrolysis (CSP) technique," Mater. Lett, vol. 164, pp. 547–550, 2016.

[2] P. Ravikumar, B. Kisan, and A. Perumal, "Thickness dependent ferromagnetism in thermally decomposed NiO thin films," J. Magn. Magn. Mater, vol. 418, pp. 86–91, 2016.

[3] S. Aydemir, "Effects of withdrawal speed on the microstructural and optical properties of sol-gel grown ZnO:Al thin films," Vacuum, vol. 120, pp. 51–58, 2015.

[4] E. Mosquera, C. Rojas-michea, M. Morel, F. Gracia, V. Fuenzalida, and R. A. Zárate, "Zinc oxide nanoparticles with incorporated silver : Structural , morphological , optical and vibrational properties," Appl. Surf. Sci, vol. 347, pp. 561–568, 2015.

[5] Z. Nazir, M. Anwar, Z. Saddiqe, S. Riaz, and S. Naseem, "Biological and optical properties of sol – gel derived ZnO using di ff erent percentages of silver contents," Colloids Surfaces B Biointerfaces, vol. 171, no. July, pp. 383–390, 2018.

[6] M. Karyaoui, A. Mhamdi, H. Kaouach, A. Labidi, and A. Boukhachem, "Some physical investigations on silver-doped ZnO sprayed thin films," Mater. Sci. Semicond. Process, vol. 30, pp. 255–262, 2015.

[7] S. C. Tjong and H. Chen, "Nanocrystalline materials and coatings," Mater. Sci.and Eng., R: Reports, vol. 45, pp. 1–88, 2004.

[8] K. Thongsuriwong, P. Amornpitoksuk, and S. Suwanboon, "Photocatalytic and antibacterial activities of Ag-doped ZnO thin films prepared by a sol – gel dip-coating method," J. of sol-gel sci. and tech., vol. 62, pp. 304–312, 2012.

[9] Karunakaran, C., V. Rajeswari, and P. Gomathisankar. "Antibacterial and photocatalytic activities of sonochemically prepared ZnO and Ag–ZnO." J. Alloys Compd, vol. 508.2, pp. 587-591, 2010.

[10] Jin, Yunxia, Qiliang Cui, Kai Wang, Jian Hao, Qiushi Wang, and Jian Zhang. "Investigation of photoluminescence in undoped and Ag-doped ZnO flowerlike nanocrystals." J. Appl. Phys, vol. 109.5, pp. 053521, 2011.

[11] S. M. H. A. Sabah, H. S. Ali, and A. T. Hussein, "Studying structural , morphological and optical properties of nanocrystalline ZnO : Ag fi lms prepared by sol – gel method for antimicrobial activity," J Solgel Sci Technol, vol. 87.2, pp. 362-371, 2018.

[12] S. Ali and A. Farooq, "Structural and optical properties of pure and Ag doped ZnO thin films obtained by sol gel spin coating technique," Mater. Sci-Poland, vol. 33.3, pp. 601-605, 2015.

[13] S. Y. Purwaningsih and S. Pratapa, "Synthesis of Nano-sized ZnO Particles by Co-precipitation Method with Variation of Heating Time," In AIP Conference Proceedings, vol. 1710.1, pp. 030040, 2016.

[14] I. C. Studies, "Synthesis of Silver-Doped Zinc Oxide Nanocomposite by Pulse Mode Synthesis of Silver-Doped Zinc Oxide Nanocomposite by Pulse Mode Ultrasonication and Its Characterization Studies," J. of Nanoscience, 2013.

[15] Gayathri, Sethuraman, OS Nirmal Ghosh, S. Sathishkumar, S. Sudhakara, J. Jayaramudu, S. S. Ray, and Annamraju Kasi Viswanath. "Investigation of physicochemical properties of Ag doped ZnO nanoparticles prepared by chemical route." Appl. Sci. Lett., Vol. 1(1),pp. 8-13, 2015.

[16] Srithar, A., J. C. Kannan, and T. S. Senthil. "Preparation and Characterization of Ag doped ZnO nanoparticles and its Antibacterial Applications." J.of adv. in chem., vol. 13.6, pp. 6273-6279, 2017.

[17] Z. R. Khan, M. S. Khan, M. Zulfequar, and M. S. Khan, "Optical and Structural Properties of ZnO Thin Films Fabricated by Sol-Gel Method," Mater. Sci. and applications, vol. 2011, pp. 340–345, 2011.

[18] R. R. Prabhu, A. C. Saritha, M. R. Shijeesh, and M. K. Jayaraj, "Fabrication of p-CuO / n-ZnO heterojunction diode via sol-gel spin coating technique," Mater. Sci. Eng. B, vol. 220, pp. 82–90, 2017.

[19] Fang, Jiabin, Yiping Zhu, Dajun Wu, Chi Zhang, Shaohui Xu, Dayuan Xiong, Pingxiong Yang, Lianwei Wang, and Paul K. Chu. "Gas sensing properties of NiO/SnO2 heterojunction thin film." Sensors And Actuators B: Chem, vol. 252, pp. 1163-1168, 2017.

[20] M. Sultan, S. Mumtaz, A. Ali, M. Y. Khan, and T. Iqbal, “Band alignment and optical response of facile grown NiO/ZnO nano-heterojunctions,” Superlattices Microstructures, vol. 112, pp. 210-217, 2017.

[21] Y. Luo *et al*., “Applied Surface Science Piezoelectric effect enhancing decay time of p-NiO / n-ZnO ultraviolet photodetector,” Appl. Surf. Sci., vol. 361, pp. 157–161, 2016.

[22] G. Turgut and S. Duman, “Sol-gel growth and characterization of a new p-NiO / n-GaAs structure,” J. Alloys Compd, vol. 664, pp. 547–552, 2016.

[23] Y. Zhao, H. Wang, C. Wu, W. Li, F. Gao, and G. Wu, “Study on the electroluminescence properties of diodes based on n-ZnO / p-NiO / p-Si heterojunction,” Opt. Commun, pp. 3–6, 2014.

[24] F. Tian and Y. Liu, “Synthesis of p-type NiO/n-type ZnO heterostructure and its enhanced photocatalytic activity,” Scr. Mater, vol. 69, no. 5, pp. 417–419, 2013.

[25] Y. Liu, G. Li, R. Mi, C. Deng, and P. Gao, “Sensors and Actuators B : Chemical An environment-benign method for the synthesis of p-NiO / n-ZnO heterostructure with excellent performance for gas sensing and photocatalysis,” Sensors And Actuators B: Chem, vol. 191, pp. 537–544, 2014.

[26] V. Sushmitha, V. Maragatham, P. Deepak Raj, and M. Sridharan, “Structural, electrical, optical and magnetic properties of NiO/ZnO thin films,” IOP Conf. Ser. Mater. Sci. Eng, vol. 310, no. 1, 2018.

[27] A. M. Soleimanpour, Y. Hou, and A. H. Jayatissa, “Evolution of hydrogen gas sensing properties of sol-gel derived nickel oxide thin film,” Sensors And Actuators, B: Chem, vol. 182, pp. 125–133, 2013.

[28] Zhang, P., R. Y. Hong, Q. Chen, and W. G. Feng. "On the electrical conductivity and photocatalytic activity of aluminum-doped zinc oxide." Powder technol., vol. 253, pp. 360-367, 2014.

[29] Alzahrani, Ahmed Obaid M., M. Sh Abdel-wahab, Meshari Alayash, and M. S. Aida. "Effect of ZnO layer thickness upon optoelectrical properties of NiO/ZnO

heterojunction prepared at room temperature." J. mater. Sci. mater. el., vol. 29.19, pp. 16317-16324, 2018.

[30] Kaneva, N., A. Bojinova, K. Papazova, D. Dimitrov, I. Svinyarov, and M. Bogdanov. "Effect of thickness on the photocatalytic properties of ZnO thin films," Bulg Chem Commun,vol. 47.1, pp. 395-401, 2015.

GENERAL CONCLUSION

Conclusion

The main goal of this thesis is the preparation and characterization of thin films based on ZnO and other oxides, and in order to achieve that, the whole experimental work has been done at the Laboratory of Active Components and Materials (LCAM) at Larbi Ben M'hidi University-Oum El Bouaghi, Algeria.

This work is started with the preparation of samples using sol-gel dip-coating method, alcoholic solutions (methanol, ethanol), zinc acetate, nickel acetate, silver nitrate and monoethanolamine (MEA) as solvent, precursors, dopant, and stabilizer, respectively. The compositional, morphological and optical features of the films were investigated using XRD, AFM, FTIR and UV-visible spectrophotometer.

Starting with the effect of withdrawal speed which is an essential parameter that affecting the properties of thin films prepared by sol-gel dip-coating method, NiO thin films were prepared with withdrawal speed of 30, 50 and 70 mm/min. The structural results revealed that the films are polycrystalline and the crystallinity deteriorated which confirmed by the decreasing of the grain size when the withdrawal speed increased, the morphological properties shows that all films have a uniform and dense NiO grain and the thin NiO layers became denser as the withdrawal speed increased. RMS values had been raised up within the increase in withdrawal speed. They were found to be 3.78, 10.02 and 15 nm for withdrawal speeds of 30, 50 and 70 mm / min, respectively. The optical analysis showed that the transmittance of thin layers dropped down with the increased of withdrawal speeds, the values of the optical band gap were 3.88, 3.91 and 3.97 eV for the withdrawal speeds 30, 50 and 70 mm / min, respectively.

As the second part of this study, we used doping to enhance the properties of zinc oxide; silver doped ZnO thin films were prepared using sol-gel dip-coating method. It was found that the crystallinity of the thin films deteriorated with the increase of Ag doping and that attributed to the shift of diffraction peak (101) toward higher 2θ. The surface roughness was found to be decreased with the increase of Ag-doping concentration, the RMS values were increased from 8.60 nm for pure ZnO to 9.35 nm for 1Wt % Ag doping then slightly decreased to 7.96 and 4.62 nm for 3Wt % and 5Wt % Ag concentration, respectively. This decreasing is might attributed to the decrease in the grain size. The optical transmittance was increased with the increasing of Ag doping concentration, the recorded Eg values were 3.26

eV for both pure ZnO and 1Wt% Ag-doped ZnO thin films which indicate that doping with small concentration has not much effect on the optical band gap. However, the Eg slightly decreased to 3.25 and 3.24 eV for 3Wt% and 5Wt% Ag doping. The FTIR results confirm the successful synthesized of ZnO thin films.

In the final section, ZnO/NiO heterostructure thin films were prepared by sol-gel dip-coating method with different ZnO thickness (2, 6, 9 and 12 coats), the XRD results revealed the existence of two sets of diffraction peaks belong to ZnO hexagonal wurtzite structure and to NiO cubic structure confirming the composition of NiO and ZnO in the heterostructure. The transmittance spectra exhibit a shift toward lower energies when the ZnO coating number increased and of course lower transmittance due to the increased in the thickness of the film.

A high photocatalytic activity performance of the ZnO/NiO heterostructure thin films was achieved which ascribe to the high separation of the photogenerated electrons and holes. In addition, the ZnO film thickness plays an important role in the photocatalytic performance of ZnO/NiO heterostructure. The optimal thickness of 6 coats gives the highest degradation rate after 4.5 h of solar irradiation exposure.

Abstract

In this work, we studied the effect of the withdrawal speed on the properties of nickel oxide thin films, the effect of silver doping on the properties of zinc oxide and the elaboration of p-NiO/n-ZnO heterostructure thin films. All thin films were deposited onto glass substrates using the sol-gel dip-coating method. The structural, optical and morphological properties of the films were investigated using X-ray diffraction, spectrophotometer and atomic force microscopy (AFM), respectively.

It was found that the increase in withdrawal speed leads to the deterioration of the crystallinity of NiO thin films and to the decrease in the optical transmittance. However, the surface roughness was found to be increased when the withdrawal speed increased.

With regard to the effect of Ag-doped ZnO thin films, the XRD results revealed that the crystalline quality decreased when the Ag concentration increased with a shift of the diffraction peak (101) toward higher angles. This shift suggests the substitution incorporation of Ag species into the ZnO lattice. For the morphological study, films with high Ag-doping concentration showed low surface roughness, the RMS values were decreased from 8.60 to 4.62 nm for pure and 5Wt % Ag-doped concentration, respectively. The optical analysis showed that the Ag-doping increase the optical transmittance of ZnO thin films. Hence, these results revealed that the Ag-doped ZnO thin films can be used in different applications especially optoelectronics.

Finally, n-ZnO/p-NiO heterostructure thin films with different coating number of n-ZnO layer (2, 6, 9 and 12) were prepared. The XRD results confirmed the formation of the n-ZnO/p-NiO heterostructure through the existence of two sets of diffraction belonging to NiO and ZnO. The photocatalytic properties of the p-NiO/n-ZnO heterostructure were investigated by measuring the degradation of Methylene Blue dye under solar light irradiation. It was found that the thickness of the n-type layer plays a critical role in the heterostructure performance. The thickness obtained for 6 coating layers shows the best photocatalytic activity with degradation rate in the order of 98.67% for 4.5h of irradiation exposure.

Keywords: ZnO, NiO, thin films, photocatalysis, Sol-Gel method.

Résumé

Dans ce travail, nous avons étudié l'effet de la vitesse de tirage sur les propriétés des couches minces d'oxyde de nickel, l'effet du dopage à l'argent sur les propriétés de l'oxyde de zinc et l'élaboration de couches minces hétérostructure p-NiO / n-ZnO. Tous les films minces ont été déposés sur des substrats de verre en utilisant la méthode de sol-gel trempage-tirage. Les propriétés structurales, optiques et morphologiques des films ont été étudiées par diffraction des rayons X, spectrophotométrie et microscopie à force atomique (AFM), respectivement.

Il a été constaté que l'augmentation de la vitesse de retrait entraîne une détérioration de la cristallinité des couches minces de NiO et une diminution de la transmission optique. Cependant, la rugosité de surface s'est accrue avec un accroissement de la vitesse de retrait.

Concernant l'effet de dopage à l'Ag des couches minces de ZnO, les résultats obtenus par DRX ont révélé une diminution de la qualité cristalline avec l'augmentation de la concentration de Ag. Un décalage du pic de diffraction (101) vers des angles plus élevés a été observé. Ceci est dû à la substitution des atomes Zn par Ag dans le réseau ZnO. Pour l'étude morphologique, les films avec une concentration élevée en dopage Ag montrent une faible rugosité de surface. Une diminution des valeurs RMS a été aussi observée, de 8,60 à 4,62 nm pour ZnO pure et ZnO dopé-Ag à 5Wt%, respectivement. L'analyse optique montre que le dopage à l'Ag augmente la transmittance optique des couches minces de ZnO. Ainsi, ces résultats obtenus peuvent suggérer la possibilité de l'utilisation des couches minces de ZnO dopées à l'Ag dans différentes applications, notamment l'optoélectronique.

Enfin, des films minces à hétérostructures n-ZnO / p-NiO avec différent nombre de revêtements de la couche de n-ZnO (2, 6, 9 et 12) ont été préparés. Les résultats de DRX confirment la formation de l'hétérostructure n-ZnO / p-NiO grâce à l'existence de deux ensembles de diffraction appartenant à NiO et à ZnO. Les propriétés photocatalytiques de l'hétérostructure p-NiO / n-ZnO ont été étudiées en mesurant la dégradation du colorant bleu de méthylène sous irradiation solaire. Il a été constaté que l'épaisseur de la couche de type n joue un rôle critique dans la performance de l'hétérostructure. L'épaisseur obtenue par 6

couches de revêtement montre une meilleure activité photocatalytique avec un taux de dégradation de l'ordre de 98,67% pour 4,5 h d'exposition à l'irradiation.

Mots-clés: ZnO, NiO, films minces, photocatalyse, méthode Sol-Gel.

الملخص

في هذا العمل ، قمنا بدراسة تأثير سرعة السحب على خواص الافلام الرقيقة لأكسيد النيكل NiO ، تأثير منشط الفضة Ag على خواص أكسيد الزنك ZnO و في الاخير تم تصنيع الأفلام الرقيقة المتغايرة ل n-ZnO / p-NiO. تم تحضير هذه الأفلام الرقيقة على ركائز زجاجية باستخدام تقنية سول جال Sol-Gel عن طريق الغمس. تم دراسة الخواص البلورية ,الضوئية ,و المورفولوجية لهذه الافلام باستخدام حيود الأشعة السينية DRX ، مقياس الطيف UV-vis ومجهر القوة الذرية AFM، على التوالي.

اظهرت النتائج من جهة , أن الزيادة في سرعة السحب تؤدي إلى تدهور البنية البلورية للأفلام الرقيقة لـ NiO وإلى انخفاض النفاذية الضوئية .ومن جهة اخرى وجد ان خشونة السطح تزداد بزيادة سرعة السحب.

فيما يتعلق بالافلام الرقيقة للاكسيد الزنك المطعمة ب Ag ،كشفت نتائج XRD أن الجودة البلورية انخفضت عندما زاد تركيز Ag مع انزياح ذروة الانعراج (101) نحو زوايا اكبر. يرجع هذا الانزياح إلى الدمج من نوع الاستبدال لذرات Ag مكان Zn في شبكة ZnO. بالنسبة للدراسة المورفولوجية ، تظهر الأفلام ذات تركيز Ag العالي خشونة سطح منخفضة ،حيث انخفضت قيمة RMS من 8.60 إلى 4.62 نانومتر بسبب تطعيم ب ٪ Wt 5 من الفضة . أظهر التحليل البصري ايضا أن التنشيط يزيد من النفاذية الضوئية للأفلام الرقيقة ل ZnO .تشير هذه النتائج الى أنه يمكن استخدام الافلام الرقيقة للاكسيد الزنك المطعمة ب Ag في تطبيقات مختلفة وخاصة الكهروضوئية.

أخيرًا، تم تحضير الأفلام الرقيقة المتغايرة لـ n-ZnO / p-NiO و تم دراسة تأثير عدد طبقات n-ZnO (2 , 6 ,9 و 12). تؤكد نتائج XRD على تشكل مزيج من n-ZnO و p-NiO و ذالك من خلال وجود طورين بلوريين لكل من NiO وZnO . تم دراسة خصائص التحفيز الضوئي للبنية المغايرة n-ZnO / p-NiO عن طريق دراسة تفكك صبغة الميثيلين الزرقاء تحت إشعاع الضوء الشمسي ، وقد وجد أن سمك الطبقة n-ZnO يلعب دورًا مهمًا في أداء البنية المغايرة , حيث ان 6 طبقات من n-ZnO تظهر أفضل نشاط تحفيز ضوئي مع معدل تفكك بنسبة ٪ 98.67 خلال 4.5 ساعات تحت الاشعاع الشمسي.

كلمات مفتاحيه : ZnO، NiO، الأفلام الرقيقة ، التحفيز الضوئي ، طريقة Sol-Gel